

## **INFORMATION TO USERS**

**This manuscript has been reproduced from the microfilm master. UMI films the text directly from the original or copy submitted. Thus, some thesis and dissertation copies are in typewriter face, while others may be from any type of computer printer.**

**The quality of this reproduction is dependent upon the quality of the copy submitted. Broken or indistinct print, colored or poor quality illustrations and photographs, print bleedthrough, substandard margins, and improper alignment can adversely affect reproduction.**

**In the unlikely event that the author did not send UMI a complete manuscript and there are missing pages, these will be noted. Also, if unauthorized copyright material had to be removed, a note will indicate the deletion.**

**Oversize materials (e.g., maps, drawings, charts) are reproduced by sectioning the original, beginning at the upper left-hand corner and continuing from left to right in equal sections with small overlaps.**

**Photographs included in the original manuscript have been reproduced xerographically in this copy. Higher quality 6" x 9" black and white photographic prints are available for any photographs or illustrations appearing in this copy for an additional charge. Contact UMI directly to order.**

**ProQuest Information and Learning  
300 North Zeeb Road, Ann Arbor, MI 48106-1346 USA  
800-521-0600**

**UMI<sup>®</sup>**



**University of Alberta**

**Scanning Force Microscopic Investigation of Oxidized  
Glassy Carbon Electrodes**

**By**

**Gregory Gabriel Kiilu Kiema**



**A thesis submitted to the faculty of Graduate Studies and Research in partial  
fulfillment of the requirements for the degree of Doctor of Philosophy**

**Department of Chemistry**

**Edmonton, Alberta.**

**Spring 2002**



**National Library  
of Canada**

**Acquisitions and  
Bibliographic Services**

**395 Wellington Street  
Ottawa ON K1A 0N4  
Canada**

**Bibliothèque nationale  
du Canada**

**Acquisitions et  
services bibliographiques**

**395, rue Wellington  
Ottawa ON K1A 0N4  
Canada**

*Your file Votre référence*

*Our file Notre référence*

**The author has granted a non-exclusive licence allowing the National Library of Canada to reproduce, loan, distribute or sell copies of this thesis in microform, paper or electronic formats.**

**The author retains ownership of the copyright in this thesis. Neither the thesis nor substantial extracts from it may be printed or otherwise reproduced without the author's permission.**

**L'auteur a accordé une licence non exclusive permettant à la Bibliothèque nationale du Canada de reproduire, prêter, distribuer ou vendre des copies de cette thèse sous la forme de microfiche/film, de reproduction sur papier ou sur format électronique.**

**L'auteur conserve la propriété du droit d'auteur qui protège cette thèse. Ni la thèse ni des extraits substantiels de celle-ci ne doivent être imprimés ou autrement reproduits sans son autorisation.**

0-612-68590-X

**Canada**

**University of Alberta**

**Library Release Form**

**Name of Author:** Gregory Gabriel Kiilu Kiema  
**Title of Thesis:** Scanning Force Microscopic Investigation of Oxidized Glassy Carbon Electrodes  
**Degree:** Doctor of Philosophy  
**Year this Degree Granted:** 2002

Permission is hereby granted to the University of Alberta Library to reproduce single copies of this thesis and to lend or sell such copies for private, scholarly or scientific research purposes only.

The author reserves all other publication and other rights in association with the copyright in the thesis, and except as herein before provided, neither the thesis nor any substantial portion thereof may be printed or otherwise reproduced in any material form whatever without the author's prior written permission.



---

5716 110 Street  
Edmonton, Alberta  
Canada T6H 3E3

December, 2001

**University of Alberta**

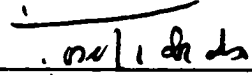
**Faculty of Graduate Studies and Research**

The undersigned certify that they have read, and recommend to the Faculty of Graduate Studies and Research for acceptance, a thesis entitled "Scanning Force Microscopic Investigation of Oxidized Glassy Carbon Electrodes" submitted by Gregory Gabriel Kiilu Kiema in partial fulfillment of the requirements for the degree of Doctor of Philosophy in Chemistry.

  
Dr. Mark T. McDermott

  
Dr. Frederick F. Cantwell

  
Dr. John-Bruce D. Green

  
Dr. Joseph Takats

  
Dr. Jingli Luo

  
Dr. Greg M. Swain, External  
Examiner, Michigan State  
University

Oct-26, 2001  
Date

**“Kidole kimoja hakivunji chawa”**

***(One finger cannot kill a louse)***

**To My Parents**

**Gregory and Marietta Kiema**

**And To My Loving Wife**

**Andrene**

**And To My Brothers**

**Chris, John, Domi, George, Alex, Gilbert**

## **ABSTRACT**

Efforts to enhance the selectivity and sensitivity of glassy carbon (GC) electrodes have led to several pathways for chemically modifying these interfaces. Electrochemical pretreatment (ECP) method is one of the most commonly utilized surface preparation procedure for activating GC electrodes due to its simplicity, relatively low cost and *in situ* capabilities.

Tapping mode scanning force microscopy (TM SFM) was utilized in this work, to characterize topographic and compositional changes induced on GC surface following ECP in acidic and basic electrolytes. Several electrochemical characterizations were carried out on the oxidized GC surface to track compositional variations and correlate them with TM SFM images. Results obtained showed that phase contrast TM SFM is able to differentiate between oxidized GC and the original polished surface on patterned electrodes. The unmodified regions in both media exhibited a darker contrast (greater phase lag) relative to the modified ones. The observed phase contrast was found to be dependent on differences in mechanical properties. Topographic images showed no morphological changes for GC electrodes oxidized in acid. However, ECP in base resulted in removal of carbon material from the GC surfaces.

A simple and rapid electrochemical procedure was developed to remove contaminants from carbon electrodes. Electrochemical measurements obtained on the electrochemically cleaned GC surface showed a highly reproducible surface with reactivity comparable to polished

GC. The etching effect induced by ECP in basic media opens pathways for fabricating microstructures on GC. Initial exploration of these possibilities demonstrated the potential of the base etching procedure towards micromachining structures on GC.

It is important to understand the activation mechanism of the various treatment methods applied to carbon electrodes. This would allow electrochemists to gain control of reactivity at electrode surfaces. In view of this, *in situ* frictional force SFM was utilized to track oxidation nucleation of the ECP process in acidic media. Regions oxidized in acid exhibited a lower frictional signal relative to the unmodified regions for images collected in pH 3 buffer. An inversion in frictional contrast was observed when imaging was done in basic media. Results showed that the electrochemical oxidation process nucleate at the defects. The polishing layer was found to direct the oxidation nucleation mechanism.

## **ACKNOWLEDGEMENTS**

This has been a long journey and has been made possible by many people whom I would like to take this opportunity to thank. I foresee myself forgetting to mention some people who were instrumental to my success and in case I forget to mention you, I do hope that you will accept my sincere apologies.

First and foremost, I would like to thank my supervisor, Dr. Mark McDermott. Thank you Mark for your guidance and advice at all stages in my study. I'm at a loss to find adequate words to describe my gratefulness. The many discussions we had and your fruitful suggestions made this work possible. I will always be grateful for the conducive environment you natured in our research lab. Your advice on issues outside the lab was also greatly appreciated. Thank you for the confidence you have in me and for your positive recommendations that made me land my first job. I know that you will continue to keep your door open for future consultations. I pray for greater success for the McDermott research group. Finally, I wish you and your family the very best in life.

I take this opportunity to thank all the McDermott Group members for their encouragement and the many discussions we had during group meetings. Special thanks go to the three pioneer members of the McDermott group, namely Michael, James and Truong. You made me feel welcomed to the group from day one. We enjoyed together many outside lab activities (and thankfully all were lawful) and I will always treasure those memories. It was a privilege to work with you guys. I consider all of you true friends and I hope that we shall continue keeping in touch. Remember, our Safari to Kenya is still on. Let's make it happen! Mirwais, Vishal, Aaron, Solomon, Francis, Sykes and Ryan, it was an honor and pleasure working with you guys. All of you made life in the lab fun. More often than not we struck a balance and made work with play more worthwhile. I wish you all success in completing

your studies and also take this opportunity to wish you all success in your future endeavors.

A very special thank you goes to my family and wife. To my Dad, thanks for teaching me the importance of education. Mum, thank you very much for your endless love, support and faith in me. I would never have asked God for a better mum and hope that I have made you proud. I love you very much. To my wife Andrene, thank you very much for your love, patience and support during my studies. Many thanks go to all my brothers, Chris, John, Domi, George, Alex and Gilbert. Thank you all for your love and encouragement since “them days”. I’m proud of you all. To my Grandma Silu and late Grandpa Kiilu, thank you for all the sacrifices you made for us.

I would like to thank all my relatives and friends in Kenya for their love and support over the years. To all my friends in Canada, Sam, Derrick, Tariq, Okwado, Jimmy, Bosire, Patrick, Oliver, and others not mentioned here, thanks for making my life outside grad school exciting. To my mother-in-law Emelia, thank you for your constant encouragement while I was writing up my thesis and also for putting up with my absence during your stay with us.

I would like to thank the Department of Chemistry for offering me a Teaching Assistantship and also for supporting my research. I would also like to acknowledge the Natural Science and Engineering Research Council (NSERC) of Canada for funding our research group. I wish to express my gratitude to Dr. Glen Fitzpatrick of Micralyne for doing the initial microfabrication work and Dr. Authur Moore (Advanced Ceramics) for the generous gift of Glassy Carbon. I would also like to thank Microfab, University of Alberta for providing facilities for doing the microfabrication work. I thank George Braybrook of Earth Sciences, University of Alberta, for the SEM images. Last, but not least, I acknowledge Jomo Kenyatta University of Agriculture and Technology for granting me a study leave to pursue my PhD studies.

# TABLE OF CONTENTS

## CHAPTER I: GENERAL INTRODUCTION

Glassy Carbon Electrodes	1
Treatment of Glassy Carbon Electrodes	4
Scanning Probe Microscopy	18
Tapping Mode Scanning Force Microscopy	19
Research Objectives	25
References	27

## CHAPTER II: PROBING MORPHOLOGICAL AND COMPOSITIONAL VARIATIONS OF ANODIZED GLASSY CARBON WITH TAPPING-MODE SCANNING FORCE MICROSCOPY

Introduction	35
Experimental	36
Results and Discussion	42
Conclusions	67
References	68

## CHAPTER III: REMOVAL OF POLISHING CONTAMINANTS FROM POLISHED CARBON SURFACES VIA AN ELECTROCHEMICAL PRETREATMENT METHOD

Introduction	72
Experimental	74
Results and Discussion	77
Conclusions	94
References	94

## **CHAPTER IV: FABRICATION OF MICROSTRUCTURES ON GLASSY CARBON SUBSTRATES VIA AN ELECTROCHEMICAL ETCHING PROCEDURE**

Introduction	97
Experimental	99
Results and Discussion	100
Conclusions	110
References	111

## **CHAPTER V: REAL TIME MAPPING OF THE ELECTROCHEMICAL OXIDATION OF GLASSY CARBON ELECTRODES WITH FRICTION FORCE MICROSCOPY**

Introduction	113
Experimental	115
Results and Discussion	116
Conclusions	136
References	137

## **CHAPTER VI: CONCLUSIONS AND FUTURE WORK**

Overall Conclusions	140
Suggestions for Future Works	143
References	145

## LIST OF TABLES

<b>Table 2.1</b>	Electrochemical and TM SFM result for polished GC ECPed at 1.8 V in 1.0 M H <sub>2</sub> SO <sub>4</sub> .	43
<b>Table 2.2</b>	Electrochemical and TM SFM result for polished GC ECPed at 1.8 V in 0.1 M NaOH.	44
<b>Table 2.3</b>	Results of adhesion and elastic modulus measured on various GC surfaces.	60
<b>Table 3.1</b>	Table of rate constants measured on polished and base oxidized GC.	85

## LIST OF FIGURES

<b>Figure 1.1</b>	Schematic representation of GC.	3
<b>Figure 1.2</b>	Schematic illustration of surface architecture of polished and ECPed GC.	14
<b>Figure 1.3</b>	Diagram illustrating major SFM components.	20
<b>Figure 1.4</b>	Schematic illustration of cantilever damping.	21
<b>Figure 1.5</b>	Schematic illustration of phase shift between input driver signal and cantilever oscillation.	23
<b>Figure 1.6</b>	Schematic illustration of phase contrast on surfaces of segregated composition.	24
<b>Figure 2.1</b>	Schematic illustration of standard photo-resist based microfabrication techniques.	38
<b>Figure 2.2</b>	Schematic illustration of ECP conditions.	39
<b>Figure 2.3</b>	Topographic SFM images of polished GC, base oxidized GC and acid oxidized GC.	47
<b>Figure 2.4</b>	SFM images of patterned GC ECPed in acid.	50
<b>Figure 2.5</b>	SFM images of patterned GC ECPed in base and cross-sectional profile of etched depression.	52
<b>Figure 2.6</b>	Example of a force-displacement curve.	56
<b>Figure 2.7</b>	Force-displacement curve for polished GC and polished GC ECPed in base.	58
<b>Figure 2.8</b>	Force-displacement curve for polished GC and polished GC ECPed in acid.	59
<b>Figure 2.9</b>	Indentation curves obtained on polished GC ECPed in base and polished GC.	61

<b>Figure 2.10</b>	Indentation curves obtained on polished GC ECPed. in acid and polished GC.	62
<b>Figure 2.11</b>	Schematic model illustrating tip interactions during TM SFM imaging of patterned GC electrodes ECPed in base.	65
<b>Figure 2.12</b>	Schematic model illustrating tip interactions during TM SFM imaging of patterned GC electrodes ECPed in acid.	66
<b>Figure 3.1</b>	Scheme illustration of technique used to pattern polished GC with polystyrene mask.	75
<b>Figure 3.2</b>	SFM images of polished GC partially masked with polystyrene and ECPed in base for 10 s at 1.8 V.	78
<b>Figure 3.3</b>	A zoom in on SFM images obtained in Figure 3.2 on both modified and unmodified regions.	80
<b>Figure 3.4</b>	XPS spectra obtained on polished GC and GC ECPed in base for 10 s at 1.8 V.	82
<b>Figure 3.5</b>	Cyclic voltammograms of $\text{Fe}(\text{CN})_6^{3-/4-}$ on polished GC and polished GC ECPed in base at 1.8 V for 10 s.	86
.		
<b>Figure 3.6</b>	Cyclic voltammograms of $\text{Eu}^{3+}(\text{aq})$ on polished GC and polished GC ECPed in base at 1.8 V for 10 s.	88
<b>Figure 3.7</b>	Cyclic voltammograms of 2,6-AQDS on polished GC and polished GC ECPed in base at 1.8 V for 10 s.	90
<b>Figure 4.1</b>	Plot of etching depth vs. oxidation time for polished GC ECPed at 1.8 V in 0.1 M NaOH.	101
.		
<b>Figure 4.2</b>	Plot of etching depth vs. anodization potential (versus Ag /AgCl reference electrode).	103

<b>Figure 4.3</b>	Scanning electron micrograph showing a cross-sectional profile of a depression.	106
<b>Figure 4.4</b>	Scanning electron micrograph showing picovials fabricated on GC substrate by base etching at 3.0 V for 15 min.	107
<b>Figure 4.5</b>	Scanning electron micrograph showing a network of microchannels machined on GC substrate via base etching procedure at 3.0 V for 5 min.	108
<b>Figure 4.6</b>	Scanning electron micrograph showing magnification of Figure 4.5 at the “double T” junction.	109
<b>Figure 5.1</b>	SFM images of a GC surface oxidized for 5 min. in acid and imaged in pH 3 and pH 10 buffer solutions.	117
<b>Figure 5.2</b>	Schematic representation of an electrolytic SFM cell used for <i>in situ</i> experiments.	123
<b>Figure 5.3</b>	<i>In situ</i> SFM images of a GC surface collected in pH 3 and 10 buffer solutions.	124
<b>Figure 5.4</b>	<i>In situ</i> SFM images of a GC surface collected in pH 3.	129
<b>Figure 5.5</b>	Schematic representation of a polished GC surface covered with a polishing layer.	134
<b>Figure 5.6</b>	<i>In situ</i> SFM images of a GC surface initially ECPed in base then Ecped in acid and imaged in pH 3.	135

## LIST OF SYMBOLS

$A$	Electrode area
$A_o$	Free oscillation amplitude
$A_{sp}$	Setpoint amplitude
$\text{\AA}$	Distance unit in angstroms
$C^\circ$	Differential capacitance
$D_o$	Diffusion coefficient for oxidized species
$D_R$	Diffusion coefficient for reduced species
$E$	Elastic modulus
$E_r$	Reduced elastic modulus
$E_{pa}$	Anodic peak potential
$E_{pc}$	Cathodic peak potential
$\Delta E_p$	Cathodic-anodic peak separation
$E^\circ$	Standard electrode potential
$i_{pa}$	Anodic peak current
$i_{pc}$	Cathodic peak current
$v$	Scan rate
$F$	Faraday's constant
$F_N$	Force applied in the normal direction to the surface
$f$	Friction force
$\mu$	Friction coefficient
$\bar{P}_{ts}$	Average tip-sample power dissipation

$\phi$	Phase shift
pL	Picoliter
Q	Quality factor of the free oscillating cantilever
R	Radius of the SFM tip
$\Gamma$	Amount of surface bound quinone
$r_{sp}$	Ratio of setpoint (or imaging) amplitude to free oscillation amplitude
S	Slope of unloading portion of a load-displacement Curve
$\dot{\gamma}$	Interfacial energy
k	Cantilever spring constant
$k^0$	Heterogeneous rate constant
$L_a$	Intraplanar microcrystallite size
$L_c$	Interplanar microcrystallite size
V	Volts
$\nu$	Poisson's ratio
$w_{ts}$	Work of adhesion between tip and sample

## **LIST OF ABBREVIATIONS**

<b>AFM</b>	<b>Atomic force microscopy</b>
<b>AC</b>	<b>Alternating current</b>
<b>CV</b>	<b>Cyclic voltammetry</b>
<b>ECP</b>	<b>Electrochemical pretreatment</b>
<b>EGO</b>	<b>Electrochemical graphitic oxide</b>
<b>ET</b>	<b>Electron-transfer</b>
<b>FTIR</b>	<b>Fourier transform infrared spectroscopy</b>
<b>FWHM</b>	<b>Full width at half maximum</b>
<b>GC</b>	<b>Glassy carbon</b>
<b>HOPG</b>	<b>Highly oriented pyrolytic graphite</b>
<b>IC</b>	<b>Integrated circuit</b>
<b>IR</b>	<b>Infrared spectroscopy</b>
<b>MEMS</b>	<b>Microelectromechanical systems</b>
<b>RF</b>	<b>Radio frequency</b>
<b>SCE</b>	<b>Standard calomel electrode</b>
<b>SEM</b>	<b>Scanning electron microscopy</b>
<b>SFM</b>	<b>Scanning force microscopy</b>
<b>SPM</b>	<b>Scanning probe microscopy</b>
<b>STM</b>	<b>Scanning tunneling microscopy</b>
<b>TM SFM</b>	<b>Tapping mode scanning force microscopy</b>
<b>XPS</b>	<b>X-ray photoelectron spectroscopy</b>

# CHAPTER I

## GENERAL INTRODUCTION

### **Glassy Carbon Electrodes**

Glassy carbon (GC) has been a widely utilized material in electrochemistry due to its importance in electrocatalysis [1], in electroanalysis [2], and in biological sensing [3-8]. Its extensive usage is due to its attractive properties such as low porosity, chemical stability, wide potential window, mechanical stability and relatively low cost. The rich surface chemistry of GC allows tailoring of its interfacial properties by physisorption or chemisorption of molecules, polymers, and metals [1-4]. Sensors and biosensors have been prepared by immobilization of recognition elements and enzymes on the GC electrode surface [2].

GC is a special form of carbon made from controlled thermal decomposition of polymeric resins such as phenol-formaldehyde or polyacrylonitrile under an inert atmosphere. These precursor materials are used because of their high carbon yield upon pyrolysis. The polymer is heated to a high temperature, typically in the range of 1000-3000 °C and results in an extensive conjugated  $sp^2$  carbon structure [2-6]. Carbonization starts to occur at a temperature above 300 °C. Non-carbon atoms such as nitrogen and oxygen present in the precursor polymer are released and only carbon is left. Depending on the processing temperature and polymer resin used, the yields of GC are usually 40-60% [6,7]. The widely accepted

schematic representation of the structural model for GC proposed by Jenkins *et al.* is shown in Figure 1.1 [6]. The tangled ribbon-like structure is a result of the precursor polymer and prevents long range graphitization. However, some local graphitization occurs during the final heating stage. The physical properties of the GC material are dependent on the final temperature at which the polymer is heated. Higher heat treatment temperature generally results in greater ordering of the GC. Three grades of GC are commonly available based on this final temperature: GC-10 (1000 °C), GC-20 (2000 °C), and GC-30 (3000 °C). GC-20 is the electrode material used throughout this research.

The microcrystallite size of  $sp^2$  hybridized carbon can be defined by the intraplanar microcrystallite size,  $L_a$ , and the interplanar microcrystallite size,  $L_c$ , which provide a measure of the extent of graphitization.  $L_a$  defines the extent of the crystal in the plane of the hexagonal lattice (a-axis) while  $L_c$  defines the extent of the crystal in the plane perpendicular to the hexagonal lattice (c-axis). The plane along the a-axis is commonly referred to as the basal plane while the plane perpendicular to the graphite lattice is termed edge plane.

X-ray diffraction studies show significant change in the microcrystallite size when the final heat treatment temperature is varied [4]. The values of  $L_a$  have been reported to change from 25 Å to 55 Å and that of  $L_c$  from 12 Å to 70 Å when the final temperature is varied from 2000 °C to 3000 °C. GC is isotropic on a scale greater than ca. 200 Å and has a lower density (1.3-1.5 g/cm<sup>3</sup>) than graphite (2.27 g/cm<sup>3</sup>) which reflects its porous microstructure [2].

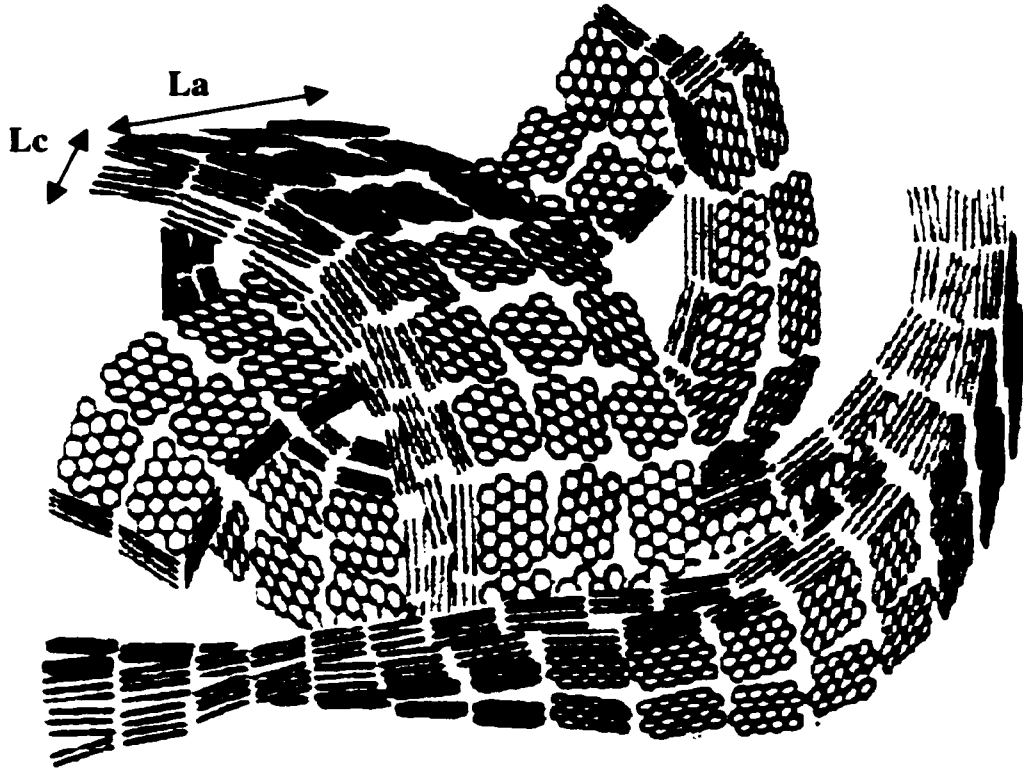


**Figure 1.1:** Schematic representation of GC [6].

However, the voids constituting the pores are not connected, which accounts for the low gas permeability observed for this material.

### **Treatment of GC Electrodes**

A number of pretreatment and activation methods have been developed to ensure highly reactive and reproducible GC electrode surfaces. Most pretreatment methods have involved polishing the GC surface with various grades, sizes, and types of abrasive materials. Polishing improves reproducibility of “as received” GC surfaces via the removal of gross surface defects and impurities that arise from the manufacturing process. Activation procedures are additional steps that are undertaken to increase the reactivity of the electrode surface. Procedures such as electrochemical pretreatment (ECP) [8-13], ambient or vacuum heat treatment [14-19], laser irradiation [20-22], and exposure to isopropanol/activated carbon mixture [23] have been employed to activate GC electrodes. These activation procedures affect the final surface structure of GC electrodes and often are found to be crucial to electrochemical performance [8, 9, 11, 15, 17, 19, 20, 24-26]. ECP of GC electrodes is the most widely utilized treatment method after polishing. Both polishing and ECP methods are used in this research and will be discussed in detail in the following sections.

**Polished GC.** Polishing procedures have been extensively used for GC electrodes [14, 16, 24, 26-29]. Polished GC is by far the most often used starting surface for other activation procedures. Generally, the procedure begins by grinding the “as received” GC with fine grit silicon carbide paper to

level any large-scale roughness. The surface is then polished in an aqueous slurry of alumina particles or in a paste of diamond particles. The polishing material is usually supported on a felt polishing cloth. The particle size of the abrasive powders used is typically in the micrometer to submicrometer range and produces a mirror like surface. Kazee *et al.* have shown that the final surface of a polished GC electrode is covered with a thin layer of finely divided carbon microparticles and polishing contaminants [29]. This layer has been found to remain even after ultrasonication in a water bath [19, 26, 29].

Changes in electrode activity following various treatments have been commonly assessed in terms of the heterogeneous electron transfer (ET) reversibility and background current. Cyclic voltammetry (CV) is commonly used in the determination of heterogeneous ET rate constants,  $k^{\circ}$  [2, 4]. Cyclic voltammetry is used in this research to assess ET reactivity on modified GC electrode surfaces. The following general redox reaction will be considered to describe the CV experiment:



where O represents the oxidized form of the redox species and R the reduced form.  $n$  represents the number of electrons needed to reduce one O molecule to R.  $E^{\circ}$  is the standard potential at which the redox reaction occurs. A CV experiment is initiated at a potential  $E_1$ , that is more positive than  $E^{\circ}$  and thus reduction of O to R does not occur. The potential is linearly scanned negatively to a final potential,  $E_2$ , at which O cannot exist at the electrode

surface without being reduced. As a result, a cathodic peak current,  $i_{pc}$ , is observed at a potential  $E_{pc}$ . At potentials negative of  $E_{pc}$ , mass transport is diffusion limited and the current decays as a function of  $t^{-1/2}$ , where  $t$  is time. On reaching  $E_2$ , the direction of the potential scan is reversed and the potential is swept back towards  $E_1$ . As the potential is scanned positively an anodic peak current,  $i_{pa}$ , is observed at a potential  $E_{pa}$  where R is oxidized back to O. At potentials positive of  $E_{pa}$ , diffusional mass transport of R to the electrode surface is again limiting and the current decays as a function of  $t^{-1/2}$ . Return of the potential to  $E_1$  signifies a potential cycle and the plot of current as a function of potential, or time is called a cyclic voltammogram. The cyclic voltammetric peak separation,  $\Delta E_p$ , is the separation of the anodic peak potential ( $E_{pa}$ ) and cathodic peak potential ( $E_{pc}$ ).

$\Delta E_p$  is useful in the determination of electrochemical reversibility and electron transfer rate constant,  $k^0$ . For a reversible system, a  $\Delta E_p$  value of  $57/n$  mV is observed and  $i_{pa}/i_{pc} = 1$ . These values are independent of scan rate,  $v$ . Reactions in which  $\Delta E_p$  varies with  $v$  are referred to as quasi-reversible reactions. Nicholson developed a mathematical model for estimating the rate constant values of quasi-reversible redox reactions by examining the variation in  $\Delta E_p$  with  $v$  [30]. The shape of a cyclic voltammogram is found to depend on the transfer coefficient,  $\alpha$ , and dimensionless parameter  $\psi$  given by the expression:

$$\psi = \frac{\left(\frac{D_O}{D_R}\right)^{\alpha/2} k^{\circ}}{[D_O \pi \nu (nF/RT)]^{1/2}} \quad \{1.2\}$$

where  $D_O$  and  $D_R$  represents the diffusion coefficients of O and R species respectively in  $\text{cm}^2/\text{s}$  and  $\nu$  is the scan rate in  $\text{V}/\text{s}$ . The Nicholson method uses the  $\Delta E_p$  values measured from cyclic voltammograms to obtain corresponding values of  $\psi$  from a working curve of  $\log \psi$  versus  $\Delta E_p$  [30]. Upon determining  $\psi$ , the value of  $k^{\circ}$  is then calculated using equation 1.2. The smaller the  $\Delta E_p$  value, the faster the ET kinetics.

The background current on carbon electrodes is dependent on surface roughness, surface functional groups, and surface faradaic reactions. Thus, background current can provide important information about surface structure. The capacitive component of background current has been used on carbon electrodes to track changes in surface structure following surface modification [2, 4]. Cyclic voltammetry in inert electrolyte is a common technique used for examining background current. Gileadi *et al.* developed a method for determining the differential capacitance,  $C^{\circ}$ , of electrode/solution interface [31]. In this method the electrochemical cell is used as an AC differentiating circuit where a triangle potential wave input results in a square wave current output. The capacitance of the electrode/solution interface is related to the output current via:

$$C^{\circ}(\mu\text{F}/\text{cm}^2) = i_{p-p}/2\nu A \quad \{1.3\}$$

where  $i_{p-p}$  is the peak-to-peak output current in  $\mu\text{A}$ , and  $v$  is the scan rate in  $\text{mV/s}$  and  $A$  is the electrode area in  $\text{cm}^2$ .

The  $\text{Fe}(\text{CN})_6^{3-/4-}$  redox system has been commonly used as a probe to assess changes in carbon electrode activity upon various treatments. Polished GC surface exhibits higher  $k^0$  for  $\text{Fe}(\text{CN})_6^{3-/4-}$  redox system as compared to untreated GC surfaces used as received. Fagan *et al.* have reported a cathodic peak and anodic peak separation ( $\Delta E_p$ ) of 300 mV from the cyclic voltammogram for  $\text{Fe}(\text{CN})_6^{3-/4-}$  on untreated GC surface and upon polishing the untreated surface a  $\Delta E_p$  value of 75 mV was obtained [19]. Carefully polished GC surfaces (i.e., polished with 600-grit SiC; 1.0-, 0.3-, 0.05- $\mu\text{m}$   $\text{Al}_2\text{O}_3$ ) have also been reported to produce high  $k^0$  for other benchmark systems such as dopamine [26] and ascorbic acid [26, 32].

The lack of a standardized polishing procedure has contributed to a high variation in heterogeneous ET rate constant,  $k^0$ , reported for  $\text{Fe}(\text{CN})_6^{3-/4-}$  on polished GC surfaces.  $k^0$  value reported for this redox probe varies from  $\sim 10^{-4}$  to 0.14  $\text{cm/s}$  depending on polishing procedure [16]. Hu *et al.* have reported that increased cleanliness during polishing of GC with 600 grit SiC followed by successive 1.0-, 0.3-, 0.05- $\mu\text{m}$   $\text{Al}_2\text{O}_3$  slurries resulted in a  $k^0$  value for  $\text{Fe}(\text{CN})_6^{3-/4-}$  comparable to that obtained with platinum electrodes [16]. The authors also noted that use of water of lower purity resulted in lower  $k^0$  values for  $\text{Fe}(\text{CN})_6^{3-/4-}$ . The use of a polishing cloth as a base for polishing has also been suggested by some investigators to cause a decrease in the rate

constant for  $\text{Fe}(\text{CN})_6^{3-/4-}$  [9, 16]. The investigators reported improved ET kinetics when the polishing was done on a glass plate. Thornton *et al.* have demonstrated that use of finer abrasives during polishing procedure resulted in improved ET kinetics for  $\text{Fe}(\text{CN})_6^{3-/4-}$  [27]. Fagan *et al.* have reported that organic modifiers often used as carriers or deagglomerating agents in abrasive powders deactivate the polished GC surface [19].

The activation mechanism following polishing is not clear since several surface variables change during polishing. For example, Rice *et al.* have used Raman spectroscopy to show that intraplanar microcrystallite size,  $L_a$ , for fractured GC-30 surface decreased with polishing [21]. This result suggests that polishing procedure changes the surface microstructure of the untreated GC electrode. Kamau *et al.* have reported an increase in oxygen/carbon ratio from 0.12 to 0.17 with polishing by employing X-ray photoelectron spectroscopy (XPS) [26]. The authors found that the majority of the oxygen on the polished surface was in phenolic form. Results from other XPS studies have also detected the presence of oxygen on the polished surface [10, 16].

In summary, careful attention to electrode polishing and cleaning could yield an electrode of very good activity. However, polished GC electrodes do show significant surface-to-surface variation. Rate constant values determined on polished GC electrodes for various redox systems show extreme sensitivity to polishing history which is a significant drawback for

these electrodes. A more detailed discussion on the poor reproducibility of polished GC surfaces is deferred to Chapter III.

**Electrochemical Pretreatment (ECP) of GC.** Electrochemical methods of pretreatment have been the subject of many studies involving carbon fibers and GC electrodes [2, 4]. The terms anodization and cathodization are frequently used to describe the ECP process with anodization indicating that the electrode is subjected to positive potentials where oxidation of the electrode may occur and cathodization indicating that the electrode is subject to negative potentials where reduction of the electrode may take place. Electrochemical methods of pretreatment have been used extensively, as they are convenient, inexpensive and rapid and they offer an additional advantage that they can be performed within the electrolyte. The procedure involves application of one of several potential waveforms to the carbon electrode in some suitable solvent.

Lord and Rogers were the first to demonstrate that anodization of a graphite electrode greatly changed the shape of a slow scan voltammetric curve for the reduction of  $\text{Fe}^{+3}$  in 0.1 M HCl [33]. Thereafter, more studies have been done on the effects of ECP on carbon electrodes in acidic solutions [10, 11, 34-39], in neutral buffered or salt solutions [9, 12, 14, 40-42], and in basic solutions [36, 37, 39, 43, 44]. As with polishing procedure, there is no standardized ECP procedure. Differences in ECP procedure arise from electrolyte composition, applied potential waveform and magnitude of the applied potential. One of the most widely applied ECP procedures involves

anodization of the electrode surface at potentials between 1.6 to 2.2 V versus standard calomel electrode (SCE). In this research, ECP was mostly performed by poisoning a GC electrode at 1.8 V versus a silver/silver chloride (Ag/AgCl) reference electrode.

Several studies have reported on the effects of ECP on the surface structure of carbon electrodes. ECP of GC electrodes in acidic or neutral buffered/salt solutions at high positive potentials effectively transforms compositionally the surface of GC with a layer of graphite oxide referred to as electrochemical graphitic oxide (EGO) [11, 29]. The investigation by Kepley and Bard revealed that the oxide film thickness increased monotonically with activation time up to at least 1  $\mu\text{m}$  [11, 29]. The authors also found the oxide film to be porous, hydrated, anionic, and non-conductive.

Nagaoka *et al.* have established that the EGO film adsorbs ions and could undergo ion exchange of cations [45]. XPS studies of the EGO film have indicated an increase of oxygen/carbon ratio from 0.08 for polished GC to 0.24 after ECP in acid, confirming formation of an oxygen rich film [9]. High resolution XPS studies have revealed that the majority of the surface oxide groups exist as phenolic, carbonyl and carboxylate functionalities [9, 28, 40, 45]. The exact nature of this oxide layer is uncertain. However, Engstrom and Strasser have reported that the amount of charge in the cathodic stripping peak indicates a multilayer structure [9]. The authors also observed that cathodization reduced the oxides, but did not remove them. In the same

study, contact angle measurements following ECP indicated increase in hydrophilicity of the acid anodized GC surface.

Anodization of GC in basic solutions has significantly different effects as compared to ECP in acidic or neutral buffered/salt solutions [9, 43, 44]. The formation of surface oxides by anodization of carbon electrodes in basic solutions was reported by Kozłowski and Sherwood [37]. However, ECP of GC in basic electrolytes does not result in an EGO film [35, 46]. Reported results imply that if a EGO film is produced by ECP in base, it is immediately removed possibly by dissolution [35, 44]. ECP of GC in basic media at high positive potentials results in lower background current values than those observed on acid anodized GC surfaces [11, 43]. The high background noted on acid modified GC surfaces have been attributed to redox functional groups produced by ECP and the increased porosity and anionic character of the EGO film.

ECP of carbon electrodes in basic electrolytes at mild conditions ( $\sim 1.8$  V versus SCE) has been found to etch away the carbon material, unlike in acidic media [37, 46]. Beilby and Carlsson have reported removal of pyrolytic carbon films deposited on polished GC substrates upon ECP in NaOH. The authors stated that they were able to visually observe the underlying GC substrate following anodization in basic electrolyte [43]. Also, a study by Kozłowski and Sherwood reported the presence of carbon fragments in the working electrode solution after electrochemical oxidization of carbon fibers in

NaOH solution [37]. Their observation suggested breakup of the carbon fiber lattice.

Acid anodized GC surfaces display different colors [10, 35, 46] that have been attributed to optical interference in the transparent EGO film [11, 35]. No color changes have been reported on GC surfaces anodized in basic solutions [46]. Anjo and coworkers have established that GC electrodes ECPed in basic electrolytes show better performance in the analysis of dopamine than those anodized in acidic solutions [35]. The authors attributed the differences to a significant reduction in dopamine adsorption on base anodized GC surfaces as compared to GC surfaces ECPed in acidic media. Figure 1.2 provides a schematic illustration of the surface architecture for both base and acid anodized GC based on reported studies. More details on the differences between acid and base anodized GC surfaces will be discussed in Chapter II.

ECP alters the physical and chemical properties of carbon surfaces in several ways. Examples of these changes include increase in both microscopic area and hydrophilicity. As stated earlier, the electrode may also be modified with an oxide film that promotes charge interactions. Other observed effects of ECP include removal of impurities from the carbon surface and mediation by promoting proton transfer for some reactions or by promoting catalytic sites. Redox systems have been found to respond differently to the above ECP induced changes in surface variables.

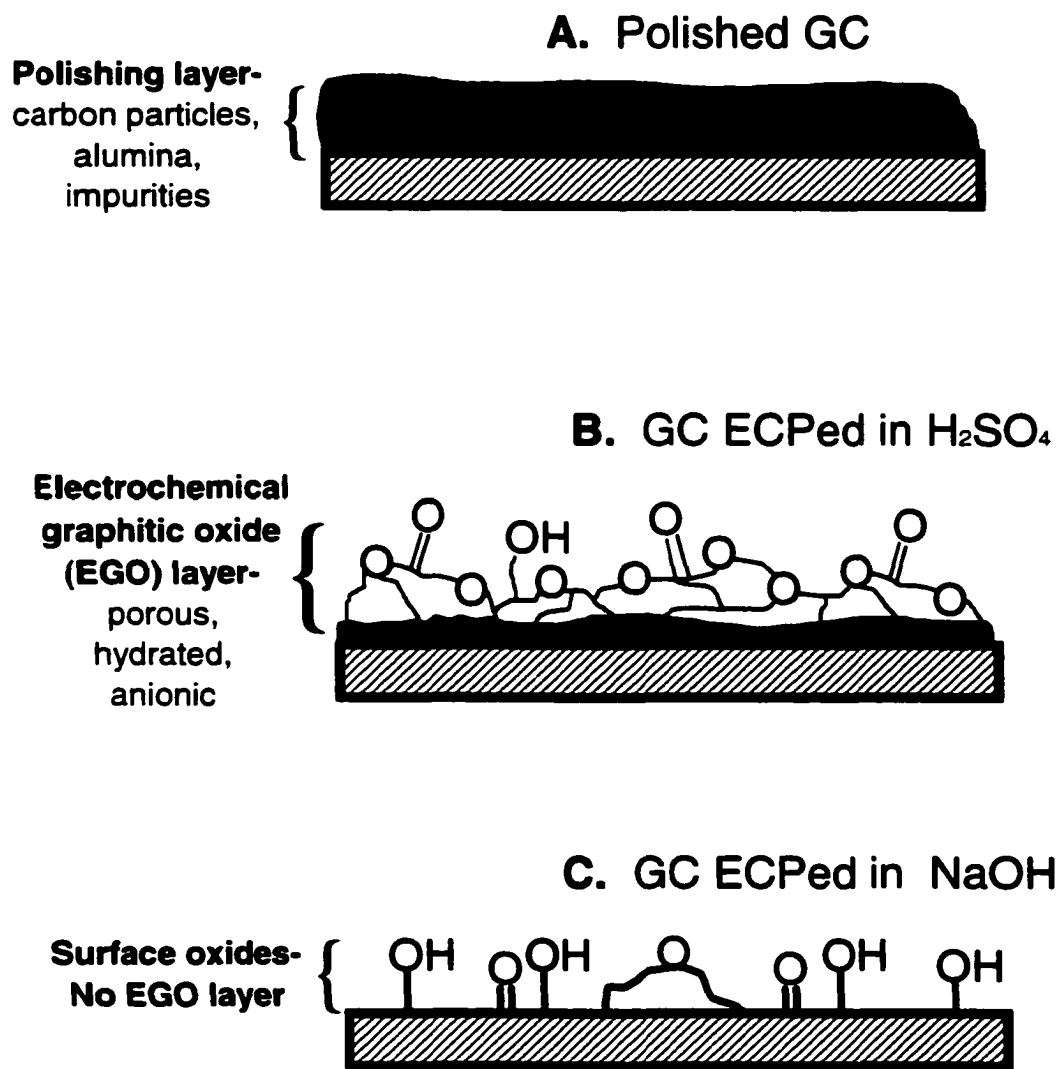


**Figure 1.2:** Schematic illustration of the surface architecture for (A) polished GC (B) polished GC ECPed in acid and (C) polished GC ECPed in base.

For example, Armstrong *et al.* have described the importance of oxide sites to cytochrome c charge transfer on carbon electrodes [47, 48]. The authors found that binding of the cytochrome c to surface oxides greatly accelerated the electron transfer process. Gonon *et al.* reported the first application of ECP carbon fiber microelectrodes for *in vivo* analysis in brain tissue [12]. The investigators observed that ECP of carbon microelectrodes in acidic media improved ET kinetics sufficiently enough to separate overlapping ascorbic acid and dopamine voltammetric peaks. The success in the detection of dopamine *in vivo* was attributed to suppression of ascorbic acid response by EGO film due to electrostatic effect.

Kovach *et al.* have also reported large effects on the behavior of several metal complexes as well as dopamine and ascorbic acid on carbon electrodes ECP in acid [49]. Results from this study showed that ECP increased sensitivity for dopamine (a cation) and had little effect on 4-methyl catechol (a neutral), while the sensitivity for ascorbic acid and dihydroxyphenyl acetic acid (anions at pH 7.2) decreased. The authors concluded that the enhanced sensitivity was due to preferential ion exchange of cations with the EGO film, thereby leading to preconcentration on the electrode surface. McDermott *et al.* have demonstrated that presence of surface oxides generated by ECP of GC in acidic media provided sites for inner sphere catalysis of aquated metal complexes [50]. Kuwana and coworkers have demonstrated that dihydronicotinamide adenine dinucleotide (NADH) is catalytically oxidized by surface bound quinone groups [16].

Cabaniss *et al.* have shown that the proton-assisted ET mechanism for NADH based on hydrogen/deuterium isotope effect required surface oxides, particularly phenols [10].

Other studies have pointed out that the presence of oxides is not necessary to increase the electrocatalytic activity of GC surfaces. Arguments against surface oxides involvement are supported by achievement of activation by non-oxidative pretreatment methods such as vacuum heat treatment [19], laser activation [51], and solvent extraction [14]. For example, the increase in the rate constant for  $\text{Fe}(\text{CN})_6^{3-/4-}$  redox system at carbon surfaces has been attributed to surface cleanliness and exposure of active sites [16, 20, 52]. Engstrom and Strasser [9] have found that anodization of GC in acidic media resulted in improved ET kinetics for  $\text{Fe}(\text{CN})_6^{3-/4-}$ . The investigators attributed improved kinetics to removal of impurities from the electrode surface following ECP. XPS analysis of polished GC surface prior to and after ECP showed decreased level of impurities associated with Teflon, a contaminant from the electrode housing that are introduced on the surface during polishing.

Bowling *et al.* have suggested that oxidation plays an important role during ECP of GC by creating strain on the lattice which causes more active edge plane sites to form, thereby enhancing ET kinetics for  $\text{Fe}(\text{CN})_6^{3-/4-}$  [53]. Barbero *et al.* proposed that formation of micropores due to ECP of GC in acid expose graphitic edges leading to increased electrocatalytic activity of GC electrode towards several benchmark systems [54]. The importance of

the double layer properties and surface wettability have been demonstrated by Bjelica and Jovanovic [55]. The authors measured the ET kinetics for  $\text{Fe}^{2+/3+}$  redox couple on GC activated in aqueous and non-aqueous electrolytes and found that unlike in aqueous media, ECP activation had no effect in non-aqueous media.

Scanning electron microscopy (SEM) and scanning probe microscopy (SPM) techniques have been used in the surface analysis of electrochemically modified carbon electrodes. Results from these microscopic studies have mainly revealed topographic changes and increase in surface roughness following pretreatment. For example, Smyrl *et al.* have observed formation of “mesa” using SEM following anodic pretreatment in basic electrolyte [56]. The authors attributed the swelling of the carbon matrix to injection of species from the electrolyte, likely hydroxide ions. Picq *et al.* have investigated anodized GC electrodes using SEM [57]. The authors observed formation of small pores during the activation process.

Morita and Shimizu have reported etching of carbon fiber-epoxy composite using SEM upon anodic pretreatment in acid [58]. SPM studies by Freund *et al.* and Wang *et al.* have reported surface roughening following ECP of GC electrodes [59, 60]. However, Engstrom and Strasser using SEM have reported no significant changes in topography on GC surface activated in acidic media [9].

## **Scanning Probe Microscopy**

Scanning probe microscopy (SPM) has emerged as an active and exciting area of research since the invention by Binnig *et al.* of the scanning tunneling microscope (STM) in 1982 [61] and the creation of atomic force microscope (AFM) by Binnig *et al.* in 1986 [62]. Among the more exciting advances in SPM methodology has been the development of AFM also known as scanning force microscopy (SFM) for compositional mapping of surfaces at nanometer length scales [63-73]. The first report of this ability utilized the most common imaging mode of SFM known as contact mode SFM. In this study, Overney *et al.* used contact mode SFM, operated in lateral (or friction) mode to distinguish between different chemical domains [63]. These studies were extended to employ SFM probe tips of controlled chemistry, which generated images with contrast based on predictable chemical interactions [64, 66, 71, 72, 74]

Tapping mode SFM (TM SFM) is a more recent imaging mode of SFM which was developed to overcome the problems of sample damage often experienced when imaging soft or weakly bound samples in contact mode SFM. Topographically induced shear forces experienced in contact mode SFM are greatly reduced in TM SFM [75], thereby allowing imaging of delicate samples. Both contact and tapping imaging modes are utilized in our laboratory. However, the bulk of the research work presented in this dissertation was obtained using TM SFM. Thus, TM SFM is discussed in some detail in the following section while a brief discussion on contact mode

SFM is deferred to Chapter III where the imaging mode is employed to investigate ECPed GC electrodes.

### **Tapping Mode SFM.**

A scanning force microscope consists of four major components: a cantilever-mounted tip, a piezoelectric micropositioner, a cantilever deflection sensor, and an electrical feedback mechanism for the micropositioner. A laser beam is reflected off the back of the cantilever and directed onto a position sensitive photodiode detector as depicted in Figure 1.3. In tapping mode SFM, imaging is implemented by externally oscillating the cantilever-tip assembly close to its resonance frequency (~ 300 kHz). This is generally accomplished through a small piezoelectric transducer that contacts the cantilever base.

The sample surface is then moved towards the vertically oscillating tip until the tip begins to intermittently contact the surface. The contact with the surface reduces the amplitude as shown in Figure 1.4. The feedback control is set to detect the perturbation on the free oscillation amplitude ( $A_0$ ) caused by the intermittent contact with the surface. The modified oscillation amplitude is used as a setpoint amplitude ( $A_{sp}$ ) such that as the tip scans laterally, the vertical position is adjusted with the feedback control to maintain the  $A_{sp}$  at a constant value. For example, a region of high topography will decrease the cantilever amplitude momentarily. The height change of the sample is plotted versus x-y position to generate a topographic image. The

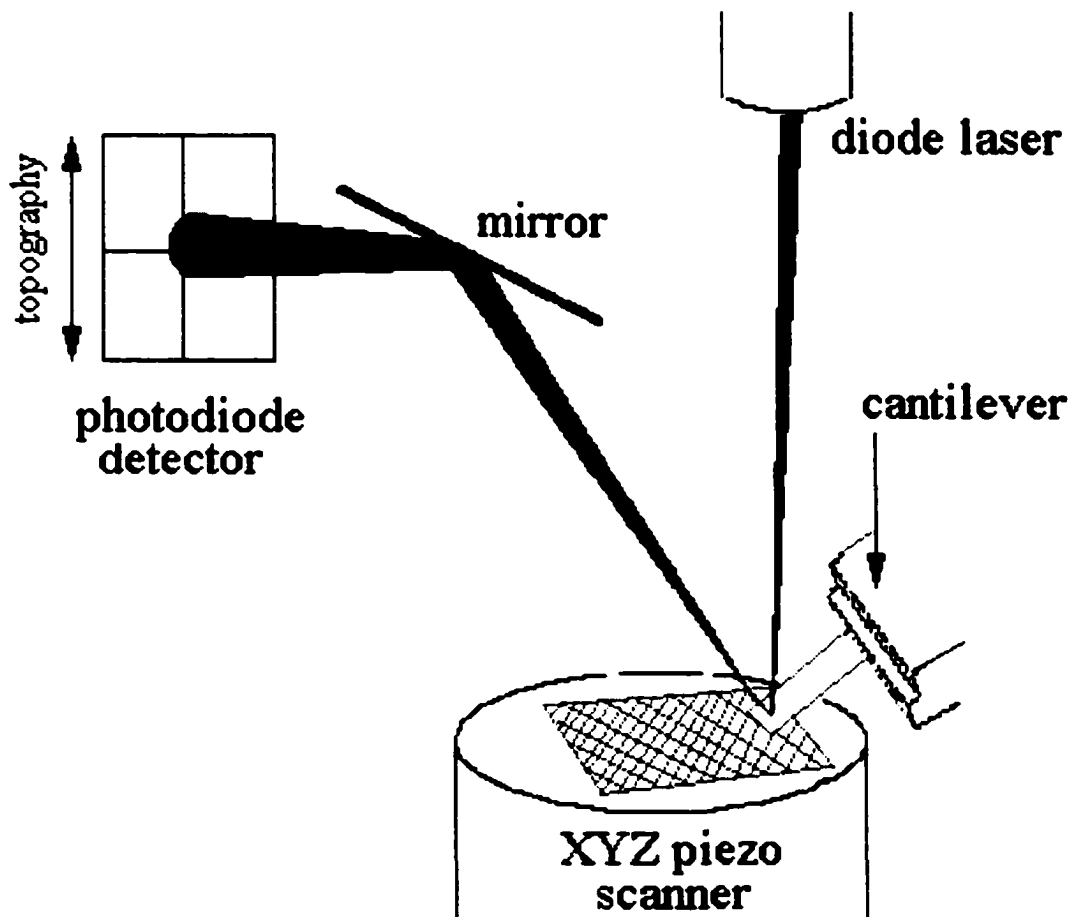


**Figure 1.3:** Diagram illustrating the major components of a scanning force microscope. The probe tip is mounted on the bottom side of the cantilever and cannot be seen in this figure.

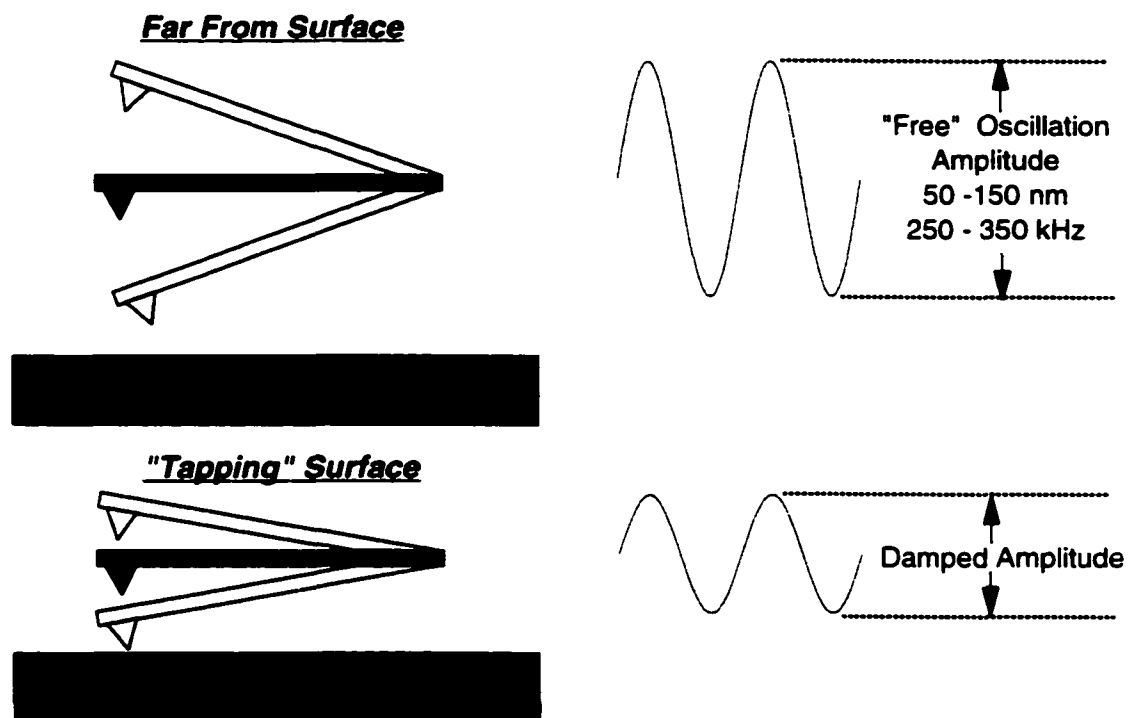


**Figure 1.4:** Schematic illustration of a vertically oscillating cantilever-tip assembly. Amplitude reduces on contact with the sample surface.

feedback loop will lower the sample height to adjust the amplitude back to  $A_{sp}$ . The change in sample height is recorded as a topographic feature in the image.

Phase imaging is a powerful extension of TM SFM that is sensitive to variations in local material properties and hence goes beyond simple topographic mapping of surfaces. In phase imaging, the difference between the phase of the input driver signal and response of the cantilever oscillation is monitored as a phase shift, ( $\phi$ ), as shown in Figure 1.5. Several modeling efforts aimed at predicting factors that influence phase contrast in TM SFM have been reported [76-84]. It has been suggested that interactions between the tip and surface that damp the cantilever oscillation are responsible for phase lags in TM SFM [78, 80, 83, 84].

Tamayo and Garcia treated the vibration of the cantilever-tip assembly as a simple harmonic oscillator, and based on the equation of motion, the authors found that tip-sample energy dissipation is essential for a phase shift to occur [78]. Cleveland *et al.* have investigated the relationship between phase shift ( $\phi$ ) and the energy dissipated by the tip-sample contact ( $P_{ts}$ ) from the energy conservation perspective [80]. The authors proposed that the  $\phi$  and the set-point amplitude ( $A$ ) of a tapping cantilever at the drive resonance frequency  $\omega_b$  are related to the average tip-sample power dissipation,  $\bar{P}_{ts}$ , by equation 1.4 provided below:

$$\sin\phi = \left( \frac{2Q}{k\omega_b A_0 A} \right) \bar{P}_{ts} + \frac{A}{A_0} \quad \{1.4\}$$

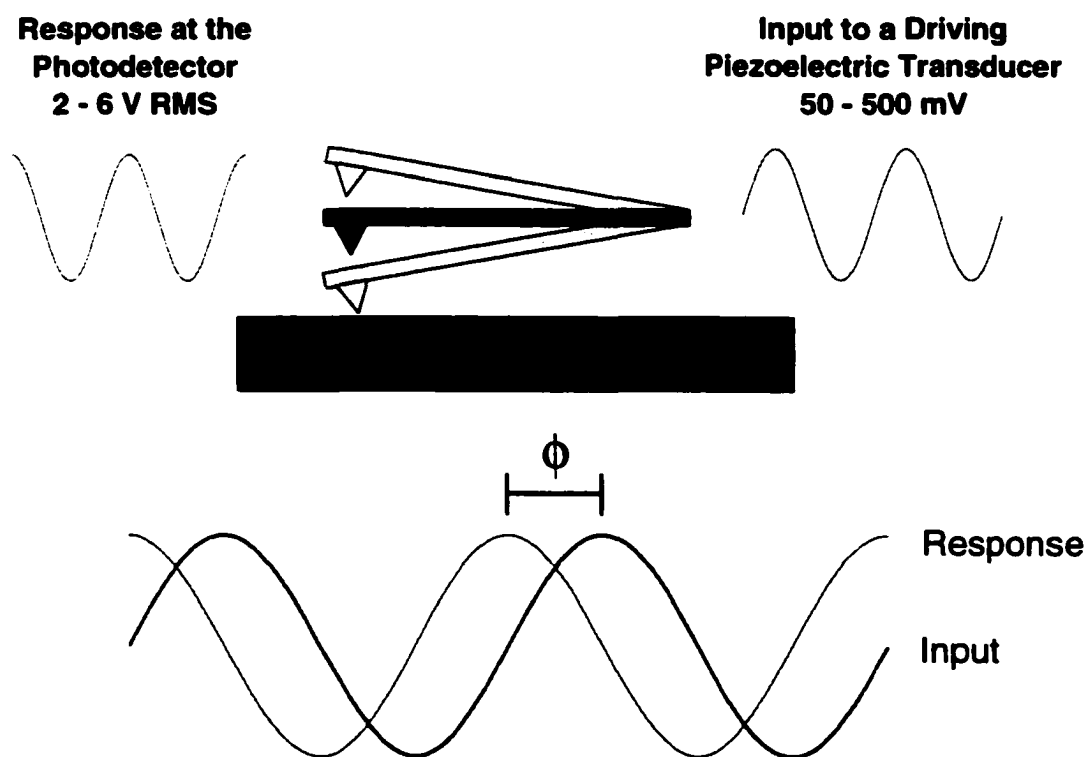


**Figure 1.5:** Schematic illustration of a phase shift ( $\phi$ ) between the input driver signal and the response of the cantilever oscillation.

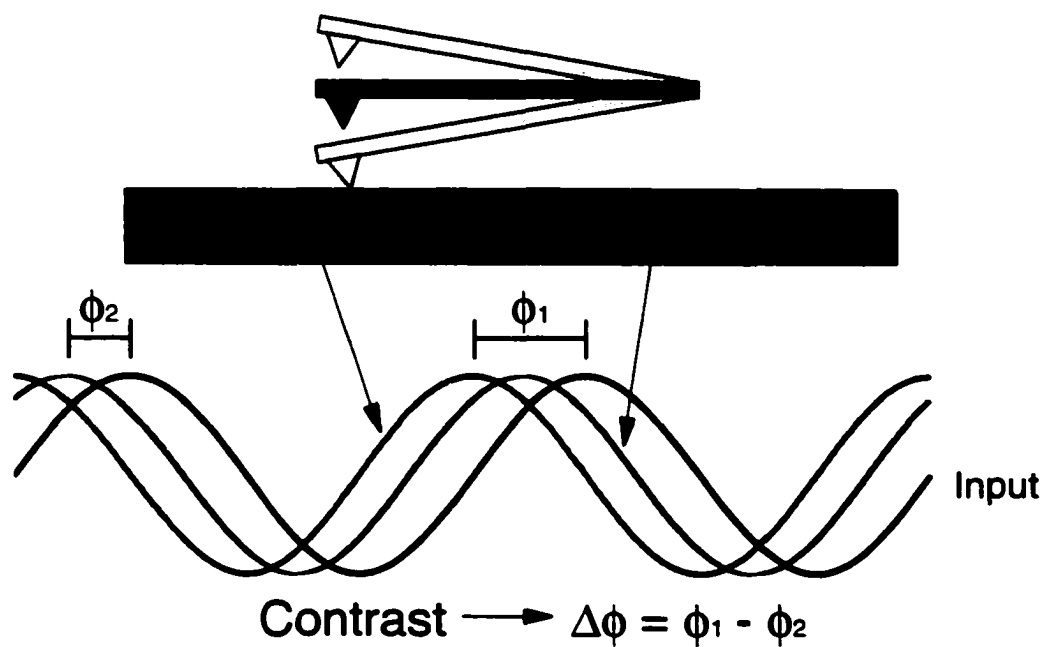


**Figure 1.6:** Schematic illustration of phase contrast ( $\Delta\phi$ ) observed in TM SFM when imaging surfaces of segregated composition.

where  $k$ ,  $A_0$ , and  $Q$  are the spring constant of the cantilever, free oscillation amplitude and quality factor of the free oscillating cantilever, respectively. As stated earlier, phase imaging is performed with the amplitude held constant by the feedback loop. Thus, equation 1.4 importantly indicates that when imaging surfaces of segregated composition with TM SFM, variations in the energy dissipated by the tip at each region will result in phase contrast as illustrated in Figure 1.6. This suggests that phase contrast images can be considered maps of local energy dissipation. It has been recently shown that phase contrast TM SFM can be utilized to map surfaces compositionally based on differences in surface mechanical properties and chemistry [39, 75, 76, 85-90]. The specific sample properties that govern phase contrast in TM SFM are not clearly understood. However, surface parameters such as viscoelasticity, plastic deformation and adhesion hysteresis have been shown to give rise to energy dissipative interactions resulting in phase shifts [78, 83, 84]. With respect to the direction of contrast, a region exhibiting greater energy dissipating processes will produce a greater phase shift and is plotted as a darker contrast in all the TM SFM images presented in this dissertation.

### **Research Objectives**

Efforts to enhance the selectivity and sensitivity of GC electrodes have led to several pathways for chemically modifying these interfaces. Electrochemical pretreatment (ECP) method is one of the most commonly utilized surface preparation procedure for activating GC electrodes due to its simplicity, relatively low cost and *in situ* capabilities. The changes induced on

the GC surface via ECP have been characterized in terms of their influence on electron transfer kinetics, capacitance and adsorption. Most of these studies were characterized using macroscopic techniques such as XPS, Raman spectroscopy and electrochemistry. However, such techniques only provide an average representation of the electrode surface structure. SEM studies have provided details of ECPed GC electrodes at microscopic resolution. However, only topographic information is provided. SPM techniques permit topographic investigation of modified GC surfaces at scales comparable to SEM but is also able to provide compositional mapping of the modified surfaces.

SPM techniques have been successfully employed to characterize the two dimensional structure of electrode surfaces. However, only a handful of SPM studies have focused on the widely utilized GC electrodes. This is likely due to the rough and ill-defined surface structure of GC electrodes compared to atomically smooth SPM substrates such as annealed gold and highly ordered pyrolytic graphite (HOPG). The first objective of this research is to apply compositionally sensitive contrast mechanisms in SFM to track both morphological and compositional variations induced on GC by ECP in acidic and basic electrolytes. Results obtained will more completely characterize the effects of ECP on GC surface structure and facilitate assessment of tapping mode SFM (TM SFM) for compositional mapping of relatively rough, polished electrode surfaces.

Polished GC is often used as the starting surface for other activation procedures, including ECP. However, electrochemical measurements obtained at these surfaces show significant surface-to-surface variation from laboratory to laboratory. This is partly attributed to differences in the amount and/or composition of polishing contaminants present on the polished surfaces. The second objective is to develop a simple and rapid electrochemical cleaning procedure aimed at removing polishing impurities from polished carbon surfaces. Overcoming surface variation of the starting GC surface would result in better understanding of the relationship between surface structure and ET reactivity.

The activation mechanism of ECP processes is not clearly understood. The third objective of this research is therefore to track the oxidation nucleation mechanism following ECP of GC in acidic media using chemically sensitive lateral or friction mode SFM. A more in-depth understanding of the ECP activation mechanism would allow better control of reactivity at the electrode surface. The work described herein describes my efforts and progress towards achieving these objectives.

### References

1. N. L. Pocard, D. C. Alsmeyer, R. L. McCreery, T. X. Neenan, and M. R. Callstrom, *J. Mater. Chem.* 2:771 (1992).
2. K. Kinoshita, , John Wiley & Sons Inc., New York, 1988, p. 226 .
3. W. E. van der Linden and J. W. Dieker, *Anal. Chim. Acta* 119:1 (1980).

4. R. L. McCreery, , Vol. 17 (A. J. Bard, ed.), Marcel Dekker, New York, 1991, p. 221.
5. S. Yamada and H. Sato, *Nature* 193:261 (1962).
6. G. M. Jenkins and K. Kawamura, *Nature* 231:175 (1971).
7. D. W. McKec, *Annu. Rev. Mater. Sci.* 3:195 (1973).
8. R. C. Engstrom, *Anal. Chem.* 54:2310 (1982).
9. R. A. Engstrom and V. A. Strasser, *Anal. Chem.* 56:136 (1984).
10. G. E. Cabaniss, A. A. Diamantis, W. R. Murphy, R. W. Linton, and T. J. Meyer, *J. Am. Chem. Soc.* 107:1845 (1985).
11. L. J. Kepley and A. J. Bard, *Anal. chem.* 1988:1459 (1988).
12. F. G. Gonon, C. M. Fombarlet, M. J. Buda, and J. F. Pujol, *Anal. Chem.* 53:1386 (1981).
13. L. Falat and H. Y. Cheng, *Anal. Chem.* 54:2108 (1982).
14. R. M. Wightman, M. R. Deakin, P. M. Kovach, W. G. Kuhr, and K. J. Sturts, *J. Electrochem. Soc.* 131:1578 (1984).
15. K. J. Stutts, P. M. Kovach, W. G. Kuhr, and R. M. Wightman, *Anal. Chem.* 55:1632 (1983).
16. I.-F. Hu, D. H. Karweik, and T. Kuwana, *J. Electroanal. Chem.* 188:59 (1985).
17. M. R. Deakin, K. J. Stutts, and R. M. Wightman, *J. Electroanal. Chem.* 182:113 (1985).
18. P. Chen and R. L. McCreery, *Anal. Chem.* 68:3958 (1996).
19. D. T. Fagan, I. Hu, and T. Kuwana, *Anal. Chem.* 57:2759 (1985).

20. M. Poon and P. McCreery, *Anal. Chem.* 58:2745 (1986).
21. R. J. Rice and R. L. McCreery, *Anal. Chem.* 61:1637 (1989).
22. R. J. Rice, N. M. Pontikos, and R. L. McCreery, *J. Am. Chem. Soc.* 112 (1990).
23. S. Ranganathan, T.-C. Luo, and R. L. McCreery, *Anal. Chem.* 71:3574 (1999).
24. D. Tse and T. Kuwana, *Anal. Chem.* 50:1315 (1978).
25. I. F. Hu and T. Kuwana, *Anal. Chem.* 58:3235 (1986).
26. G. N. Kamau, W. S. Willis, and J. F. Rusling, *Anal. Chem.* 57:545 (1985).
27. D. C. Thornton, K. T. Corby, V. A. Spendel, J. Jordan, A. Robbat, D. J. Rutstrom, M. Gross, and G. Ritzler, *Anal. chem.* 57:150 (1985).
28. J. F. Evans and T. Kuwana, *Anal. Chem.* 49:1632 (1977).
29. B. Kazee, D. E. Weisshaar, and T. Kuwana, *Anal. Chem.* 57:2736 (1985).
30. R. S. Nicholson, *Anal. Chem.* 37:1351 (1965).
31. E. Gileadi, N. Tsherniskovski, and M. Babai, *J. Electrochem. Soc.* 119:1018 (1972).
32. J. J. Ruiz, A. Aldaz, and M. Dominguez, *Can. J. Chem.* 56:1533 (1978).
33. S. S. Lord and L. B. Rogers, *Anal. Chem.* 26:284 (1954).
34. A. Rojo, A. Rosenstratten, and D. Anjo, *Anal. Chem.* 58:2988 (1986).
35. D. M. Anjo, M. Kahr, M. M. Khodabakhsh, S. Nowinski, and M. Wanger, *Anal. Chem.* 61:2603 (1989).

36. M. Noel and P. N. Anantharaman, *Analyst* 110:1095 (1985).
37. C. Kozlowski and P. Sherwood, *J. Chem. Soc. Faraday Trans. 1* 81:2745 (1985).
38. K. M. Sundberg, *J. Electrochem. Soc.* 136:434 (1989).
39. G. K. Kiema and M. T. McDermott, *Anal. Chem.* 71:4306 (1999).
40. T. Nagaoka and T. Yashino, *Anal. Chem.* 58:1037 (1986).
41. R. C. Engstrom, *Anal. Chem.* 54:2310 (1982).
42. L. Bodalbhai and A. Brajter-Toth, *Anal. Chem.* 63:1047 (1991).
43. A. L. Bielby, T. A. Sasaki, and H. M. Stern, *Anal. Chem.* 67:976 (1988).
44. A. L. Bielby, T. A. Sasaki, and H. M. Stern, *Anal. Chem.* 67:976 (1995).
45. T. Nagaoka, T. Fukunaga, and T. Yoshino, *Anal. Chem.* 60:2766 (1988).
46. A. L. Beilby and A. Carlsson, *J. Electroanal. Chem.* 248:283 (1988).
47. F. A. Armstrong and K. J. Brown, *J. Electroanal. Chem.* 219:31325 (1987).
48. F. A. Armstrong, A. M. Bond, H. A. O. Hill, B. N. Olive, and I. S. M. Psalti, *J. Am. Chem. Soc.* 111:9185 (1989).
49. P. M. Kovach, M. R. Deakin, and R. M. Wightman, *J. Phys. Chem.* 90:4612 (1986).
50. C. A. McDermott, K. R. Kneten, and R. L. McCreey, *J. Electrochem. Soc.* 140:2593 (1993).

51. N. M. Pontikos and M. R. L., *J. Electroanal. Chem.* 324:229 (1992).
52. R. L. McCreery, K. K. Cline, C. A. McDermott, and M. T. McDermott, *Colloids Surfaces A* 93:211 (1994).
53. R. J. Bowling, R. T. Packard, and R. L. McCreery, *J. Am. Chem. Soc.* 111:1217 (1989).
54. C. Barbero and R. Kotz, *J. Electrochem. Soc.* 140:1 (1993).
55. L. J. Bjelica and J. L. S., *Electrochim. Acta* 37:371 (1992).
56. W. H. Smyrl, R. T. Atanasoski, L. Atanasoska, L. Hartshorn, M. Lien, K. Nygren, and E. A. Fletcher, *J. Electroanal. Chem.* 264:301 (1989).
57. G. Picq, R. Reeves, P. Ribourg, and P. Vennerau, *J. Electroanal. Chem.* 162:225 (1984).
58. K. Morita and Y. Shimizu, *Anal. Chem.* 61:159 (1989).
59. M. S. Freund, A. Brajter-Toth, T. M. Cotton, and E. R. Henderson, *Anal. Chem.* 63:1047 (1991).
60. J. Wang, D. Martinez, R. Yaniv, and L. D. McCormick, *J. Electroanal. Chem.* 278:379 (1990).
61. G. Binnig, H. Rohrer, C. Gerber, and E. Weibel, *Phys. Rev. Lett.* 49:57 (1982).
62. G. Binnig, C. F. Quate, and C. Gerber, *Phys. Rev. Lett.* 12:930 (1986).
63. R. M. Overney, E. Meyer, J. Frommer, D. Brodbeck, R. Lüthi, L. Howard, H.-J. Güntherodt, M. Fujihira, H. Takano, and Y. Gotoh, *Nature* 359:133 (1992).

64. C. D. Frisbie, L. F. Rozsnyai, A. Noy, M. S. Wrighton, and C. M. Lieber, *Science* 265:2071 (1994).
65. J. L. Wilbur, H. A. Biebuyck, J. C. MacDonald, and G. M. Whitesides, *Langmuir* 11:825 (1995).
66. J.-B. D. Green, M. T. McDermott, and L. M. Siperko, *J. Phys. Chem.* 99:10960 (1995).
67. J.-B. D. Green, M. T. McDermott, and M. D. Porter, *J. Phys. Chem.* 100:13342 (1996).
68. T. Han, J. M. Williams, and T. P. J. Beebe, *Anal. Chim. Acta* 307:361 (1995).
69. A. Noy, C. D. Frisbie, L. F. Razsnyai, M. S. Wrighton, and C. M. Lieber, *J. Am. Chem. Soc.* 117:7943 (1995).
70. S. K. Sinnah, A. B. Steel, J. C. Miller, and J. E. Reutt-Robey, *J. Am. Chem. Soc.* 118:8925 (1996).
71. E. W. van der Vegte and G. Hadziioannou, *J. Phys. Chem. B* 101:9563 (1997).
72. D. I. Vezenov, A. Noy, L. F. Rozsnyai, and C. M. Lieber, *J. Am. Chem. Soc.* 119:2006 (1997).
73. D. I. Vezenov, A. Noy, and C. M. Lieber, *Annu. Rev. Mater. Sci.* 27:381 (1997).
74. A. Noy, D. V. Vezenov, and C. M. Lieber, *Annu. Rev. Mater. Sci.* 27:381 (1997).
75. M. O. Finot and M. T. McDermott, *J. Am. Chem. Soc.* 119:8564 (1997).

76. S. N. Magonov, V. Elings, and M.-H. Whangbo, *Surface Science* **375**:L385 (1997).
77. J. Tamayo and R. Garcia, *Langmuir* **12**:4430 (1996).
78. J. Tamayo and R. Garcia, *Appl. Phys. Lett.* **71**:2394 (1997).
79. N. A. Burnham, O. P. Behrend, F. Oulevey, G. Gremaud, P.-J. Gallo, D. Gourdon, E. Dupas, A. J. Kulik, H. M. Pollock, and G. A. D. Briggs, *Nanotechnology* **8**:67 (1997).
80. J. P. Cleveland, B. Anczykowski, A. E. Schmid, and V. B. Elings, *Appl. Phys. Lett.* **72**:2613 (1998).
81. G. Bar, R. Brandsch, and M.-H. Whangbo, *Surf. Sci.* **411**:L802 (1998).
82. R. Garcia, J. Tamayo, M. Calleja, and F. Garcia, *Appl. Phys. A* **66**:S309 (1998).
83. A. Paulo and R. Garcia, *Surf. Sci.* **471**:71 (2001).
84. G. Bar, R. Brandsch, M. Bruch, L. Delineau, and M.-H. Whangbo, *Surf. Sci.* **444**:L11 (2000).
85. D. A. Chernoff, *Proc. Microscop. Microanal.*:888 (1995).
86. A. J. Howard, R. R. Rye, and J. E. Houston, *J. Appl. Phys.* **79**:1885 (1996).
87. P. Leclère, R. Lazzaroni, J. L. Brédas, J. M. Yu, P. Dubois, and R. Jérôme, *Langmuir* **12**:4317 (1996).
88. R. Viswanathan, J. Tian, and D. W. Marr, *Langmuir* **13**:1840 (1997).
89. A. Noy, C. H. Sanders, D. V. Vezenov, S. S. Wong, and C. M. Lieber, *Langmuir* **14**:1508 (1998).

90. K. Sasaki, Y. Koike, H. Azebara, H. Hokari, and M. Fujihara, *Appl. Phys. A* 66:S1275 (1998).

## CHAPTER II

### **Probing Morphological and Compositional Variations of Anodized Glassy Carbon Electrodes with Tapping-Mode Scanning Force Microscopy \***

#### **Introduction**

The work presented in this chapter will demonstrate the application of tapping mode scanning force microscopy (TM SFM) for the compositional mapping of electrochemically modified glassy carbon (GC) electrodes. The motivation of this work stems from a previous study in our laboratory that noted phase contrast TM SFM is more precise in generating compositional maps of rough surfaces compared to the widely utilized contact-mode SFM [1]. This is because the intermittent contact between the tip and sample in TM SFM significantly reduces lateral forces experienced by the tip.

The ability to rationally design electroanalytical devices hinges largely on the capacity to characterize interfaces compositionally. In many cases, the development of an analytical electrode involves modification of its surface at the molecular level [2-4]. A powerful approach for the characterization of modified electrodes involves combining techniques that probe surface architecture at both macroscopic and microscopic length scales. Traditionally, electrochemical techniques as well as spectroscopic methodologies have been employed to provide a spatially averaged picture of

---

\*A form of this Chapter has been published in *Anal. Chem.*, 1999, 71, 4306-4312

electrode surface structure. More recently, the ultra- high resolution of scanning probe microscopy (SPM) has been exploited to provide molecular-scale descriptions [4].

As reviewed in Chapter I, electrochemical pretreatment (ECP) has been widely employed to activate the surface of carbon electrodes towards a variety of redox systems [5-13]. Although ECP is a facile and flexible modification scheme, its effect on the morphology and surface architecture of GC has not been thoroughly explored. A few microscopic studies have reported on changes in topography and surface roughness following ECP [14-18]. The present work is focused on applying compositionally sensitive contrast mechanism in SFM to characterize compositional changes induced on GC upon ECP and to assess the ability of TM SFM to perform this analysis. In this Chapter, electrochemical measurements and TM SFM images are correlated to track both topographic and compositional variations in GC induced by ECP in acidic and basic media. Results obtained in this study show that phase contrast TM SFM is able to differentiate between oxidized GC and the original polished surface on patterned electrodes. These results illustrate that TM SFM is able to map compositionally relatively rough, polished electrode surfaces.

## **Experimental**

**Reagents.**  $\text{Ru}(\text{NH}_3)_6^{3+}(\text{aq})$  in 1 M KCl and  $\text{Fe}(\text{CN})_6^{4-}(\text{aq})$  in 1 M KCl solutions were prepared at 1 mM concentrations from  $\text{Ru}(\text{NH}_3)_6\text{Cl}_3$  (Strem Chemicals) and  $\text{K}_4\text{Fe}(\text{CN})_6$  (BDH Chemicals) respectively.  $\text{Eu}^{3+}(\text{aq})$  in 0.2 M

$\text{NaClO}_4$  solution was prepared at 5 mM concentrations from  $\text{Eu}(\text{NO}_3)_3 \cdot 5\text{H}_2\text{O}$  (Aldrich). All reagents were used as received. Aqueous solutions were prepared using distilled/deionized (18 M $\Omega$ /cm) water (Barnstead, Dubuque, IA) and purged with nitrogen gas for 10 min. prior to use.

**Electrode Preparation and Electrochemical Measurements.** The GC-20 electrodes (Tokai GC-20, Electrosynthesis Corp., NY) were prepared by polishing with successive slurries of 1.0, 0.3 and 0.05  $\mu\text{m}$  alumina (Buehler) in distilled/deionized water on polishing microcloth (Buehler). The GC electrodes were sonicated for 10 min. between polishing. Polished GC electrodes were patterned by using standard photoresist-based microfabrication techniques (Figure 2.1). The HPR 504 photoresist (OCG Chemicals) was spin-coated on a polished GC surface. The substrate (coated GC electrode) was illuminated through a copper grid mask (Pelco, CA) with UV light (~405 nm) and then developed with Shipley 354 developer. This produced an electrode with masked and unmasked regions. Electrochemical pretreatment was achieved by poisoning a polished electrode at +1.80 V for a selected period of time in either acidic electrolyte (1.0 M  $\text{H}_2\text{SO}_4$ ) or basic solution (0.1 M NaOH) as illustrated in Figure 2.2. A three-electrode cell was used with a Ag/AgCl reference electrode and a Pt wire counter electrode. The cell was connected to a Model 175 (Princeton Applied Research, NJ) potentiostat. Electrochemically treated GC electrodes were sonicated in

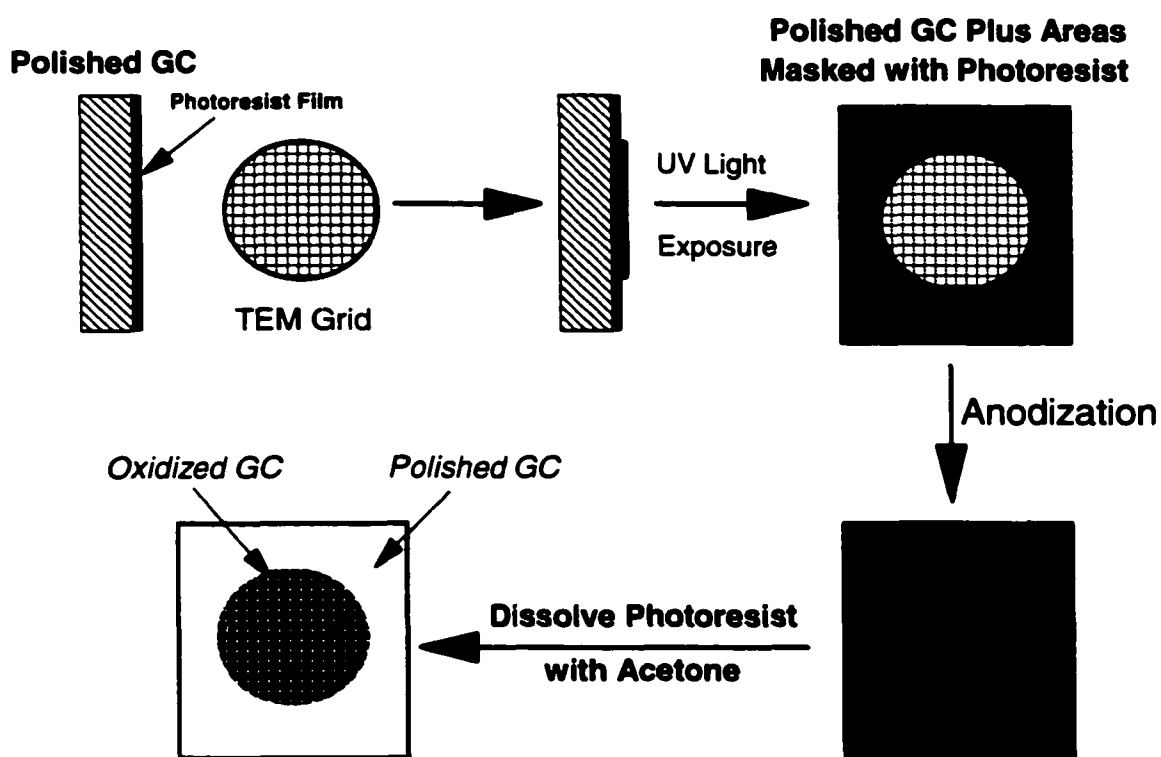
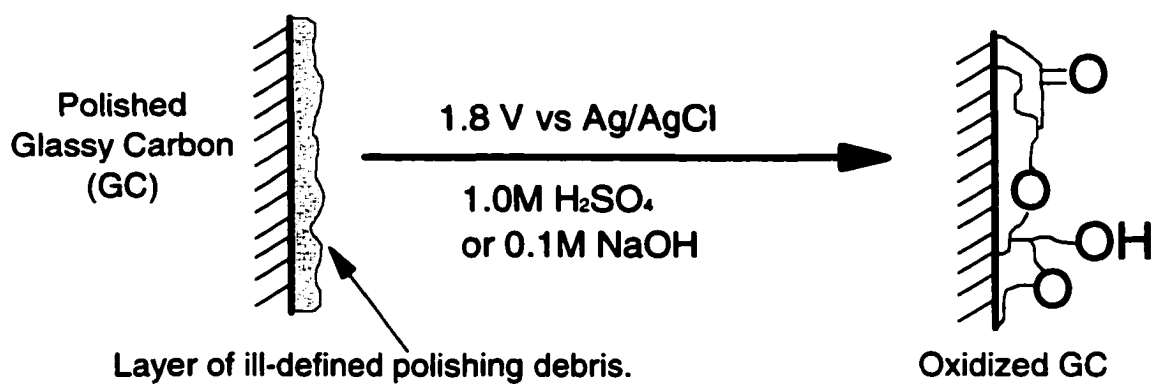


**Figure 2.1:** Scheme illustrating standard photoresist-based microfabrication techniques utilized to create patterned GC electrode surfaces.



### Potential Program

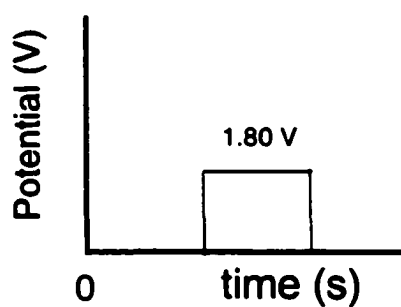


**Figure 2.2:** Scheme illustrating electrochemical conditions employed to activate the polished GC electrodes

acetone for 10 min. to remove the mask. Cyclic voltammetry was performed at a scan rate of 0.1 V/s. Differential capacitance was determined using a 100 Hz, 20 mV peak-to-peak triangle wave centered at 0.0 V. The peak-to-peak current of the output waveform is proportional to the capacitance [19] as described in Chapter I.

**Control Experiments.**  $\text{Fe}(\text{CN})_6^{3-/4-}(\text{aq})$  was used as a probe to assess the removal of the photoresist mask upon sonication of the ECPed GC electrode in acetone. Polished GC electrodes were coated with photoresist followed by sonication in acetone for 10 min. and then allowed to air dry. The cyclic voltammetric peak separation ( $\Delta E_p$ ) for  $\text{Fe}(\text{CN})_6^{3-/4-}(\text{aq})$  was then measured and found to be similar to values obtained on freshly polished GC electrodes. The charge under  $\text{Fe}(\text{CN})_6^{3-/4-}$  voltammetric reduction wave was also found to be similar to that obtained on freshly polished GC electrodes. These results imply that acetone is effective in completely removing the mask without altering the electrochemical reactivity. Similar electrochemical characterization was performed to establish whether acetone affected the graphitic oxide layer formed upon activation of polished GC in 1.0 M  $\text{H}_2\text{SO}_4$ .  $\Delta E_p$  values for  $\text{Eu}^{2+/3+}(\text{aq})$  were found to be similar on oxidized GC electrodes before and after sonication in acetone. These results indicate that sonication in acetone does not significantly alter the graphitic oxide layer formed upon anodization.

**Nanoindentation Studies.** Nanoindentation experiments were performed with a Triboscope® (Hysitron Inc) nanomechanical-testing instrument interfaced to a Digital Instrument (Santa Barbara, CA) Dimensions 3000 scanning probe microscope controller allowing *in situ* imaging of the sample before and after an indent. Indents were performed with a cube corner diamond tip (Hysitron Inc) at a force of  $\sim 100 \mu\text{N}$  and a loading rate of  $10 \mu\text{N} / \text{sec}$ . The radius of curvature of the tip is approximately 178 nm. Many different regions of each sample were analyzed. A more detailed discussion on nanoindentation curves is presented below.

**SFM Conditions.** TM SFM images were obtained in air using Nanoscope III (Digital Instruments, Santa Barbara CA). Si cantilevers were oscillated at their resonance frequency ( $\sim 300 \text{ kHz}$ ). Scanning was carried out with a constant amplitude of oscillation. An important parameter in TM SFM phase contrast imaging is the ratio of the set point (or imaging) amplitude,  $A_{sp}$ , to the free oscillation amplitude,  $A_o$  where  $r_{sp} = A_{sp}/A_o$  [20]. This ratio governs the tapping force between the tip and the sample. All images shown here were collected with  $r_{sp}$  between 0.55 to 0.65 (moderate tapping force). The imaging scan rate was between 0.5 and 1.0 Hz. The images presented here are representative of many images taken at different points on each sample. All topographic and phase contrast images presented in this study were collected simultaneously. Force curves were collected at a scan rate of 9.77 Hz. The cantilever deflection signal in volts was converted to nm by dividing

by detector sensitivity (0.18 V/nm). A more detailed discussion on force curves is presented below.

## Results and Discussion

**Electrochemical characterizations of ECPed GC.** Studies of electrochemically pretreated GC electrodes have provided evidence that this procedure alters surface composition [21]. As noted earlier in Chapter I, ECP in acidic solutions produces a surface film termed electrochemical graphitic oxide (EGO) [22, 23] which is found to be porous, hydrated and nominally anionic [22]. Anodization of GC in basic solutions produces interfacial carbon-oxygen functionalites [24] but does not result in an EGO film [9, 10]. Although the effect of ECP on electrochemical parameters has been documented before, several electrochemical characterizations of polished GC surfaces after ECP have been carried out in this research to track compositional changes and to correlate with TM SFM results. These data are listed in Tables 2.1 and 2.2. Table 2.1 provides results from electrochemical and TM SFM characterizations of polished GC surfaces oxidized in 1.0 M H<sub>2</sub>SO<sub>4</sub>. The cyclic voltammetric peak separations ( $\Delta E_p$ ) for three redox systems (Ru(NH<sub>3</sub>)<sub>6</sub><sup>2+/3+</sup>, Fe(CN)<sub>6</sub><sup>3-/4-</sup>, and Eu<sup>2+/3+</sup>) were utilized to assess the changes in ET reactivity induced by ECP for various anodization timescales.

ECP of GC in H<sub>2</sub>SO<sub>4</sub> affects the ET for Fe(CN)<sub>6</sub><sup>3-/4-</sup> and Ru(NH<sub>3</sub>)<sub>6</sub><sup>2+/3+</sup> in opposite ways. The trends in Table 2.1 likely reflect an electrostatic effect resulting from the formation of an anionic EGO film causing  $\Delta E_p$  for the

Oxidation Time ( s )	$\Delta E_p$ (mV) <sup>a</sup>			$C^o$ ( $\mu\text{F}/\text{cm}^2$ ) <sup>b</sup>	$\Delta\phi$ (degrees)
	$\text{Fe}(\text{CN})_6^{3-/4-(b)}$	$\text{Ru}(\text{NH}_3)_6^{3+/2+(b)}$	$\text{Eu}^{3+/2+(c)}$		
Polished	$82 \pm 13$	$82 \pm 8$	$265 \pm 35$	$41 \pm 10$	—
30	$85 \pm 4$	$78 \pm 4$	$130 \pm 9$	$99 \pm 8$	$5.4 \pm 1.4$
60	$94 \pm 3$	$69 \pm 4$	$105 \pm 5$	$128 \pm 7$	$7.7 \pm 1.6$
90	$100 \pm 4$	$65 \pm 3$	$80 \pm 6$	$140 \pm 7$	$10.2 \pm 1.9$

a.  $v = 100$  mV/s for all systems

b. 1 M KCl

c. 0.2 M HClO<sub>4</sub>

d. Statistics based on  $N = 6$  for both  $\Delta E_p$  and  $C^o$ , and  $N = 4$  for  $\Delta\phi$

**Table 2.1:** Results from electrochemical and TM SFM characterizations of polished GC electrodes electrochemically pretreated at 1.8 V in 1.0M H<sub>2</sub>SO<sub>4</sub>.

Oxidation Time ( s )	$\Delta E_p$ (mV) <sup>a</sup>			$C^\circ$ ( $\mu\text{F}/\text{cm}^2$ ) <sup>a</sup>	$\Delta\phi$ (degrees)
	$\text{Fe}(\text{CN})_6^{3-/4-(b)}$	$\text{Ru}(\text{NH}_3)_6^{3+/2+(b)}$	$\text{Eu}^{3+/2+(c)}$		
Polished	$82 \pm 13$	$82 \pm 8$	$265 \pm 35$	$41 \pm 10$	—
30	$82 \pm 5$	$83 \pm 7$	$223 \pm 17$	$80 \pm 11$	$6.3 \pm 1.3$
60	$83 \pm 4$	$81 \pm 6$	$184 \pm 19$	$101 \pm 9$	$8.1 \pm 1.5$
120					$12.2 \pm 1.6$

a.  $v = 100$  mV/s for all systems

b. 1 M KCl

c. 0.2 M  $\text{NaClO}_4$

d. Statistics based on  $N = 6$  for both  $\Delta E_p$  and  $C^\circ$ , and  $N = 4$  for  $\Delta\phi$

**Table 2.2:** Results from electrochemical and TM SFM characterizations of polished GC electrodes electrochemically pretreated at 1.8 V in 0.1M NaOH.

negatively charged  $\text{Fe}(\text{CN})_6^{3-/4-}$  system to increase slightly with oxidation time and decrease for  $\text{Ru}(\text{NH}_3)_6^{2+/3+}$ . For  $\text{Eu}^{2+/3+}$ , Table 2.1 shows a significant decrease in  $\Delta E_p$  with oxidation time. This dependence is consistent with reports that show ET for aquated metal ion systems like  $\text{Eu}^{2+/3+}$  is governed by surface carbon-oxygen groups at carbon electrodes [25]. Table 2.1 also shows a drastic increase in differential capacitance ( $C^0$ ) with oxidation time probably due to the combination of redox active functional groups produced by ECP and the increased porosity and anionic character of the resulting film. These electrochemical results point to the increasing growth of an anionic EGO layer with ECP time and are consistent with those from previous studies [22].

Similar electrochemical characterizations were performed on GC electrodes anodized in 0.1 M NaOH. The trends shown in Table 2.2 indicate that ECP in basic media has little effect on ET for  $\text{Fe}(\text{CN})_6^{3-/4-}$  and  $\text{Ru}(\text{NH}_3)_6^{2+/3+}$  for the oxidation times investigated. In addition, although oxidation in NaOH induces an overall decrease in  $\Delta E_p$  for  $\text{Eu}^{2+/3+}$ , the effect for similar modification time is significantly less than ECP in acidic solution (Table 2.1). A similar observation is made for the trend in  $C^0$ . These results are all consistent with the generation of surface oxygen functionalities in the absence of an EGO film. Overall, the results from electrochemical characterizations listed in Tables 2.1 and 2.2 illustrate the influence of ECP in acidic and basic solutions on electrochemical reactivity of GC.

**TM SFM imaging of ECPed GC.** Initial efforts in tracking ECP induced transformations of GC surfaces with TM SFM proved problematic due to the similarity between the oxidized surface and the original polished electrode. This is illustrated in Figure 2.3, which contains  $40 \times 40 \mu\text{m}$  topographical TM SFM images of polished GC (Figure 2.3-A) and polished GC anodized for 2 min. in 1.0 M  $\text{H}_2\text{SO}_4$  (Figure 2.3-B) and in 0.1 M NaOH (Figure 2.3-C). The morphology shown in these images is similar to that noted in previous studies of polished GC where the main features are polishing scratches [18, 23, 26]. Overall, these three surfaces appear qualitatively similar and require identical height scales. Images collected employing a range of  $r_{\text{sp}}$  from 0.8 (low tapping force) to 0.2 (high tapping force) do not appear substantially different from those in Figure 2.3. However, features in Figure 2.3-C do appear more defined and “focused”. This is a general observation for GC surfaces oxidized in 0.1 M NaOH and is discussed in more detail below.

The lack of a clear differentiation among the GC surfaces studied prompted the need to develop an electrode preparation method that would permit the direct comparison of oxidized and non-oxidized regions in the same image. Preselected regions of polished GC electrodes can be masked from the ECP procedure by employing standard integrated circuit patterning techniques (Figure 2.1). Electrochemical oxidation is then restricted to areas patterned into a layer of photoresist. Dissolution of the photoresist mask after anodization yields a GC surface with adjacent oxidized and polished regions that can then be differentiated within the same image. Figure 2.4 contains

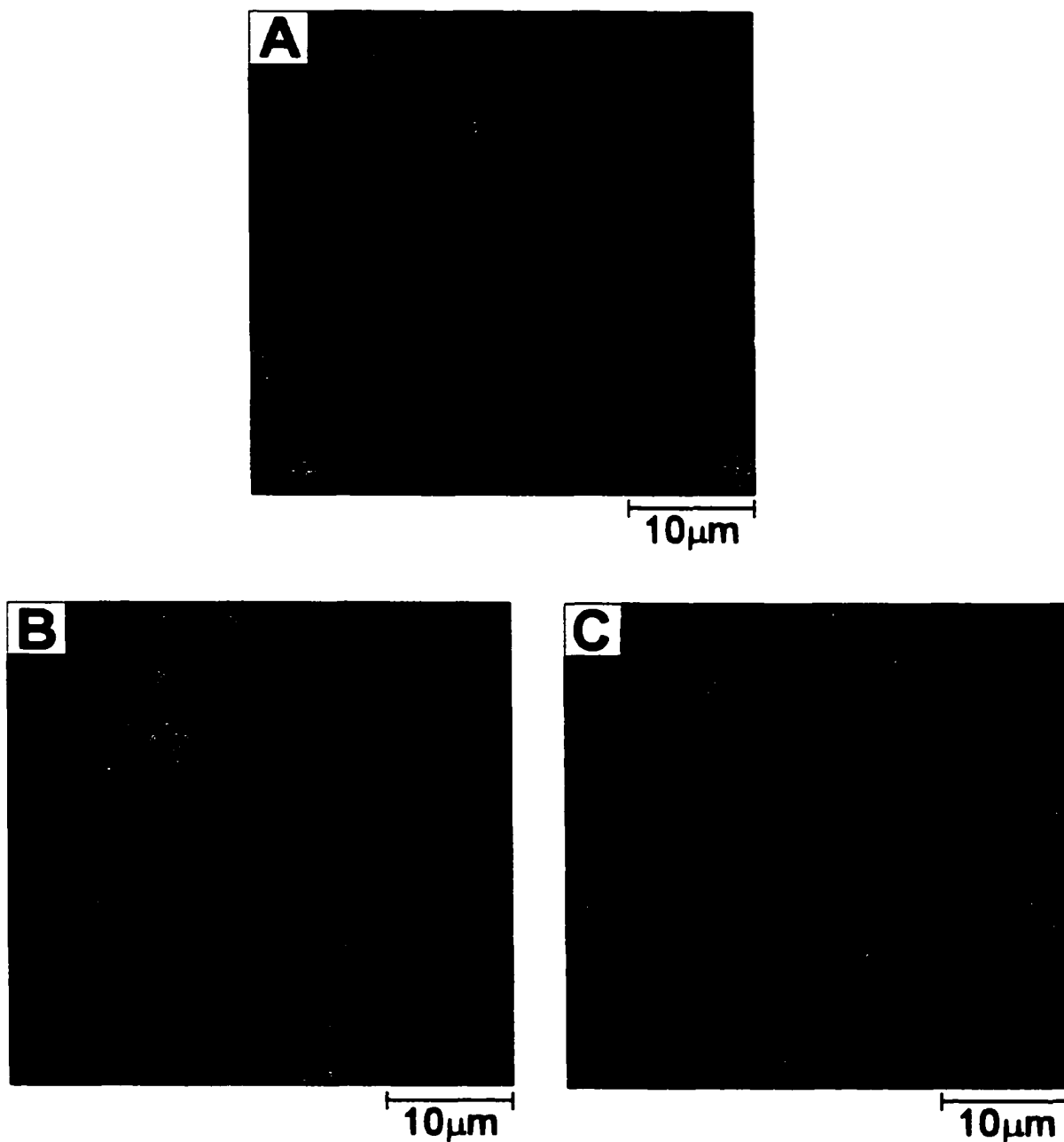


**Figure 2.3:** 40 x 40  $\mu\text{m}$  TM SFM topographic images of polished GC (Figure 1A), acid oxidized polished GC (Figure 1B), and base oxidized polished GC (Figure 1C). Z-scale = 55nm for all the images.

56 × 56 μm TM SFM images of a GC electrode prepared in this way and oxidized in 1.0 M H<sub>2</sub>SO<sub>4</sub> at 1.8 V for 90 s. Note from Table 2.1 that this pretreatment has a large effect on electrochemical reactivity implying the generation of an EGO film.

Figure 2.4-A shows that ECP in H<sub>2</sub>SO<sub>4</sub> induces minor morphological changes in the GC surface. Several rings of raised topography are apparent which are located at the boundary that existed between the exposed GC and the photoresist mask. These rings are not residual photoresist and are likely due to an enhanced oxidation at this boundary. The areas inside and outside the rings appear qualitatively similar with polishing scratches traversing the modified regions uninterrupted. In fact, if the rings outlining the pattern boundary were not present, the location of the oxidized regions would not be discernible in topographic TM SFM images. All topographic images obtained do not show any evidence for a distinct EGO layer in any of the topographic images including those from surfaces oxidized for 5 min. In general, a morphology similar to Figure 2.4-A is observed for oxidation periods from 10 s to 5 min. at 1.8 V.

Significant differentiation between oxidized and non-oxidized GC is observed in the phase image of Figure 2.4-B. In this image, the circular regions that were exposed to the ECP procedure through the mask exhibit brighter contrast relative to the unmodified, polished GC. At resonance, the phase of the cantilever lags the driver signal by 90 degrees. This phase lag is mapped to 0 degrees via the Nanoscope software before imaging. This

allows measurement of phase shift relative to the resonant peak. The phase measurement obtained from the Nanoscope III is actually the cosine of the phase angle and not the actual angle. The cosine of phase is expressed in Bocek degrees and is proportional to the actual phase. The relationship between real degrees and Bocek degrees is given by the expression:

$$\text{Real degrees} = A \cos (\text{Bocek degrees}/90) \quad \{2.1\}$$

where  $A$  is the amplitude of the driver signal.

Thus, phase contrast in Figure 2.4-B reflects differences in the phase lag of the oscillating cantilever/tip assembly with a greater phase lag manifested as darker contrast. The oxidized regions in Figure 2.4-B exhibit a phase lag that is  $\sim 10$  degrees less than the polished regions. Qualitatively, the observed phase lag difference ( $\Delta\phi$ ) can be interpreted as differences in cantilever energy dissipation resulting from variations in tip-sample interactions as discussed in Chapter I. Thus, it can be inferred that the  $\Delta\phi$  observed between the polished and oxidized regions in Figure 2.4-B is due to an ECP induced transformation of the GC surface architecture. A more detailed mechanism of the observed phase lag differences is presented below.

Along with the electrochemical data in Table 2.1 are listed  $\Delta\phi$  values measured at patterned electrodes after oxidation in 1 M  $\text{H}_2\text{SO}_4$ . The magnitude of  $\Delta\phi$  directly tracks oxidation, time arguing that the compositional change induced by ECP proceeds with continued oxidation. This is supported by the correlation between the trend in  $\Delta\phi$  and the changes in the

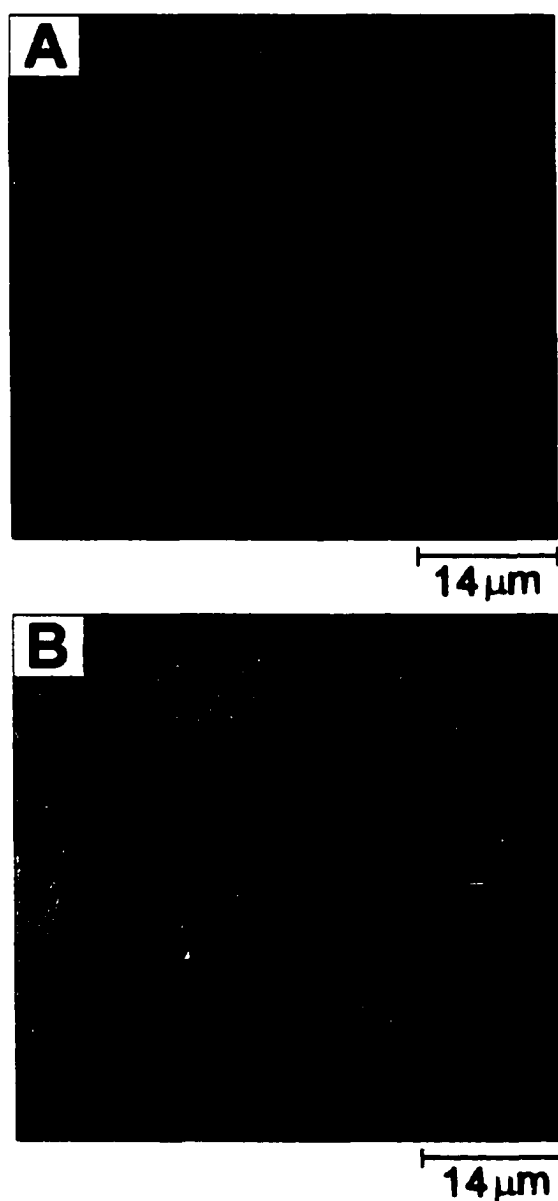


**Figure 2.4:** 56 x 56  $\mu\text{m}$  TM SFM images of a GC surface oxidized at 1.8 V in 1 M  $\text{H}_2\text{SO}_4$  for 90 s. (A) Topography (z-scale = 60 nm). (B) Phase contrast (z-scale = 40 deg).

electrochemical parameters. These observations demonstrate the utility of phase contrast TM SFM for tracking compositional changes of modified carbon electrodes.

Relative to ECP in acidic solutions, surprising morphological changes are noted for polished GC electrodes oxidized in 0.1 M NaOH. Parts A and B of Figure 2.5 are  $100 \times 100 \mu\text{m}$  topographic and phase contrast TM SFM images highlighting these changes. Contained in Figure 2.5-A are a series of  $15 \mu\text{m}$  wide depressions corresponding to areas that were exposed to oxidation at 1.8 V for 1 min. From the cross-sectional profile, the measured depth of the depressions is  $235 \pm 10 \text{ nm}$  for a 1 min. oxidation period. The flat profile of the bottom of the depressions in the cross-section indicates that the SFM tip is probing the entire depth of the depressions. However, little information is available with respect to the sides of the depressions due to inability of the pyramidal tip to probe steep walls. The directionality of the etching process is probed further in Chapter IV.

It is clear from Figure 2.5-A that ECP in 0.1 M NaOH at 1.8 V removes a significant amount of carbon material from the GC surface. Although electrochemical etching of GC in basic solutions has not been directly explored in the literature, a similar process has been noted for anodized carbon fibers [24], carbon black [27], and pyrolytic carbon films deposited on GC [28]. Ross and coworkers have analyzed the anodic reaction products formed following dissolution of carbon black in alkaline solution [27]. The

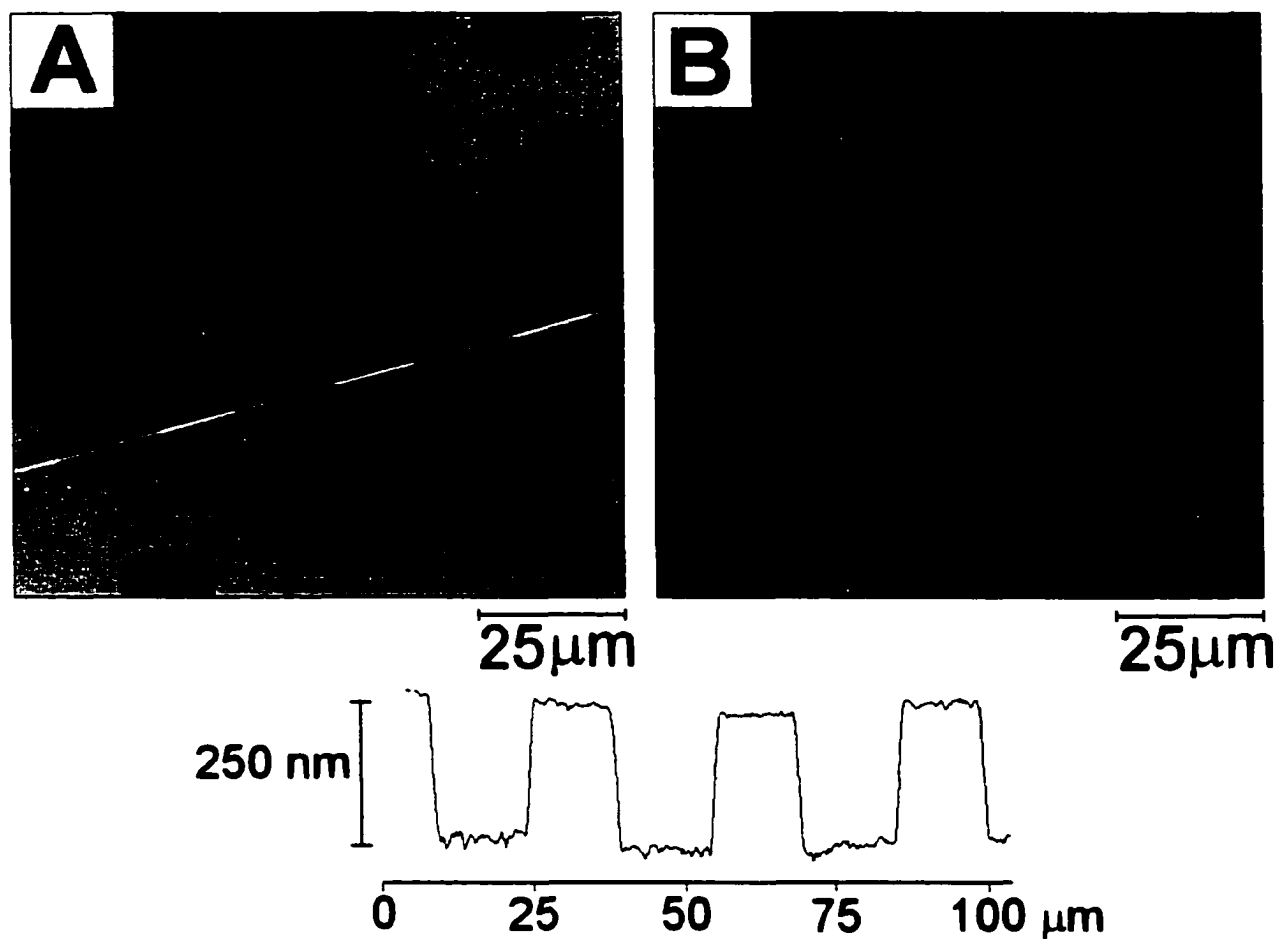
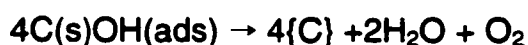


**Figure 2.5:** 100 x 100  $\mu\text{m}$  TM SFM images of a GC surface oxidized at 1.8 V in 0.1 M NaOH for 60 s. (A) Topography ( z-scale = 350 nm). (B) Phase contrast ( z-scale = 40 deg). The cross-sectional profile corresponds to the line traversing the topographic image.

authors used  $^{14}\text{C}$ -labeled carbon black and established that  $\text{O}_2$ ,  $\text{CO}$  and  $\text{CO}_2$  gaseous products were formed. Results from this study also indicated the formation of carbonate ions in solution as proposed by the following equation:



Sherwood and coworkers proposed the following processes to account for the breakup of carbon fiber lattice as well as evolution of oxygen gas during anodic treatment in sodium hydroxide:



where  $\text{C(s)}$  implies an intact carbon lattice and  $\{\text{C}\}$  indicates carbon material removed from the substrate [24]. In this study, a gas is also evolved during oxidation of GC in base which, when combined with the etching apparent in Figure 2.5, implies that the above processes effectively describe electrochemical oxidation of GC in 0.1 M NaOH at 1.8 V. The effectiveness of electrochemical oxidation for micromachining GC substrates is examined in Chapter IV.

The ability of phase contrast TM SFM to map changes in GC surface composition induced by ECP is again illustrated in Figure 2.5-B. Similar to ECP in acid (Figure 2.4-B) the polished GC exhibits a greater phase lag (darker contrast) than GC oxidized in 0.1 M NaOH. The  $\Delta\phi$  values listed in Table 2.2 track  $\Delta E_p$  for  $\text{Eu}^{+2/+3}$  and  $\text{C}^0$ , implying that ECP in base influences both phase contrast and electrochemical reactivity. Taken together, the

images in Figures 2.4 and 2.5 show the power of TM SFM for monitoring both morphological and compositional variations at modified GC electrodes.

**Mechanism of phase contrast in TM SFM images of masked GC electrodes following ECP.** As stated earlier in Chapter 1, several modeling efforts have been directed towards predicting factors that influence phase contrast in TM SFM [20, 28-34]. The interactions between the tip and surface that damp the cantilever oscillation are thought to be responsible for the observed phase lags in TM SFM [29, 33]. Surface parameters that can affect energy dissipative interactions include mechanical properties (*e.g.* viscoelasticity and plastic deformation) and adhesion hysteresis.

Although the surface composition of GC electrodes following ECP in acidic solutions varies significantly from that due to ECP in base, the direction of phase contrast and the overall trend of  $\Delta\phi$  with oxidation time is similar for both media. This argues that the observed contrast in images consisting of both polished and oxidized regions is dominated by the interaction of the SFM tip with the polished portion of the electrode. It follows that phase contrast is generated because ECP in both media removes or transforms the ubiquitous polishing layer.

The darker contrast observed at the polished regions of the segregated electrodes reflects a greater phase lag and implies that more cantilever energy is dissipated at these areas. There is no observable variation in surface topography or phase contrast during repeated imaging of a single area and thus it is believed that plastic deformation of the GC surface is

negligible. Further experiments were performed with the aim of identifying the surface parameter(s) that govern observed phase contrast. Towards this end, adhesion measurements between a  $\text{Si}_3\text{N}_4$  tip and GC surfaces were made, as well as measurements of the nanomechanical properties of the GC surfaces under investigation. These studies are discussed below.

SFM can be used to measure the long-range attractive or repulsive forces between the tip and the sample surface. This is accomplished by monitoring the cantilever deflection as the tip is brought to contact with the sample surface and also as it is pulled away from the surface. The piezoelectric scanner controls the position of the sample. A force curve is generated by plotting the z-position of the scanner versus the deflection of the cantilever. The cantilever deflection is initially expressed in detector voltage (volts). This voltage can be converted to distance (nm) by dividing by the detector sensitivity (in V/nm). Finally, the force at the tip-sample junction can be determined by multiplying the deflection distance by the cantilever force constant,  $k^0$  (nN/nm).

Figure 2.6 is an example of a force curve. The flat line from point 1 to 2 represents the approach part of the force curve where the tip is above the surface and thus no cantilever deflection. As the sample surface continues to approach the tip, attractive forces acting between the tip and surface pull the tip into contact resulting in the dip at point 2. Once the physical contact is established, further upward movement of sample surface results in a repulsive tip-sample interaction that causes the cantilever to bend. At this

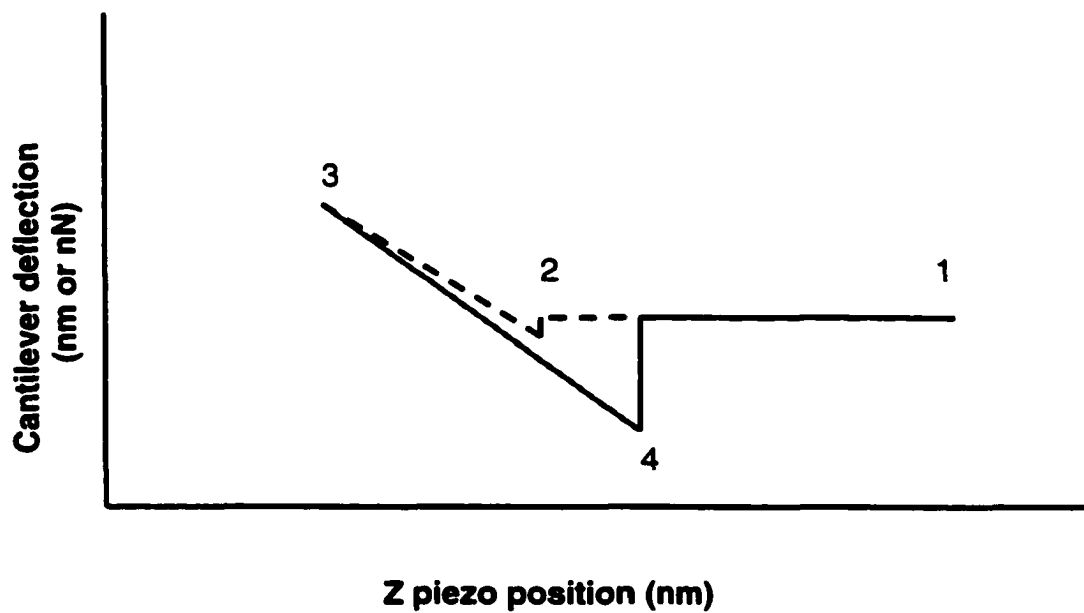


**Figure 2.6:** Example of a force–distance curve. Dotted section of the curve is the forward (approach) and solid section is the reversal (retraction) of the sample movement from the tip.

region (slanting dotted line) the cantilever deflection is proportional to the sample surface height. On the reverse scan (solid line) adhesion between the tip and sample would require the sample to be retracted further to pull the tip off the surface (adhesion hysteresis). At point 4 the tip is pulled off the surface and is referred to as the breakaway point (at breakaway voltage). Beyond this point the deflection signal springs back to the level seen at the start of the approach. The magnitude of the adhesion hysteresis is determined from the differences between breakaway force and jump-to-contact force.

Figures 2.7 and 2.8 show force curves obtained between the  $\text{Si}_3\text{N}_4$  tip and the GC surfaces studied. Values of adhesion hysteresis, measured as described in the above section are provided in Table 2.3. The force curves yield the following trend in adhesion hysteresis: base oxidized  $\approx$  polished < acid oxidized. The similarities in adhesion hysteresis between polished GC and base oxidized GC surfaces (Figure 2.7), imply that the observed contrast does not derive from adhesion hysteresis and originates from surface variables (*e.g.* from differences in mechanical properties). To verify this, nanomechanical properties of the three GC surfaces were probed.

Figure 2.9 illustrates the indentation behavior of base anodized GC (curve a) and polished GC (curve b). An indentation experiment involves engaging a sharp tip into a sample with a known force and simultaneously measuring the displacement of the tip into the sample. The load–displacement curves are usually obtained at a constant loading and unloading

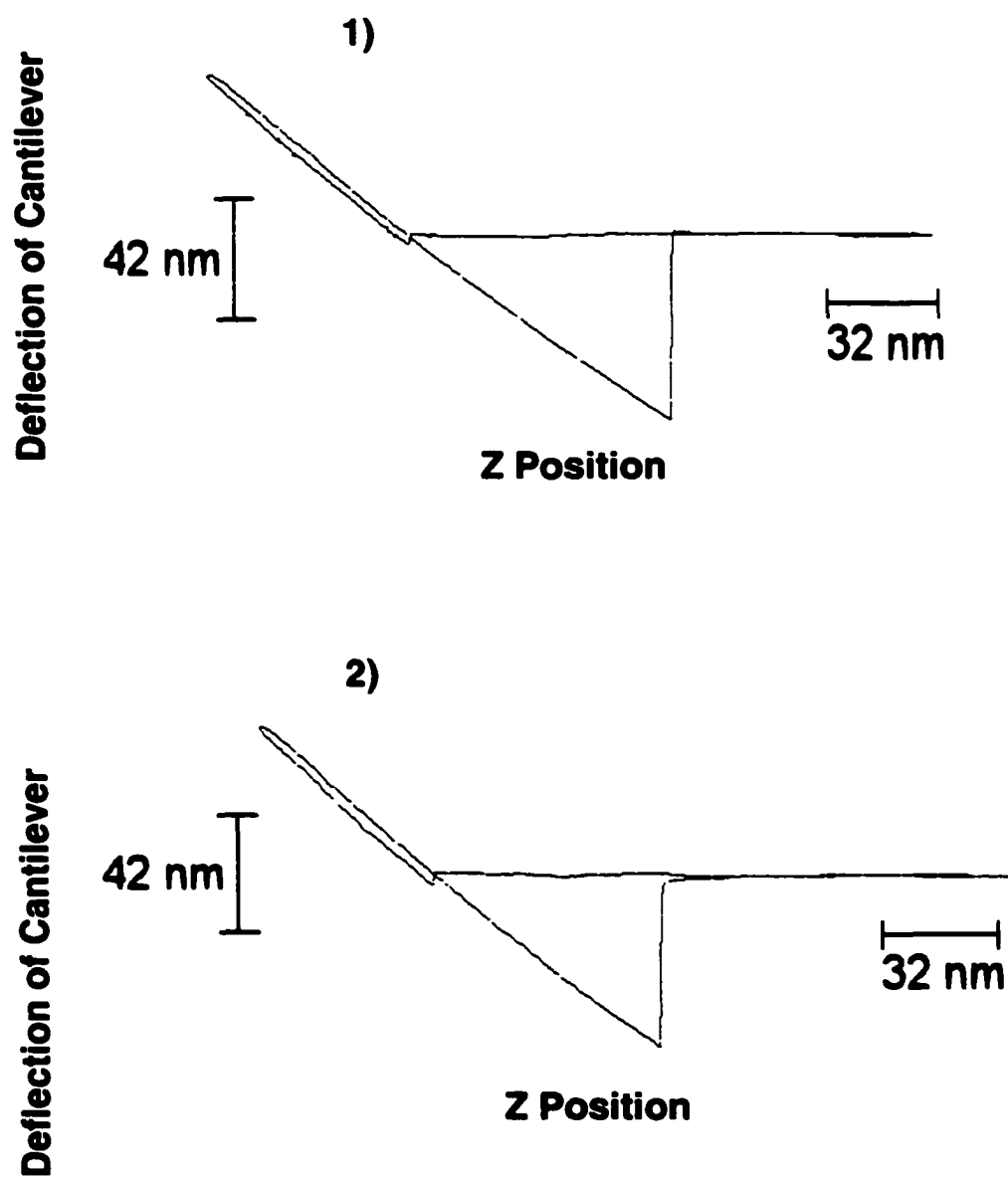


**Figure 2.7:** Force-distance curves obtained on 1) Polished GC and 2) Polished GC ECPed in base.

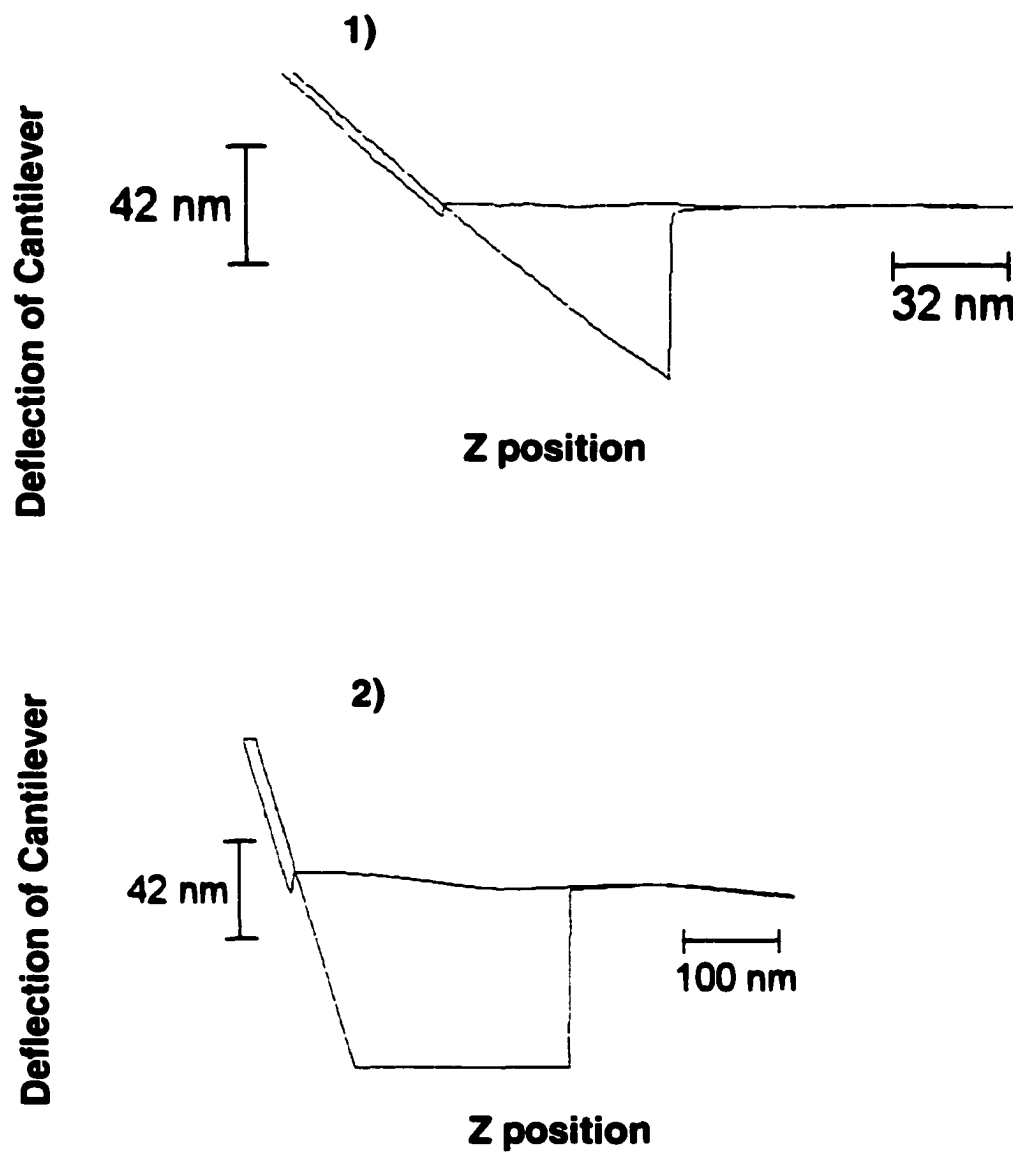


**Figure 2.8:** Force-distance curves obtained on 1) Polished GC and 2) Polished GC ECPed in acid.

GC Surface	Adhesion Hysteresis (nN)	Reduced Modulus, $E_r$ (GPa)
Polished	$8.6 \pm 1.8$	$18.2 \pm 2.1$
Base Oxidized	$8.6 \pm 0.8$	$28.1 \pm 1.2$
Acid Oxidized	$34 \pm 3$	$24.3 \pm 1.4$

Statistics based on  $N = 50$  for adhesion and  $N = 5$  for reduced modulus.

**Table 2.3:** Results from Adhesion Hysteresis and Nanoindentation Characterizations of polished GC surfaces ECPed at 1.8 V in acidic and basic media.

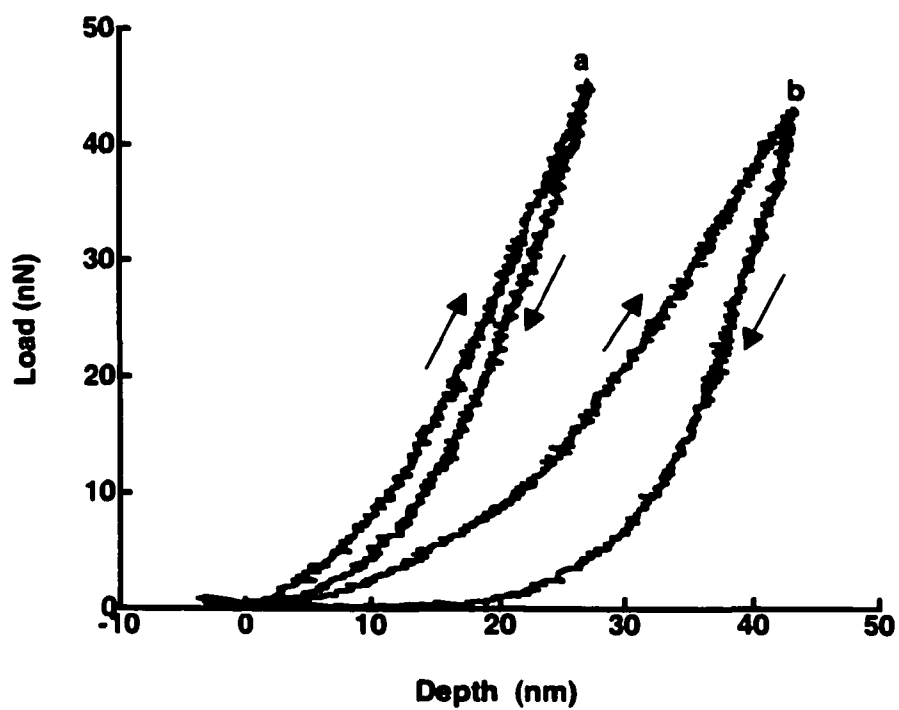


**Figure 2.9 :** Indentation curves obtained on polished GC oxidized in base (curve a) and polished GC (curve b). The arrows show the loading and unloading directions.

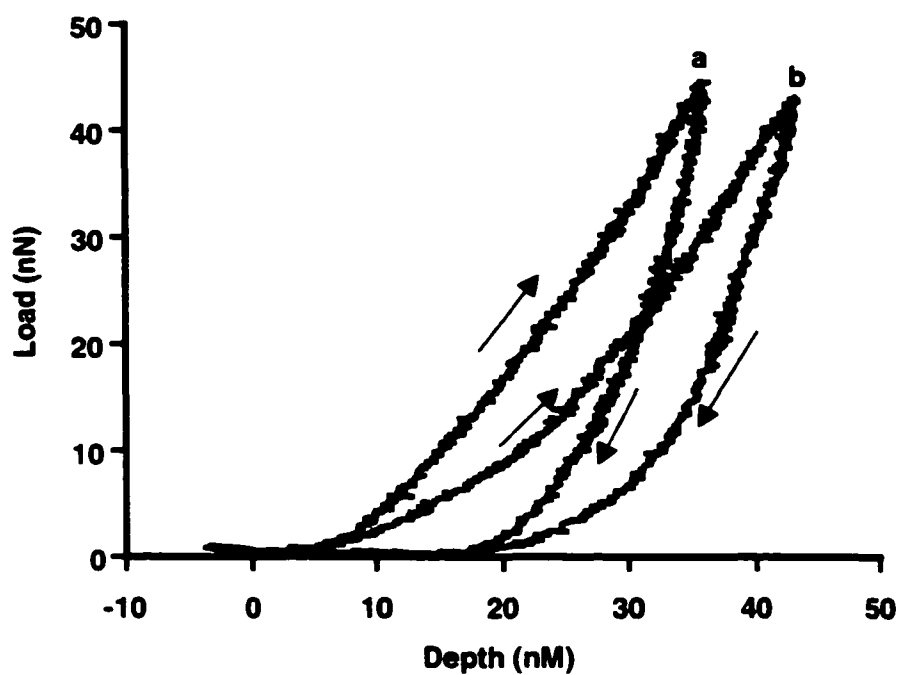


**Figure 2.10 :** Indentation curves obtained on polished GC oxidized in acid (curve a) and polished GC (curve b). The arrows show the loading and unloading directions.

rate. The initial unloading portion of the load-displacement curve (*i.e.* at maximum contact depth), represents purely elastic recovery. The slope of this unloading segment,  $S$ , is a measure of the material stiffness, and may be used to determine the reduced elastic modulus,  $E_r$  [35]. The elastic (indentation) modulus,  $E_r$ , is calculated from the slope,  $S$ , of the unloading portion of the load-displacement curve via the expression:

$$E_r = \frac{S}{2} \sqrt{\frac{\pi}{A}} \quad \{2.2\}$$

where  $A$  represents known geometric contact area of the indenter with the sample. From the indentation modulus, the elastic modulus,  $E$ , of the sample may be calculated for cases where the Poisson's ratio,  $\nu$ , is known ( $E_r = E/(1-\nu^2)$ ).  $E_r$  gives a good estimation of  $E$  for cases where  $\nu$  is unknown [36]. Table 2.3 list values of indentation modulus obtained for the GC surfaces studied.

Figure 2.9 shows that the indentation depth for a given load is larger on the polished GC reflecting a softer surface material than the base oxidized surface. Indentation modulus value obtained on polished GC was ~18.2 Gpa and is comparable to that reported [38]. Indentation modulus value measured on a base oxidized GC surface was ~28.1 GPa. These values are consistent with a softer surface material for polished GC. It is reasonable to believe that an amorphous polishing layer consisting of water, polishing debris, and carbon microparticles [23] would be mechanically soft and thus exhibit lower

elastic modulus. The elastic moduli listed in Table 2.3 are in the range where modest changes in viscosity or changes in elastic modulus at constant viscosity will induce significant differences in cantilever phase lag [29, 34]. TM SFM images reported here were collected in air where the surfaces of Si tip and GC electrodes studied are covered with a thin layer of water. The capillary forces acting between the Si tip and GC surfaces may mask the sensitivity of the tip towards detecting differences in viscoelastic properties among the GC surfaces studied. As a result, viscous damping would not be expected to contribute significantly to the observed phase shift. This implies that the phase shift noted is possibly governed by differences in elastic modulus between the unmodified and base modified GC surface. Maganov *et al.* have observed phase shift when imaging samples with regions of varying stiffness (elastic modulus) [20]. The authors observed a greater phase shift on the softer regions.

Figure 2.9 also shows that the base oxidized surface has a more elastic on-load depth recovery than polished GC following reduction of indenter load. This is evident from the unloading path of the load-displacement curve, which is close to the loading path. Thus, the different mechanical properties between polished and base oxidized GC are believed to contribute to the observed phase contrast. Specifically, as shown in Figure 2.11, on its downward cycle the cantilever/tip assembly penetrates the polishing layer and experiences greater damping relative to the base oxidized

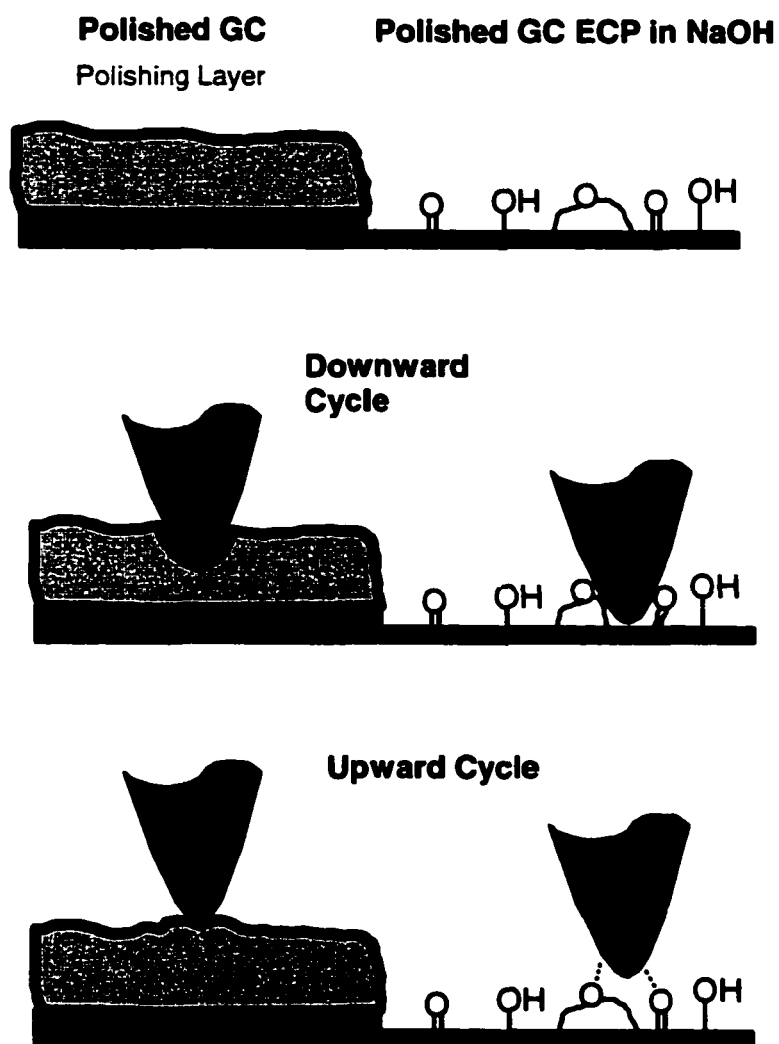


**Figure 2.11 :** Schematic model illustrating GC surface architecture and tip interactions during TM SFM imaging of patterned GC electrodes ECPed in base. For clarity, the carbon microparticles and functional groups known to exist on the polishing layer are not shown.

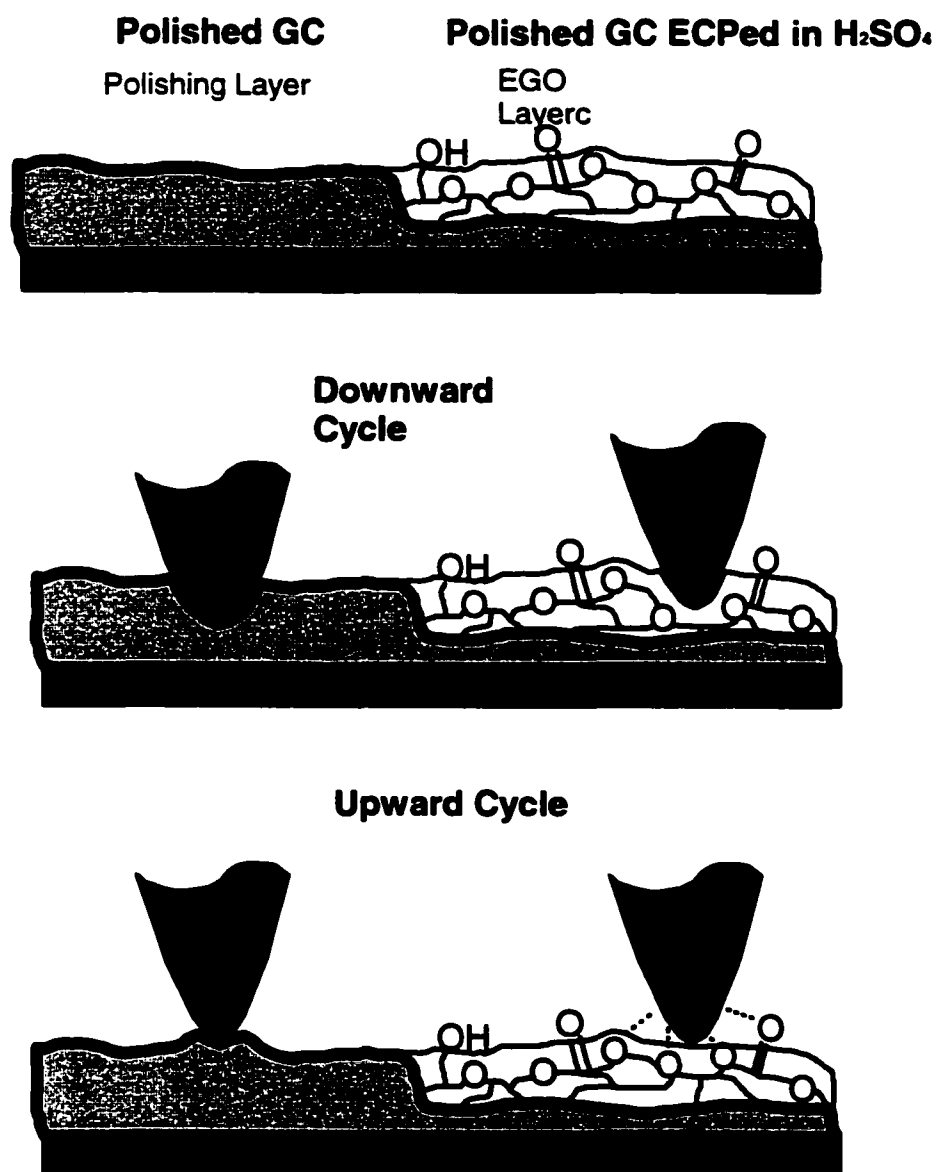


**Figure 2.12 :** Schematic model illustrating GC surface architecture and tip interactions during TM SFM imaging of patterned GC electrodes ECPed in acid.

regions. The differences in adhesion between the downward and upward cycles (adhesion hysteresis) are similar at each region.

The nature of the phase contrast observed between the polished and acid ECPed surface is less intuitively obvious. Although not suggested by the topographic TM SFM images obtained in this work, both the phase contrast images and electrochemical results indicate that the polishing layer is altered or transformed by ECP in acidic media at shorter times, consistent with literature reports [21]. Considering only the greater measured adhesion at acid oxidized GC (Figure 2.8), one would expect the acid oxidized regions in this case to appear darker in contrast. However, this is not the case, indicating that differences in elasticity dominate over adhesion hysteresis. In Figure 2.8, nanoindentation measurements show that the indentation depth at a given load is higher for polished GC as compared to a GC surface oxidized in acid. The measured values for elastic modulus on acid oxidized GC was ~24.3 GPa as compared to ~28.1 GPa on polished GC (Table 2.3). This suggests that polished GC has a slightly softer surface than the acid oxidized surface. It has been noted that a dried EGO film is more stiff and brittle than an EGO film that remains wet [22]. Therefore, it is reasonable that the elastic modulus of the polishing layer is greater than that of the EGO film. Thus, as shown in Figure 2.12, the tip penetrates more on the polished region resulting in a larger contact area. This results in a greater cantilever damping at the polished region and a darker contrast in phase images.

## Conclusions

Results obtained in this Chapter show that transformations in GC surface architecture induced by chemical modification can be tracked with TM SFM by employing partially masked electrodes. Importantly, phase contrast imaging provides compositional information that can be correlated to electrochemical reactivity. In the studies presented here, ECP of patterned GC electrodes in 1 M H<sub>2</sub>SO<sub>4</sub> does not induce topographic changes detectable by TM SFM. However, the surface compositional variations indicated by electrochemical measurements can be probed with phase contrast TM SFM. ECP in 0.1 M NaOH etches the topography of the GC surface. The potential of this etching procedure to produce micromachined GC structures is investigated in Chapter IV of this dissertation. The compositional transformation induced by ECP in NaOH is also detected with phase contrast and correlates with electrochemical reactivity. Adhesion and nanoindentation measurements indicate that the contrast in TM SFM phase images is dependent on the mechanical properties of the ubiquitous polishing layer of the unmodified regions of the patterned electrode.

## References

1. M. O. Finot and M. T. McDermott, *J. Am. Chem. Soc.* 119:8564 (1997).
2. A. J. Bard, H. D. Abruna, C. E. Chidsey, L. R. Faulkner, S. W. Feldberg, K. Itaya, M. Majda, O. Melroy, R. W. Murray, M. D. Porter, S. M.P., and H. S. White, *J. Phys. Chem.* 97:7147 (1993).

3. C.-J. Zhong and M. D. Porter, *Anal. Chem.* 67:709A (1995).
4. J.-B. D. Green, C. A. McDermott, M. T. McDermott, and M. D. Porter, *Imaging of Surfaces and Interfaces. Frontiers of Electrochemistry*, Wiley-VHC Inc., New York, 1999.
5. S. S. Lord and L. B. Rogers, *Anal. Chem.* 26:284 (1954).
6. D. Tse and T. Kuwana, *Anal. Chem.* 50:1315 (1978).
7. R. C. Engstrom, *Anal. Chem.* 54:2310 (1982).
8. G. E. Cabaniss, A. A. Diamantis, W. R. Murphy, R. W. Linton, and T. J. Meyer, *J. Am. Chem. Soc.* 107:1845 (1985).
9. A. L. Bielby, T. A. Sasaki, and H. M. Stern, *Anal. Chem.* 67:976 (1988).
10. D. M. Anjo, M. Kahr, M. M. Khodabakhsh, S. Nowinski, and M. Wanger, *Anal. Chem.* 61:2603 (1989).
11. C. A. McDermott, K. R. Kneten, and R. L. McCreery, *J. ElectroChem. Soc.* 140:2593 (1993).
12. F. A. Armstrong and K. J. Brown, *J. Electroanal. Chem.* 219:31325 (1987).
13. F. G. Gonon, C. M. Fombarlet, M. J. Buda, and J. F. Pujol, *Anal. Chem.* 53:1386 (1981).
14. L. Bodalbhai and A. Brajter-Toth, *Anal. Chem.* 63:1047 (1991).
15. P. Heiduschika, A. W. Munz, and W. Gopel, *Electrochimica Acta.* 39:2207 (1994).

16. J. Wang, D. Martinez, R. Yaniv, and L. D. McCormick, *J. Electroanal. Chem.* 278:379 (1990).
17. G. Picq, R. Reeves, P. Ribourg, and P. Vennerau, *J. Electroanal. Chem.* 162:225 (1984).
18. W. H. Smyrl, R. T. Atanasoski, L. Atanasoska, L. Hartshorn, M. Lien, K. Nygren, and E. A. Fletcher, *J. Electroanal. Chem.* 264:301 (1989).
19. E. Gileadi, N. Tsherniskovski, and M. Babai, *J. Electrochem. Soc.* 119:1018 (1972).
20. S. N. Magonov, V. Elings, and M.-H. Whangbo, *Surface Science* 375:L385 (1997).
21. R. L. McCreery, , In *Electroanalytical Chemistry* Vol. 17 (A. J. Bard, ed.), Marcel Dekker, New York, 1991, p. 221.
22. L. J. Kepley and A. J. Bard, *Anal. chem.* 1988:1459 (1988).
23. B. Kazee, D. E. Weisshaar, and T. Kuwana, *Anal. Chem.* 57:2736 (1985).
24. C. Kozlowski and P. Sherwood, *J. Chem. Soc. Faraday Trans. 1* 81:2745 (1985).
25. C. A. McDermott, K. R. Kneten, and M. R. L., *J. Electrochem. Soc.* 140:2593 (1993).
26. M. T. McDermott, C. A. McDermott, and R. L. McCreery, *Anal Chem.* 65:937 (1993).
27. R. N. Ross and H. Sokol, *J. Electrochem. Soc.* 131:1742 (1984).

28. A. L. Beilby and A. Carlsson, *J. Electroanal. Chem.* 248:283 (1988).
29. J. Tamayo and R. Garcia, *Langmuir* 12:4430 (1996).
30. J. Tamayo and R. Garcia, *Appl. Phys. Lett.* 71:2394 (1997).
31. G. Bar, R. Brandsch, and M.-H. Whangbo, *Surf. Sci.* 411:L802 (1998).
32. N. A. Burnham, O. P. Behrend, F. Oulevey, G. Gremaud, P.-J. Gallo, D. Gourdon, E. Dupas, A. J. Kulik, H. M. Pollock, and G. A. D. Briggs, *Nanotechnology* 8:67 (1997).
33. R. Brandsch, G. Bar, and M.-H. Whangbo, *Langmuir* 13:6349 (1997).
34. J. P. Cleveland, B. Anczykowski, A. E. Schmid, and V. B. Elings, *Appl. Phys. Lett.* 72:2613 (1998).
35. R. Garcia, J. Tamayo, M. Calleja, and F. Garcia, *Appl. Phys. A* 66:S309 (1998).
36. W. C. Oliver and G. M. Pharr, *J. Mater. Res.* 7:1564 (1992).
37. M. F. Doerner and W. D. Nix, *J. Mater. Res.* 1:601 (1986).
38. J. S. Field and M. V. Swain, *Carbon* 34: 1357 (1996).

## **CHAPTER III**

### **Removal of Polishing Contaminants from Carbon Surfaces via an Electrochemical Pretreatment Method.**

#### **Introduction**

As reviewed in Chapter I, polished glassy carbon (GC) electrodes show poor surface reproducibility that is attributed to variation in thickness, composition and structure of the polishing layer present at these surfaces. The surface-to-surface variation is evident from reported electrochemical measurements, which show significant variation for the same redox system [1, 2]. The work presented in this Chapter will investigate an electrochemical cleaning procedure aimed at removing polishing contaminants from polished carbon electrodes. The motivation of this study derives from results obtained in Chapter II that showed direct evidence for the removal of carbon material upon anodization of GC electrodes in basic solution.

Recently many studies have been aimed at understanding the relationship between the interfacial structure of polished carbon electrodes and electrode response [2-11]. However, a clear understanding of the factors that govern the behavior of redox systems on these surfaces is greatly limited by surface variation of the starting electrode surface. Polished GC is the most widely studied GC surface and is often used as the starting surface for other activation procedures. Various methods have been developed to remove contaminants resulting from polishing or other sources from the electrode

surface. These methods include ambient or vacuum heat treatment [1, 12], exposure to UV-generated ozone [13], laser irradiation [14, 15], exposure to RF plasma[16], and exposure to isopropanol/activated carbon mixture [17]. As a result, significant improvements on reproducibility and ET kinetics for certain redox systems have been reported following removal of contaminants by these procedures. The activation mechanism is thought to involve exposure of active sites [1, 15]. However, most of these cleaning procedures have not gained wide spread use among researchers likely due to inconvenience and high costs involved.

The work reported here describes a simple and rapid electrochemical procedure that completely removes polishing debris from polished carbon surfaces. This method involves electrochemical pretreatment (ECP) of carbon electrodes in basic media at high positive potentials for short times (~ 10 s). Tapping mode scanning force microscopy (TM SFM) and x-ray photoelectron spectroscopy (XPS) surface characterization techniques are utilized to track the removal of polishing layer. Several electrochemical characterizations of the modified GC surface are also carried out to access changes in electrode reactivity following removal of the microparticle polishing layer. Electrochemical measurements obtained on the electrochemically cleaned GC surface show a highly reproducible surface with reactivity comparable to polished GC.

## Experimental

**Reagents.**  $\text{Fe}(\text{CN})_6^{4-}$  (aq) in 1M KCl and  $\text{Ru}(\text{NH}_3)_6^{3+}$  (aq) in 1M KCl solutions were prepared at 1 mM concentrations from  $\text{K}_4\text{Fe}(\text{CN})_6$  (BDH Chemicals) and  $\text{Ru}(\text{NH}_3)_6\text{Cl}_3$  (Strem Chemicals) respectively.  $\text{Eu}^{3+}$ (aq) in 0.2 M  $\text{HClO}_4$  (Caledon) solution was prepared at 5 mM concentrations from  $\text{Eu}(\text{NO}_3)_3 \cdot 5\text{H}_2\text{O}$  (Aldrich). Disodium anthraquinone, 2,6-disulfonate (2,6-AQDS) from Aldrich was recrystallized twice from ethanol and prepared in 1 M  $\text{HClO}_4$  at 10  $\mu\text{M}$  concentration. All other reagents were used as received. Aqueous solutions were prepared using distilled /deionized (18M $\Omega$ /cm) water (Barnstead, Dubuque, IA). Solutions used for electrolysis were purged with nitrogen gas for 10 min prior to use.

**Electrode Preparation and Electrochemical Measurements.** The GC-20 electrodes (Tokai GC-20, Electrosynthesis Company, NY) were prepared as described in Chapter II. Polished GC electrodes were patterned by spraying the surface with small droplets of polystyrene dissolved in  $\text{CCl}_4$  (Figure 3.1). This produced masked and unmasked regions for direct comparison. Electrochemical pretreatment (ECP) was achieved by poisoning a polished electrode at +1.80 V for a short period of time ( $\leq 10$  s) in 0.1 M NaOH. A three-electrode cell was used with a Ag/AgCl reference electrode and a Pt wire counter electrode. The cell was connected to a Model 175 (Princeton Applied Research, NJ) potentiostat. Electrochemically treated GC electrodes were sonicated in acetone for 10 min. to remove the polystyrene

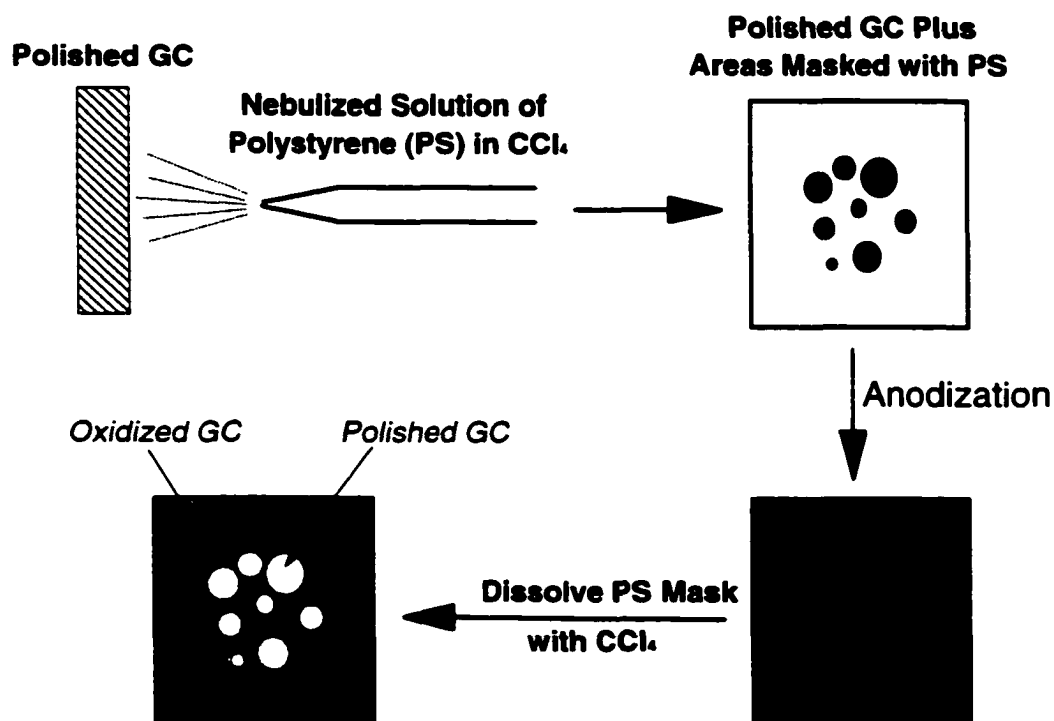


**Figure 3.1:** Scheme illustrating the technique used to mask some regions of polished GC surface with polystyrene mask.

mask. Cyclic voltammogram of 2,6-AQDS was obtained after an equilibration time of 10 min. Adsorption of 2,6-AQDS was quantified by measuring the area under the voltammetric reduction wave as described by Brown and Anson [18]. The charge under the voltammetric reduction wave,  $Q$ , is given by the equation  $Q = nFA\Gamma$ , where  $n$  is the number of electrons ( $n=2$ ),  $F$  is Faraday's constant,  $A$  is the electrode area, and  $\Gamma$  is the amount of surface bound quinone normally expressed in  $\text{pmol}/\text{cm}^2$ . Cyclic voltammetry was performed at a scan rate of 0.1 V/s. Differential capacitance was determined as described in Chapter II.

**Control Experiments.**  $\text{Fe}(\text{CN})_6^{3-/4-}(\text{aq})$  was used as a probe to assess the removal of polystyrene mask upon sonication of ECPed GC electrode in acetone. Polished GC electrodes were coated with polystyrene followed by sonication in acetone for 10 min. and then allowed to air dry. The cyclic voltammetric peak separation ( $\Delta E_p$ ) for  $\text{Fe}(\text{CN})_6^{3-/4-}(\text{aq})$  was then measured and found to be similar to values obtained on freshly polished GC electrodes. Also, the charge under the  $\text{Fe}(\text{CN})_6^{3-/4-}$  voltammetric reduction wave was found to be similar to that obtained on freshly polished GC electrodes. These results imply that acetone is effective in completely removing the polystyrene mask without altering the electrochemical reactivity.

**SFM Imaging.** Tapping mode scanning force microscopy (TM-SFM) images were obtained in air using Nanoscope III (Digital Instruments, Santa Barbara CA). The Si cantilever was oscillated at about 300 kHz. Scanning

was carried out with a constant amplitude of oscillation at a moderated tapping force as described in Chapter II. All other TM SFM imaging conditions were as described in Chapter II.

**XPS Studies.** XPS spectra were obtained before and after ECP using a Surface Science Laboratories SSX-100 spectrometer. Al K $\alpha$  radiation was used as the X-ray source with a pass energy of 150 eV. The pressure inside the analyzer was maintained at about  $10^{-9}$  torr. Resolution of the spectrometer was 0.7 eV. Acquired data was analyzed using Spectra Data Processor from XPS international.

## **Results and Discussion**

**Surface Characterization of polished GC anodized in NaOH.** In Chapter II, an electrode preparation method that allowed direct comparison of modified and unmodified regions of polished GC in the same SFM image was developed. This procedure allows differentiation of morphological and chemical modifications occurring on the polished GC surface following ECP [2]. In the present work, the polished GC surface was partially masked with polystyrene film that was delivered as small droplets from a nebulized solution (Figure 3.1). The polystyrene mask was dissolved from the GC substrate after modification and before imaging producing a surface with adjacent modified and unmodified regions. Part A and B of Figure 3.2 contains 25 x 25  $\mu\text{m}$  topographic and phase contrast TM SFM images of a partially masked

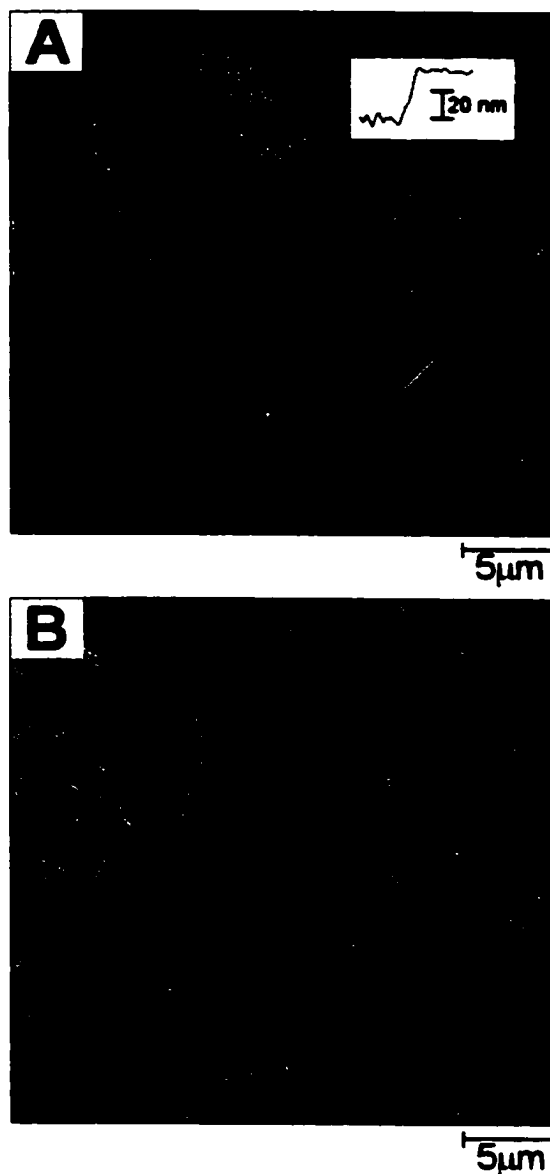


**Figure 3.2:** 25 x 25  $\mu\text{m}$  TM SFM images of a GC surface oxidized at 1.8 V in 0.1 M NaOH for 10 s through a polystyrene mask. (A) Topography (z-scale = 30 nm). (B) Phase contrast (z-scale = 20 deg).

polished GC surface oxidized at 1.8 V in 0.1 M NaOH for 10 s. Figure 3.2-A shows significant variation in morphology following the ECP procedure. The regions that were exposed to the procedure are lower in topography (darker areas). This indicates removal of material from the polished surface similar to Figure 2.5 in Chapter II. Analysis of the topographic image (Figure 3.2-A) reveals that polished surface has been etched to a depth of ~30 nm which is sufficient to account for the thickness reported for the carbon microparticle layer of 20 nm [3]. Thus, it is reasonable to believe that anodization of GC in 0.1 M NaOH for 10 s effectively removes the polishing layer known to exist on polished carbon surfaces. Figure 3.2 shows more defined polishing scratches on the modified regions, which is consistent with removal of the ubiquitous layer of polishing debris. The reappearance of focused scratches in optical micrographs of polished GC electrodes has been suggested to signify the removal of the polishing layer following heat treatment [4], laser irradiation [5], and radio frequency plasma [6].

Figure 3.2-B is the corresponding phase contrast image and provides additional evidence for the loss of the polishing layer after 10 s ECP in base. There is notable differentiation between modified and unmodified regions. The areas exposed to the ECP procedure exhibit brighter contrast relative to the unmodified polished GC surface similar to that observed in Chapter II.

A higher magnification of Figure 3.2 provides Figure 3.3, which reveals more differences in morphological features between the modified and

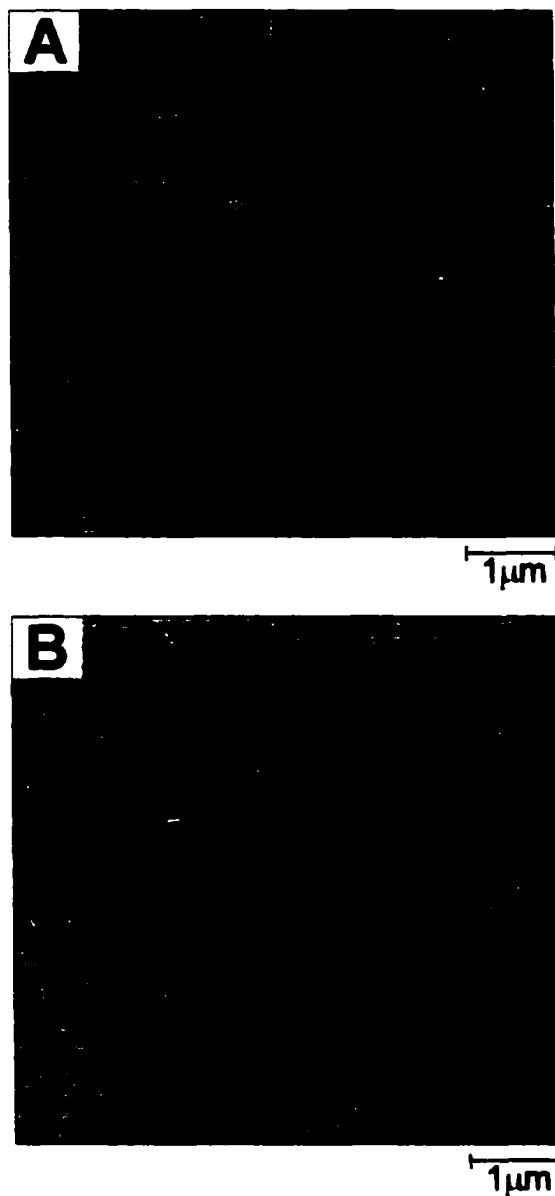


**Figure 3.3:** 5 x 5  $\mu\text{m}$  TM SFM images of A) polished GC surface and B) Polished GC oxidized at 1.8 V in 0.1 M NaOH for 10 s.

unmodified GC surface. Part A and B of Figure 3.3 are 5 x 5 $\mu$ m TM SFM phase contrast images of polished GC (Figure 3.3-A) and polished GC ECPed for 10 s in NaOH at 1.8 V (Figure 3.3-B). Phase images are used here because they provide a clearer view of the GC microstructure than topographic images. The base-activated surface exhibits nodular structures, which is consistent with absence of the polishing layer. Similar morphological structures have been reported in absence of polishing layer for fractured GC using SEM [7] and STM [8]. The dimensions of these nodular structures on average range from 140 nm to 280 nm, which is in agreement with results from the SEM (~160 nm) and STM (50-300 nm) studies mentioned above. In comparison, TM SFM phase contrast image of a polished GC surface (Figure 3.3-A) lacks these features at the same magnification. The presence of polishing layer on the GC surface covers these finer structural details and likely limits the SFM tip from probing them.

XPS analysis was also carried out to monitor change in aluminum surface concentration following base anodization of polished GC surface. Figure 3.4 shows the Al<sub>2s</sub> peak region from the XPS spectra for polished GC electrode before (spectra a) and after ECP in base for 10 s (spectra b). The peak in spectra a for polished GC at 74.3 eV corresponds to Al at a concentration of ~1.8 %. The Al source is likely the residual alumina known to exist on carbon surfaces polished in alumina/water slurries. The polishing layer consists of carbon microparticles, alumina, water and other impurities.

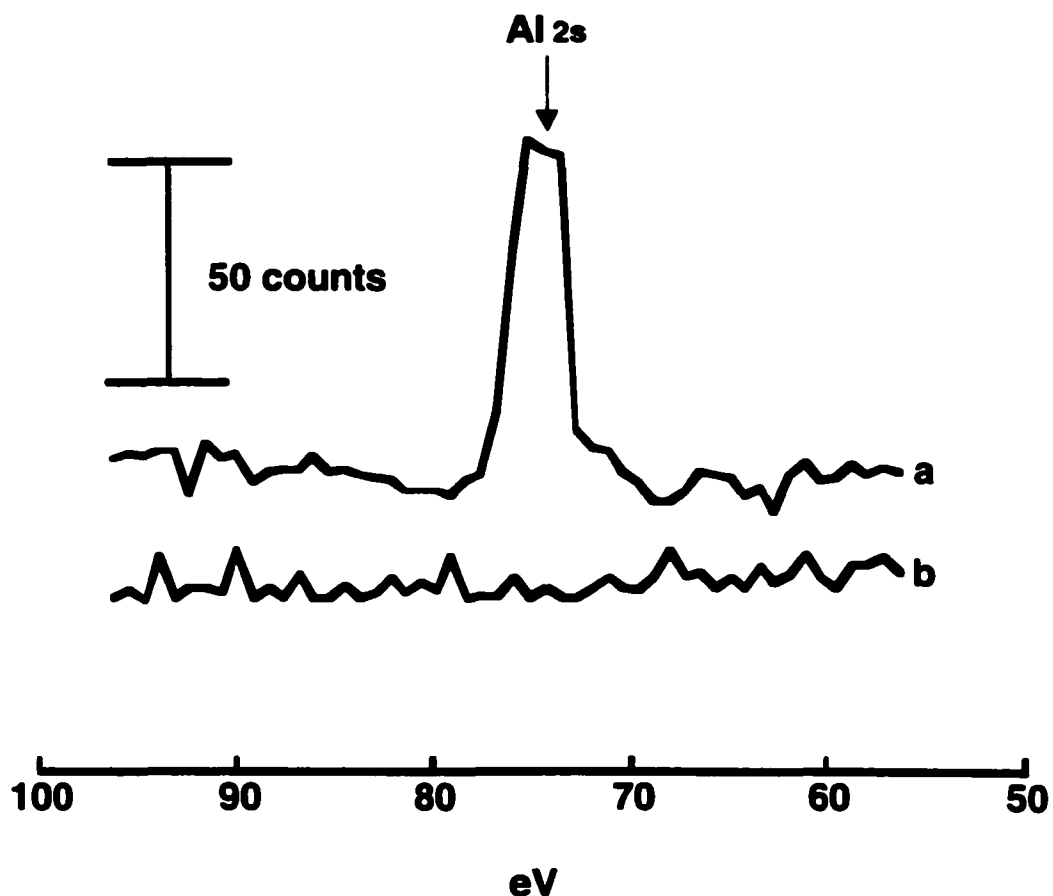


**Figure 3.4:** XPS spectra of polished GC (spectra a) and polished GC ECPed in 0.1 M NaOH at 1.8 V for 10 s (spectra b).

Previous studies have noted that this layer remains even after ultrasonic cleaning [3, 4, 9]. XPS data obtained in this work shows a reduction in Al concentration from ~5.8% to ~1.8% upon ultrasonic cleaning. These results indicate that about 30% of the initial alumina remain on the ultrasonicated surface.

Spectra b in Figure 3 shows no trace amounts of Al after 10 s anodization period. These results suggest that the polishing layer is removed from the GC surface to a degree below the detection limit of XPS. Thus, the XPS data is in agreement with TM SFM results provided in Figure 3.2 and 3.3. It is then reasonable to propose that ECP in 0.1 M NaOH at 1.8 V for 10 s removes the majority of carbon microparticle layer. It is likely that the polishing layer is removed via an oxidative process that results in corrosion of the carbon microparticle. A similar oxidative cleaning mechanism has been proposed following removal of the carbon microparticle layer by oxygen RF plasma treatment [6], laser activation [5], and UV/ozone treatment [10].

Furthermore, the oxidative ECP cleaning process could be aided further by oxygen evolution known to occur at high positive potentials in basic electrolytes [11]. The gas evolution could physically dislodge the finely divided carbon microparticles present on the polished surface. It should be noted that XPS spectra of polished GC ECPed for 10 s in base show slight increase in oxygen concentration at the surface. The O/C atomic ratio determined from the ratio of  $O_{1s}$  and  $C_{1s}$  XPS band areas increased from ~

9% to ~13% following base activation. Previous studies report that the O/C ratio for GC electrodes polished under aerobic conditions is typically 8 to 18% [1, 3, 12-14]. Thus, anodization for short time scales (~10 s) in basic electrolytes does not oxidize the GC surface extensively but is sufficient to remove the polishing layer.

**Electrochemical characterization of base-activated GC.** Three redox systems  $\text{Fe}(\text{CN})_6^{3-/4-}$ ,  $\text{Ru}(\text{NH}_3)_6^{3+/2+}$ , and  $\text{Eu}^{3+/2+}$  were utilized to assess the changes in electron-transfer (ET) reactivity induced by 10 s ECP in base. These redox systems were selected based on their known kinetic behavior on carbon surfaces. Results from previous studies show that the  $\text{Fe}(\text{CN})_6^{3-/4-}$  redox probe is sensitive to surface preparation procedures [1, 5, 15]. The ET rate of  $\text{Ru}(\text{NH}_3)_6^{3+/2+}$  is relatively insensitive to surface state [12]. The aquated  $\text{Eu}^{3+/2+}$  system has been shown to be very sensitive to the presence of surface oxides, especially surface carbonyl groups [16, 17].

Table 3.1 summarizes results from electrochemical characterizations of polished GC surfaces before and after 10 s ECP in NaOH. The figures that follow show representation data used to generate the values in Table 3.1. Figure 3.5 shows the effect of 10 s base-activation on the cyclic voltammetry of  $\text{Fe}(\text{CN})_6^{3-/4-}$ . Curve a of Figure 3.5 is the cyclic voltammogram at polished GC surface. The values for the voltammetric peak separations ( $\Delta E_p$ ) were converted to heterogeneous ET rate constants ( $k^0$ ) via the method of Nicholson as described in Chapter I [18]. A rate constant of 0.008 cm/s is

Oxidation Time ( s )	Rate Constant $k^{\circ}$ (cm/s) <sup>(a)</sup>						Capacitance		Adsorption	
	$\text{Fe}(\text{CN})_6^{3-/4-}$ <sup>(b)</sup>		$\text{Ru}(\text{NH}_3)_6^{3+/2+}$ <sup>(b)</sup>		$\text{Eu}^{3+/2+}$ <sup>(c)</sup>		$C^{\circ}$ <sup>(b)</sup> ( $\mu\text{F}/\text{cm}^2$ )	RSD (%)	$\Gamma_{2,6\text{-AQDS}}$ <sup>(d)</sup> ( $\text{pmol}/\text{cm}^2$ )	RSD (%)
	$k^{\circ}$	RSD <sup>(e)</sup> (%)	$k^{\circ}$	RSD (%)	$k^{\circ}$	RSD (%)				
Polished	$0.008 \pm 0.002$	25	$0.019 \pm 0.002$	10	$(3.2 \pm 1.2) \times 10^{-4}$	37	$41 \pm 10$	24	$172 \pm 44$	26
10	$0.015 \pm 0.001$	7	$0.022 \pm 0.002$	9	$(12.5 \pm 1.1) \times 10^{-4}$	9	$54 \pm 7$	13	$236 \pm 17$	7

a.  $v = 100$  mV/s for all systems

b. 1 M KCl

c. 0.2 M  $\text{HClO}_4$

d. 1 M  $\text{HClO}_4$

e. relative standard deviation

f. statistics based on  $N = 8$  for  $k^{\circ}$  and  $N = 7$  for both  $C^{\circ}$  and  $\Gamma$

**Table 3.1:** Results from electrochemical characterizations of polished GC electrodes electrochemically pretreated at 1.8 V in 0.1 M NaOH for 10 s.

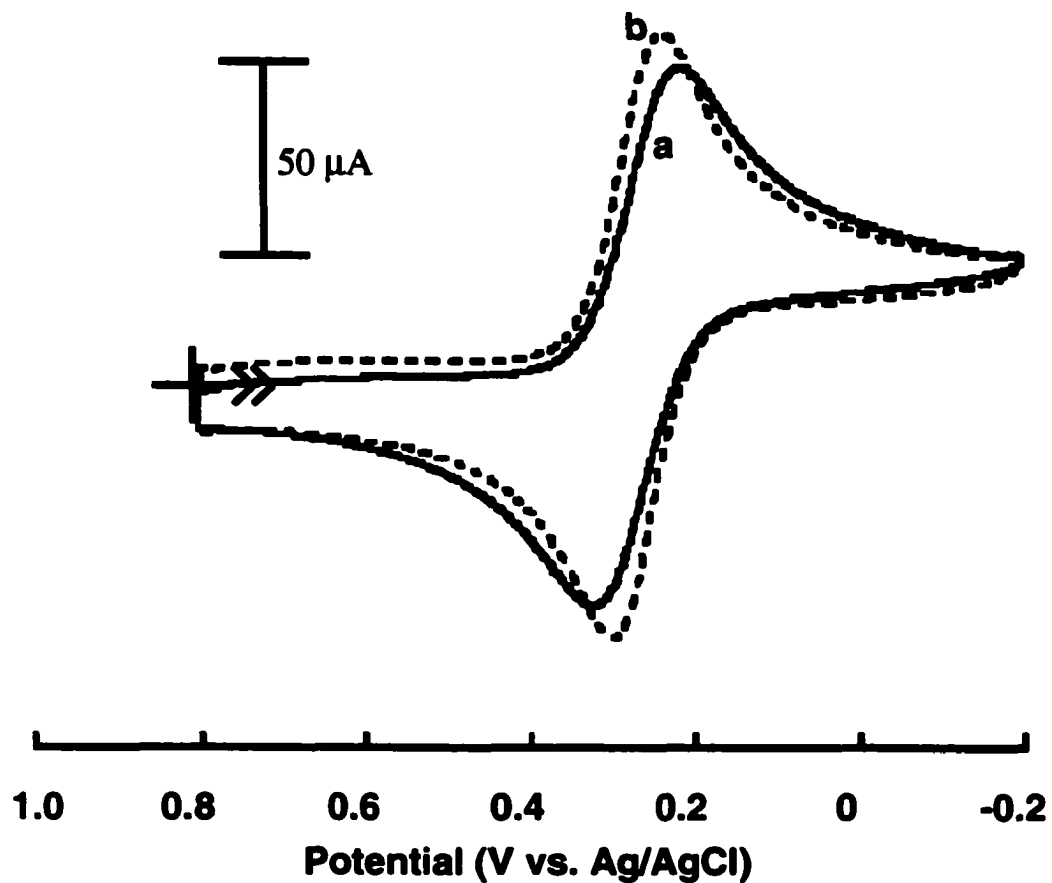


**Figure 3.5 :** Cyclic voltammograms of 1 mM  $\text{Fe}(\text{CN})_6^{3-/4-}$  in 1 M KCl on polished GC (curve a) and polished GC ECPed in base at 1.8 V for 10 s (curve b).

obtained from curve a, for the polished surface and is within the range reported for this redox system [1, 19]. Curve b of Figure 3.5 is the  $\text{Fe}(\text{CN})_6^{3-/4-}$  voltammogram on the base modified surface. Curve b exhibits slightly higher peak currents and a smaller  $\Delta E_p$  value than curve a. The measured  $k^0$  value of 0.015 cm/s (Table 3.1) reflects approximately a two-fold increase in ET rate from the unmodified GC electrode. Increase in  $k^0$  for  $\text{Fe}(\text{CN})_6^{3-/4-}$  at carbon surfaces has been attributed to surface cleanliness and active sites [1, 20]. Thus, improvements on ET rates for  $\text{Fe}(\text{CN})_6^{3-/4-}$  following base-activation is consistent with removal of the underlying polishing debris. Removal of this layer would result in exposure of the bulk GC microstructure thereby generating a more active surface.

Figure 3.6 contains cyclic voltammetric current-potential curves for the  $\text{Eu}^{3+/2+}$  redox system. Curve a of Figure 3.6 is the voltammogram at a polished GC surface and provides a  $k^0$  value of  $3.2 \times 10^{-4}$  cm/s. A rate constant of  $12.5 \times 10^{-4}$  is obtained on the base-activated surface (curve b). Aqueated  $\text{Eu}^{3+/2+}$  is an inner-sphere system and is highly dependent on surface oxides. Previous studies have shown that mild oxidation of GC surface results in large increases in  $k^0$  for  $\text{Eu}^{3+/2+}$  and increases by a factor of 500 have been reported resulting in  $k^0$  value of  $4 \times 10^{-2}$  cm/s [17]. In comparison, results obtained in this study show a slight increase in  $k^0$  for this redox system on a 10 s base-activated surface, which suggests minimum surface oxidation.

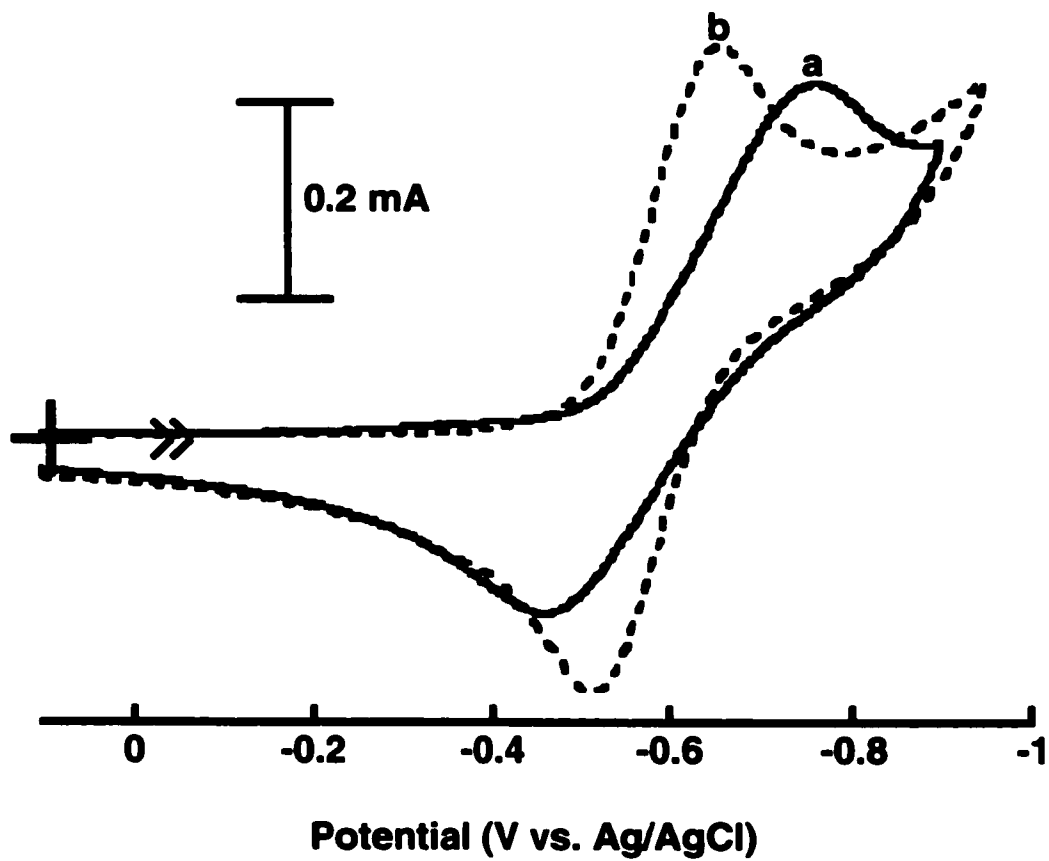


**Figure 3.6 :** Cyclic voltammograms of 5 mM  $\text{Eu}^{3+}(\text{aq})$  in 0.2 M  $\text{HClO}_4$  on polished GC (curve a) and polished GC ECPed in base at 1.8 V for 10 s (curve b).

These observations are in agreement with XPS data provided earlier that showed only ~ 4 % increase in O/C ratio following base-activation for 10 s.

No significant variation in  $k^{\circ}$  for  $\text{Ru}(\text{NH}_3)_6^{3+/2+}$  redox system is observed on the modified GC surface (Table 3.1).  $\text{Ru}(\text{NH}_3)_6^{3+/2+}$  is an outer-sphere system that shows minor kinetic effects upon surface modification even when a compact organic monolayer is chemisorbed to the GC surface [16]. Thus, removal of the polishing layer would have no significant effect on the observed rates for this outer-sphere system.

Figure 3.7 shows cyclic voltammetric current-potential curves from 10  $\mu\text{M}$  2,6-AQDS in 0.2 M  $\text{HClO}_4$  at polished GC surface before (curve a) and after 10 s base-anodization (curve b). Narrow symmetric peaks are observed at both surfaces, which is characteristic of a surface-confined redox analyte. Strong adsorption was observed on both unmodified and modified GC surfaces resulting in a  $\Delta E_p$  value of ~ 18 mV, which is close to the theoretical value of 0 mV. The full-width-at-half-maximum (fwhm) for the peaks is ~ 48 mV, which is comparable to 45 mV, expected for an ideal adsorbed species with a reversible two electron transfer [21]. The peak current of the waves increases linearly with the voltammetric scan rate.

Quantitative adsorption results obtained on polished GC (curve a) by the method described by Brown and Anson [22] yield a value of 172  $\text{pmol}/\text{cm}^2$  which is comparable to that reported [12, 23]. The theoretical saturation coverage for 2,6-AQDS adsorbing with its ring parallel to a flat surface is 132

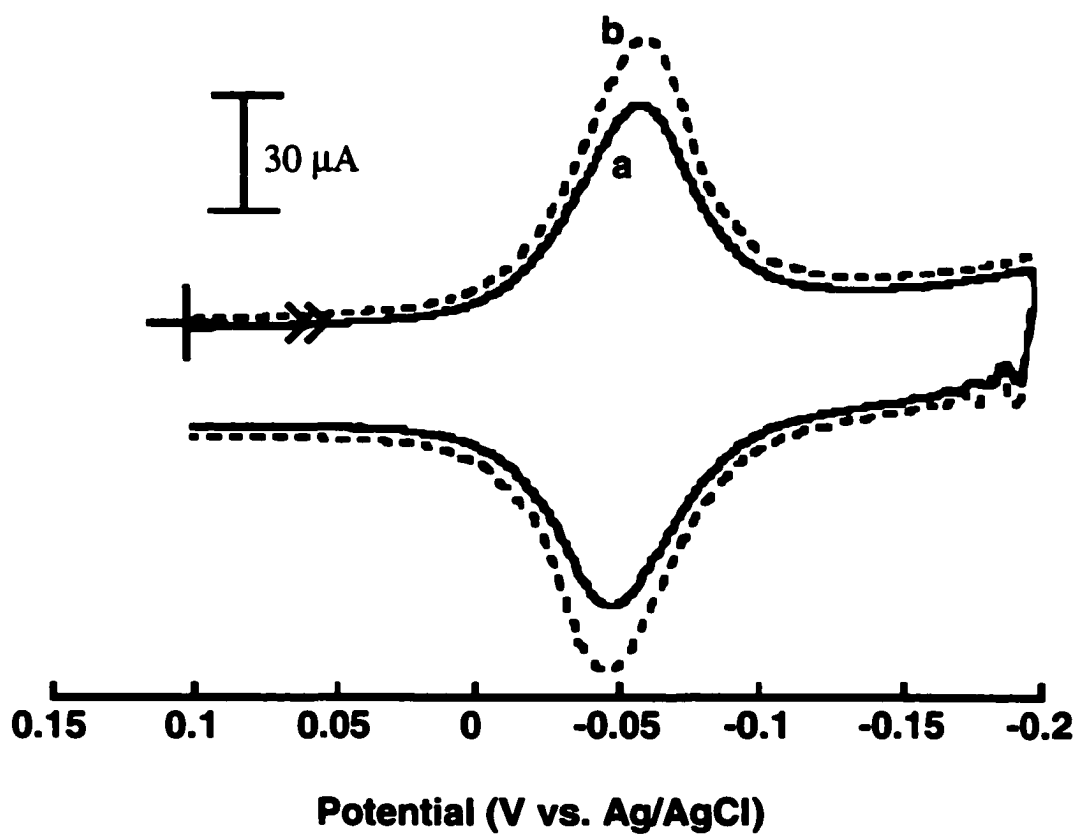


**Figure 3.7 :** Cyclic voltammograms of 10  $\mu\text{M}$  2,6-AQDS in 1 M  $\text{HClO}_4$  on polished GC (curve a) and polished GC ECPed in base at 1.8 V for 10 s (curve b).

pmol/cm<sup>2</sup> [24]. The 10 s base-activated surface shows 26% increase in 2,6-AQDS coverage to 236 pmol/cm<sup>2</sup> (Table 3.1). The increase in adsorption following ECP may be attributed to an increase in microscopic area [7, 8] and /or adsorption sites [20, 23, 25].

Assuming that 2,6-AQDS adsorbs with its ring structure parallel to the surface in a monolayer coverage, a roughness factor  $\sigma$ , can be determined via:

$$\sigma = \frac{\Gamma_{\text{AQDS,obs}}}{\Gamma_{\text{AQDS,flat}}} \quad \{3.1\}$$

where  $\Gamma_{\text{AQDS,obs}}$  is the observed coverage of 2,6-AQDS and  $\Gamma_{\text{AQDS,flat}}$  is the theoretical coverage on a flat surface based on the molecular dimension [24]. For polished GC,  $\sigma = 1.3$  and for base etched GC  $\sigma = 1.8$ . These results are consistent with those presented previously on polished GC with reported roughness factors of 1.7 [26] and 1.9 [7]. Higher roughness factors have been reported on GC surfaces exhibiting greater surface roughness. For example, scanning tunneling microscopy (STM) studies on fractured unpolished GC surface have shown that the fractured surface is significantly more rough than polished GC surface [8] with a reported roughness factor of 3.5 [7]. Therefore, in comparison, the roughness factors obtained in this work are reasonable for GC and indicate that ECP process is accompanied by a slight increase in microscopic area of the electrode.

It is also possible that surface sites that are involved in the adsorption of 2,6-AQDS increases with ECP in base for short time scales. The nature of

surface sites involved in adsorption of 2,6-AQDS is not well understood. Adsorption of 2,6-AQDS on carbon surfaces has been attributed to electronic disturbances and partial charges near edge plane defects rather than specific chemical sites [23]. However, results from another study on a variety of different carbon electrodes suggest that carbon-oxygen functionalities serve as adsorption sites [25]. As stated previously, this ECP treatment in base increases the oxygen concentration from 9 to 13% as measured by XPS. Removal of polishing debris by laser activation [5] and activated carbon/isopropanol mixture [27] has also resulted in increased adsorption for 2,6-AQDS. Adsorption of 1,2,4-trihydroxybenzene on heat-treated polished GC was larger than on unmodified polished GC surface [28]. The authors attributed this observation to removal of surface impurities which results in more exposed adsorption sites

The differential capacitance ( $C^\circ$ ) is also dependent on microscopic surface area.  $C^\circ$  measured in this work increases slightly upon 10 s anodization of polished GC in base (Table 3.1).  $C^\circ$  Thus, changes in  $C^\circ$  should be similar to that noted in the adsorption of 2,6-AQDS. However, some differences may arise since double layer capacitance is dependent on additional variables such as surface bound redox functional group, electrolyte adsorption *etc.* Presence of impurities on GC electrodes has also been found to decrease capacitance [25, 27]. In summary, increase in capacitance and adsorption measurements noted here for polished GC ECPed in base for

short time scales (~ 10 s) is consistent with increase in microscopic area and /or removal of the ubiquitous layer of polishing debris.

Importantly, the electrochemical data summarized in Table 3.1 shows that reproducibility of the polished GC surface is greatly improved by 10 s base ECP. Except for the outer-sphere  $\text{Ru}(\text{NH}_3)_6^{3+/2+}$ , the relative standard deviation of  $k^\circ$  for the redox systems studied is significantly higher (25-37%) for polished GC compared to a 10 s base anodized surface (7-9%). Adsorption measurements on polished GC yield a relative standard deviation of 26 % compared to 7 % on base anodized GC. Similarly, there is increase in precision of  $C^\circ$  for polished GC from 24 % to 13 % following 10 s ECP in base.

Even though there are no exceptionally large improvements in electrode activity following short anodization times in base (~10 s), the measured electrochemical reactivity shows significantly large improvements in reproducibility. The relative standard deviation for each set of measurements is significantly smaller relative to polished GC. This increase in precision is consistent with the removal of the polishing layer. The variability in thickness, composition, etc of this layer from surface to surface likely results in large standard deviations observed at polished GC surfaces. Thus, anodization of polished GC in basic electrolytes for short time scales (~10 s) provides a means of preferentially removing the polishing layer without large alterations in electrode reactivity. More importantly, this treatment procedure offers a highly reproducible surface, which has remained

difficult to attain on polished carbon electrodes. Thus, results obtained in this study show that use of base activation on carbon surfaces as described above will result in a starting surface that has comparable activity to polished GC but which is more reproducible from laboratory to laboratory.

## CONCLUSIONS

In this Chapter, an electrochemical oxidative procedure that removes polishing contaminants from polished carbon surfaces has been developed. The method involves 10 s ECP of polished GC electrodes in 0.1 M NaOH at 1.8 V. This procedure is simple, rapid and can be performed *in situ*. TM SFM images obtained for partially masked GC electrodes ECPed in 0.1 M NaOH at 1.8 V for 10 s shows that the etching process removes the polishing layer resulting from the polishing procedure. XPS studies confirm this result. More importantly, results from this work show that the resulting GC surface, free from polishing debris is electrochemically more reproducible than the polished GC surface. Because of the poor surface reproducibility of polished GC electrodes, the results from this work presents an important procedure for generating a starting surface with comparable activity to polished GC but with minimal surface variation. Overcoming surface variation of the starting GC surface would result in a better understanding of the relationship between surface structure and reactivity.

## References

1. I.-F. Hu, D. H. Karweik, and T. Kuwana, *J. Electroanal. Chem.* **188**:59 (1985).

2. G. K. Kiema and M. T. McDermott, *Anal. Chem.* 71:4306 (1999).
3. G. N. Kamau, W. S. Willis, and J. F. Rusling, *Anal. Chem.* 57:545 (1985).
4. B. Kazee, D. E. Weisshaar, and T. Kuwana, *Anal. Chem.* 57:2736 (1985).
5. M. Poon and P. McCreery, *Anal. Chem.* 58:2745 (1986).
6. C. W. Miller, D. H. Karweik, and T. Kuwana, *Anal. Chem.* 53:2319 (1981).
7. N. M. Pontikos and M. R. L., *J. Electroanal. Chem.* 324:229 (1992).
8. M. T. McDermott, C. A. McDermott, and R. L. McCreery, *Anal. Chem.* 65:937 (1993).
9. D. T. Fagan, I. Hu, and T. Kuwana, *Anal. Chem.* 57:2759 (1985).
10. J. Zhou and D. O. Wipf, *J. Electroanal. Chem.* 499:121 (2000).
11. C. Kozlowski and P. Sherwood, *J. Chem. Soc. Faraday Trans. 1* 81:2745 (1985).
12. P. Chen and R. L. McCreery, *Anal. Chem.* 68:3958 (1996).
13. R. A. Engstrom and V. A. Strasser, *Anal. Chem.* 56:136 (1984).
14. G. E. Cabaniss, A. A. Diamantis, W. R. Murphy, R. W. Linton, and T. J. Meyer, *J. Am. Chem. Soc.* 107:1845 (1985).
15. R. L. McCreery, K. K. Cline, C. A. McDermott, and M. T. McDermott, *Colloids Surfaces A* 93:211 (1994).
16. P. Chen, M. A. Fryling, and R. L. McCreery, *Anal. Chem.* 67:3115 (1995).

17. C. A. McDermott, K. R. Kneten, and R. L. McCreery, *J. ElectroChem. Soc.* 140:2593 (1993).
18. R. S. Nicholson, *Anal. Chem.* 37:1351 (1965).
19. S. Dong and T. Kuwana, *J. Electrochem. Soc.* 131:813 (1984).
20. R. J. Rice, N. M. Pontikos, and R. L. McCreery, *J. Am. Chem. Soc.* 112 (1990).
21. A. J. Bard and L. R. Faulkner, *Electrochemical Methods*, Wiley, New York, 1980.
22. A. P. Brown and F. C. Anson, *Anal. Chem.* 49:1589 (1977).
23. M. T. McDermott and R. L. McCreery, *Langmuir* 10:4307 (1994).
24. M. P. Soriaga and A. T. Hubbard, *J. Am. Chem. Soc.* 104:2735 (1982).
25. J. Xu, Q. Chen, and G. M. Swain, *Anal. Chem.* 70:3146 (1998).
26. M. T. McDermott, K. Kneten, and R. L. McCreery, *J. Phys. Chem.* 96:3124 (1992).
27. S. Ranganathan, T.-C. Luo, and R. L. McCreery, *Anal. Chem.* 71:3574 (1999).
28. G. W. Hance and T. Kuwana, *Anal. Chem.* 59:131 (1987).

## CHAPTER IV

### **Fabrication of Microstructures on Glassy Carbon Substrates via an Electrochemical Etching Procedure**

#### **Introduction**

The use of patterned GC electrodes in Chapter II provided direct evidence that ECP in 0.1 M NaOH at 1.8 V etches away the carbon surface. The etching effect induced by ECP in basic media opens pathways for micromachining GC structures. Initial exploration of these possibilities are discussed in this Chapter. The maximum scan size obtainable with TM SFM (Nanoscope III) employed in this work is ~ 170  $\mu\text{m}$ . In order to obtain larger scan size of the micromachined structures, scanning electron microscopy (SEM) is utilized.

As stated earlier in Chapter I, GC has several attractive properties, which make it a widely utilized material in electrochemistry [1-8]. The physical properties of GC such as good electrical conductivity, thermal stability, low gas permeability, low coefficient of thermal expansion, and low density make it an attractive material for designing microminiature systems commonly known as microelectromechanical systems (MEMS). Also, micromachined GC structures may have potential application in microbatteries [9], microsensor [10, 11], and microcapacitors [12].

MEMS have been typically prepared from silicon by microfabrication techniques that mainly involve photolithography and selective chemical etching [13]. GC may be used to substitute silicon in applications where the

microstructures need to be of low density, high resistance to strong acids or bases and thermally stable. More recently, carbon films produced by pyrolysis of photoresists at temperatures typically between 600 °C to 1100 °C have been used in electrochemically based MEMS [14]. The suitability of employing pyrolyzed photoresist as a source of carbonaceous material for MEMS is that the photoresist can be patterned by photolithographic techniques into complex structures [14].

Whitesides and coworkers have reported fabrication of GC microstructures by procedures based on micromolding of polymeric precursor resins such as phenol-formaldehyde, followed by thermal heating at high temperatures (400 –1800 °C) under inert atmosphere [14]. However, GC microstructures prepared by pyrolysis of polymeric resins as described by Whitesides and coworkers experience a major drawback due to dramatic volume reduction that occurs during carbonization. Similar shrinking of photoresist is observed during carbonization and results in dramatic change in dimensions and often in the shape of the patterned features [9, 12, 14-16]. Fabrication of microstructures on carbon films or GC substrates via the base etching procedure would overcome these problems.

The work described here demonstrates initial efforts aimed at micromachining GC structures via ECP in basic media. TM SFM is employed to track the dependency of etched depth on anodization potential. SEM is used to establish the directionality of the etching process and also provide

electron micrographs of the microstructures fabricated on GC. Results obtained in this study show that the etching procedure is able to produce GC microstructures.

## **Experimental**

**Reagents.** All reagents were used as received. Aqueous sodium hydroxide solution was prepared using distilled/deionized (18 M $\Omega$ /cm) water (Barnstead, Dubuque, IA) and purged with nitrogen gas for 10 min. prior to use.

**Electrode Preparation and Electrochemical Measurements.** The GC-20 electrodes (Tokai GC-20, Electrosynthesis Corp., NY) were prepared as described in Chapter II. Polished GC substrates were patterned by using standard photoresist-based microfabrication techniques as described in Chapter II.

**SFM Conditions.** TM SFM images were obtained as explained in Chapter II.

**SEM Conditions.** Scanning electron microscopy analysis of the GC substrates was carried out using a JOEL model 6301FXV scanning electron microscope at an acceleration voltage of 15-20 kV and a working distance of 4-5 mm. Image analysis was performed with commercial software (Image Tool, version 2.00, University of Texas Health Science Center in San Antonio) for measuring features on the GC substrates.

## Results and Discussion

The initial work reported here is aimed at determining the dependency of etched depth on anodization potential as well as establishing the etching directionality at the sidewalls of the depressions. These two important etching parameters were investigated using TM SFM and SEM surface characterization techniques. Topographic TM SFM images were obtained for GC surfaces oxidized in 0.1 M NaOH at 1.8 V for various oxidation times. The cross section line scan from these topographic images provides the etched depth as described earlier in Chapter II. All the line scans obtained exhibit flat profile of the bottom of the depressions similar to that shown in Figure 2.5. This suggests that the SFM tip is able to probe the entire depth of the depressions. The length of the tip mounted on the cantilever is about 2-3  $\mu\text{m}$ . Thus, the tip length is sufficient to probe depression depths reported in this work given that the features probed were insensitive to the tips pyramidal shape.

Figure 4.1 is a plot of the depression depth as a function of anodization time. The plot illustrates that the etched depth is controllable over the time scale studied. As established in Chapter III, initial etching involves removal of the microparticle polishing layer known to exist on polished GC surfaces. It is evident from Figure 4.1 that removal of this polishing layer proceeds more rapidly as compared to rate at which bulk carbon material is etched.

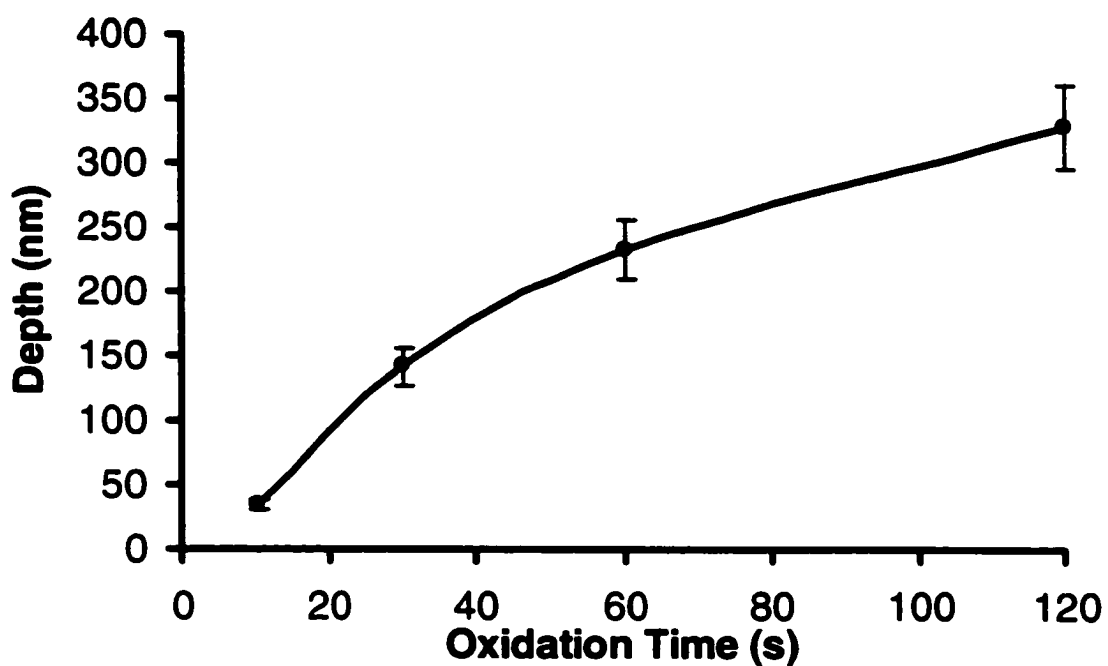


**Figure 4.1 :** Plot of etching depth (nm) vs. oxidation time (s) for ECP at 1.8 V in 0.1M NaOH. The curve through the points does not represent any theoretical fit to data. It only serves as a good guide to the eye.

The particulate nature of the polishing layer likely contributes to its rapid etching as compared to the break up of GC lattice. The polishing layer is more porous than the GC substrate and thus would allow easier penetration of the hydroxide ions, which are thought to initiate the etching process [17, 18]. Furthermore, the rapid removal of the polishing contaminants is likely assisted by gas evolution that occurs during ECP, which could physically dislodge the finely divided carbon from the surface. The plot in Figure 4.1 shows an oxidation time of 2 min. that results in a depression depth of ~ 330 nm. Dissolution of the photoresist mask in 0.1 M NaOH was found to occur between 3 to 15 min. of exposure making evaluation of longer etching times difficult. The dissolution rate is thought to depend on the photoresist film thickness and also the duration the photoresist is exposed to UV light during the patterning procedure. Towards achieving deeper etching with the same photoresist mask, the effect of increasing the anodization potential was investigated.

Figure 4.2 shows a plot of etched depth versus anodization potential at a constant oxidation time of 1 min. The plot indicates that the amount of carbon material removed by ECP in basic media is dependent on anodization potential. For example, ECP in base for 1 min. at 3.0 V etches the GC surface to a depth of ~ 989 nm as compared to a depth of ~ 235 nm etched at 1.8 V for the same oxidation period. The mechanism resulting in the removal of carbon material upon ECP in base is not clearly understood. This limits a better understanding of how various factors influence the etching process.

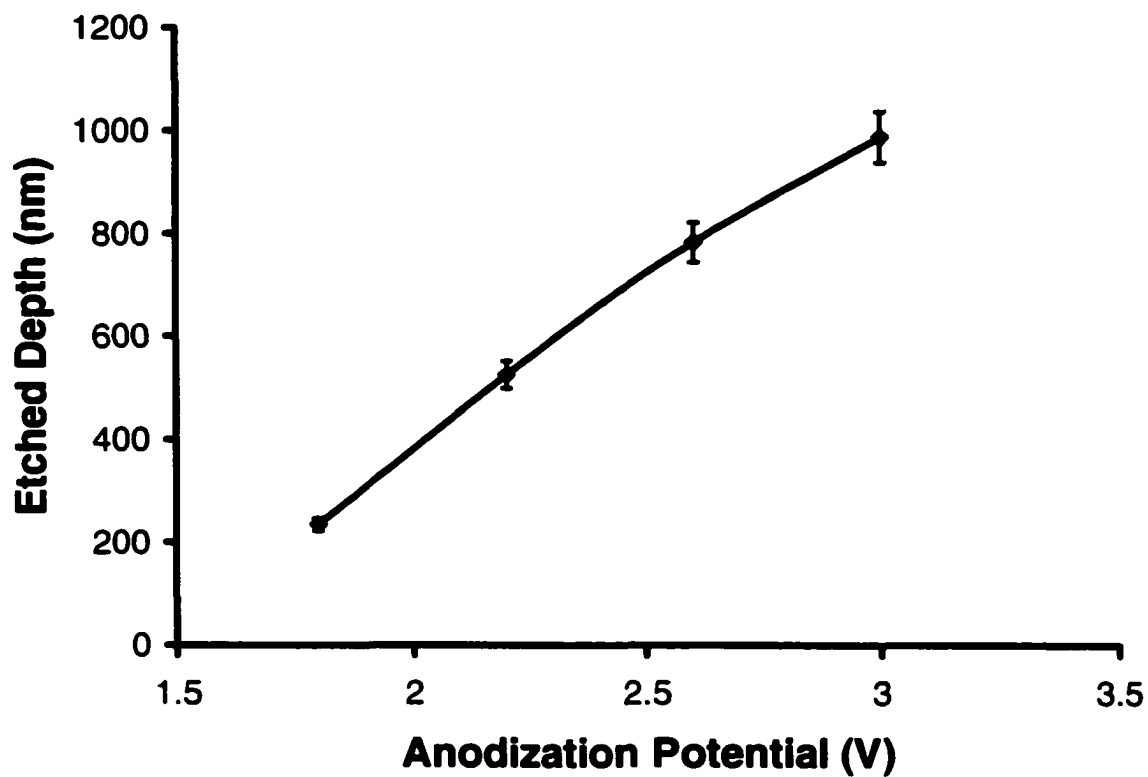


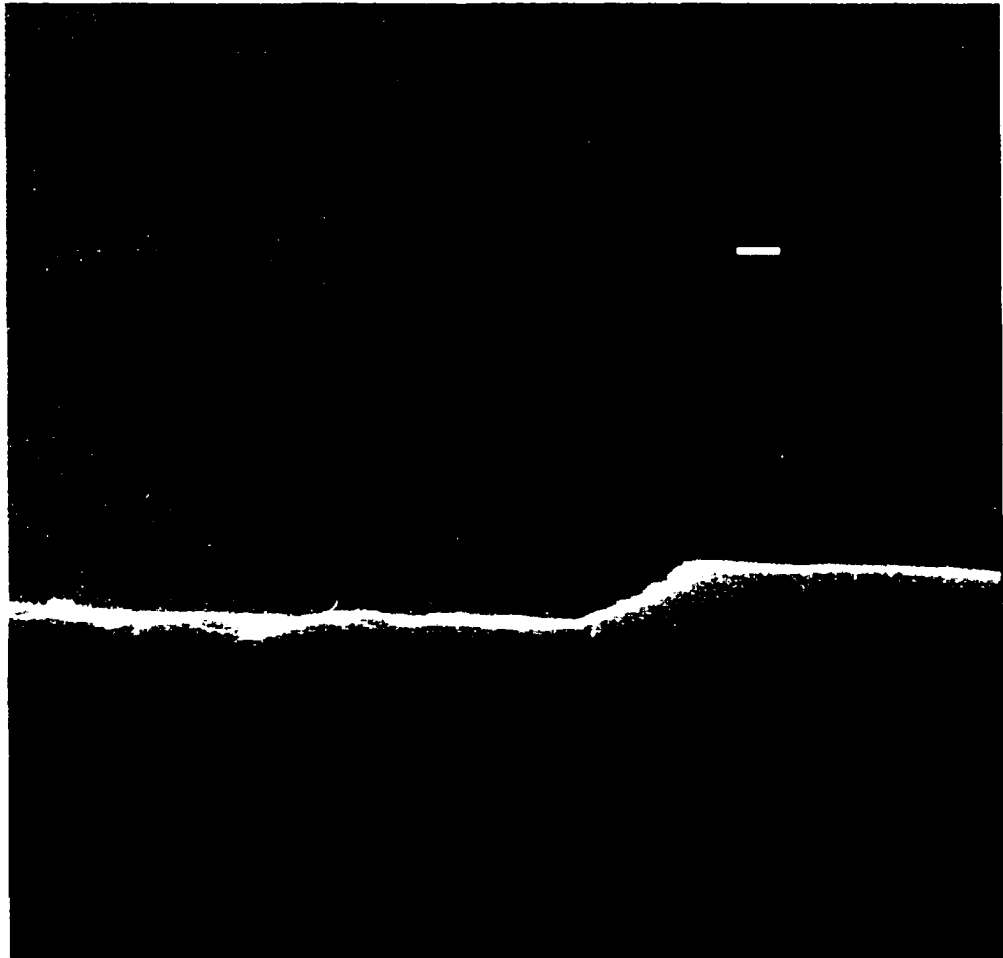
**Figure 4.2 :** Plot of etching depth (nm) vs. anodization potential (versus Ag /AgCl reference electrode). The curve through the points does not represent any theoretical fit to data. It only serves as a good guide to the eye.

However, several studies have reported injection of anions below the graphite [19, 20] and GC [17, 21] surfaces following anodic treatment. Smyrl *et al.* have proposed that anodization of GC in NaOH electrolyte leads to intercalation of ions, (*e.g.* OH<sup>-</sup>) below the GC surface. This causes localized build up of stress, swelling, and the formation of mesas [17]. Intercalation of anions under similar conditions have been observed to induce swelling of graphite. The amount of anions injected below the surface of graphite and GC has been reported to increase with anodization potential [17]. This indicates that the applied overpotential is an important parameter in determining the rate at which carbon material is removed from GC surface. In most micromachining applications, it is desirable to have some method of controlling the depth of etching. Figure 4.1 and 4.2 show that both anodization potential and time may be used to achieve control in etched depth.

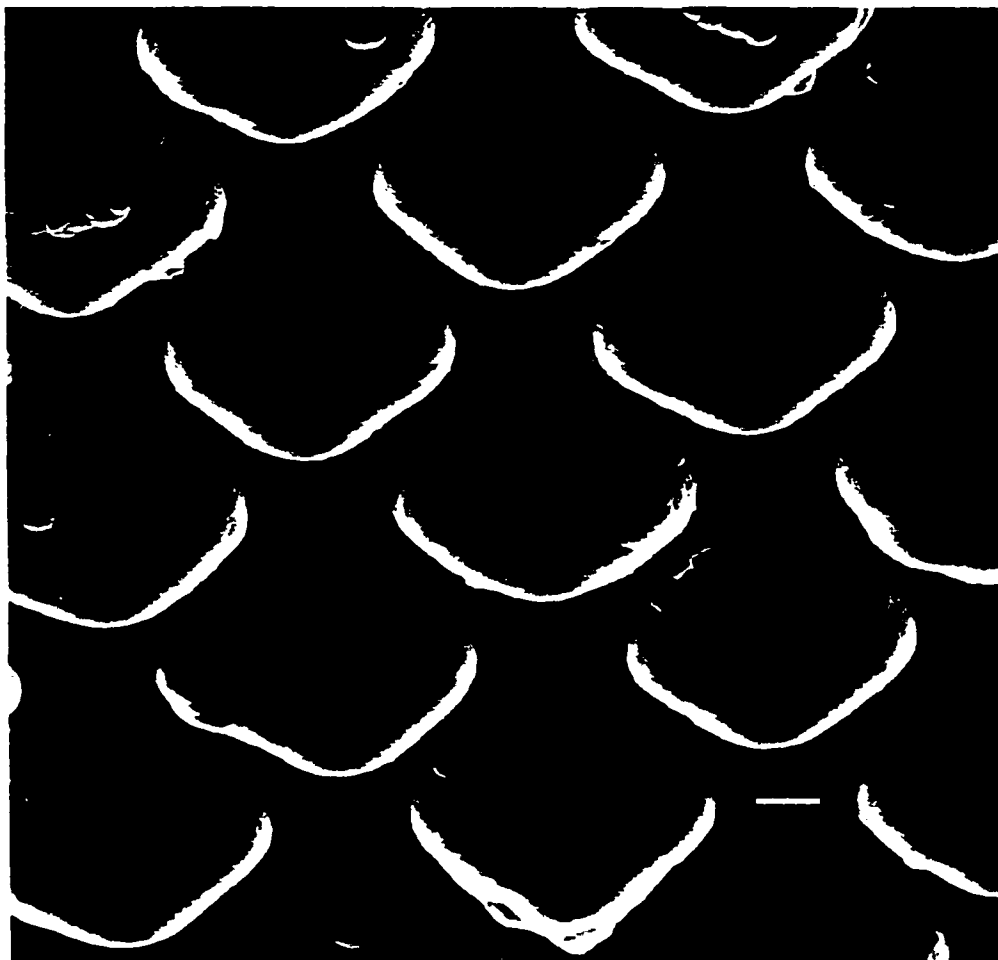
The directionality of the etching process is also probed in this study. This may be of great importance in the application of micromachined GC structures. For example, the flow of the liquids through microchannels fabricated on GC substrate would likely be influenced by the angle of the sidewalls, *i.e.* if they face inwards or are vertically oriented. As noted earlier in Chapter II, the pyramidal shaped TM SFM tip is unable to probe steep walls. Thus, SEM was employed to determine the directionality of the etching process.

Figure 4.3 shows a SEM image of a cross-sectioned sample of GC in which pits were etched by oxidation for 30 s at 1.8 V. The electron micrograph clearly shows that the sidewalls of the depressions etch inwards (pointed arrow). The direction of the etching process observed in Figure 4.3 is characteristic for isotropic etchants, in which the lateral etching under a mask proceeds at the same rate as that in the vertical direction [22].

GC microstructures with various geometries were micromachined via the base etching procedure. Figures 4.4 to 4.6 show electron micrographs for some of the structures micromachined on GC substrates. Figure 4.4 shows a series of picovials machined on GC following 15 min. ECP in 0.1 M NaOH at 3.0 V. The picovials are ~ 25  $\mu\text{m}$  wide and ~ 7  $\mu\text{m}$  in depth. The small volume of the picovials (~ 4 pL) makes them suitable for microanalysis where the amount of sample is limited. The shape of some of the picovials shown in Figure 4.4 is non-uniform especially along the walls. This is partly attributed to defective regions of the copper grid mask used in the patterning procedure. The bottom of some of the wells also exhibit defects. These defects are pits of several micrometers in diameter, which arise from trapped gas bubbles formed during the heat treatment of the precursor polymer [2, 4]. The pits get exposed during the etching process and appear to also distort the shape of the picovials especially along the walls. The etched surface appears to be rougher than that of polished GC.



**Figure 4.3:** Scanning electron micrograph showing the cross-sectional profile of a depression. The sides of the depressions etch inwards as shown by the arrow.



**Figure 4.4:** Scanning electron micrograph showing picovials fabricated on GC substrate by base etching at 3.0 V for 15 min.

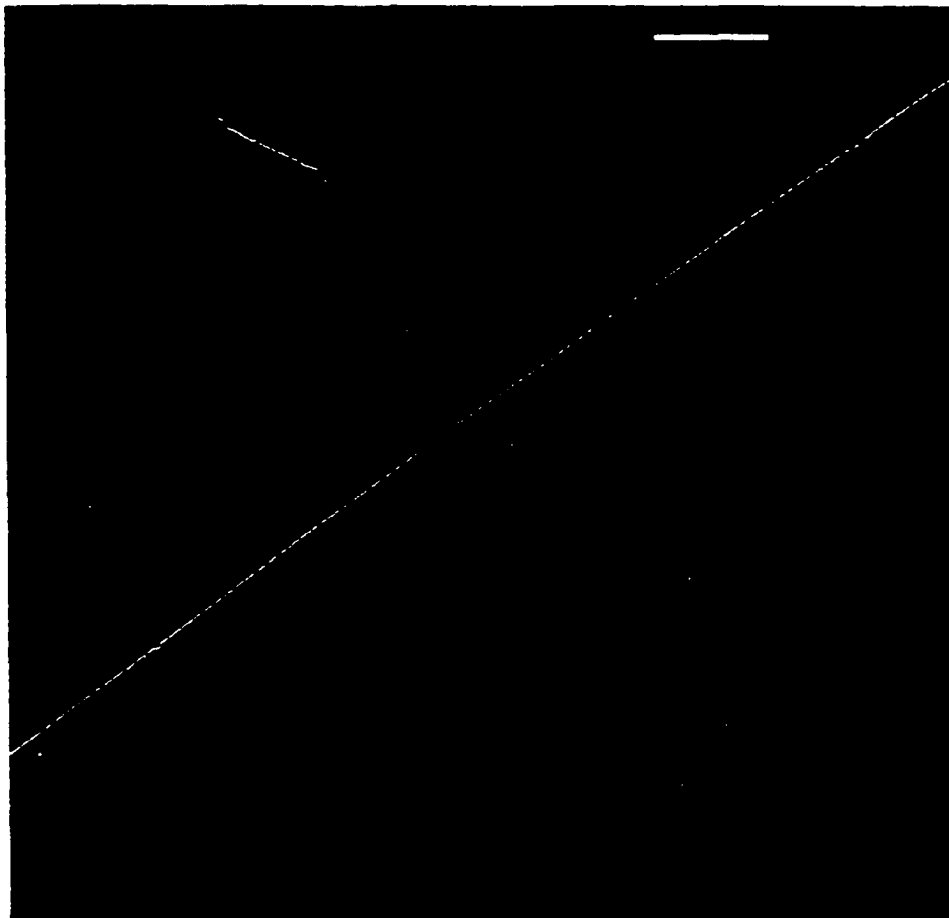


**Figure 4.5:** Scanning electron micrograph showing a network of microchannels machined on GC substrate via base etching procedure at 3.0 V for 5 min.

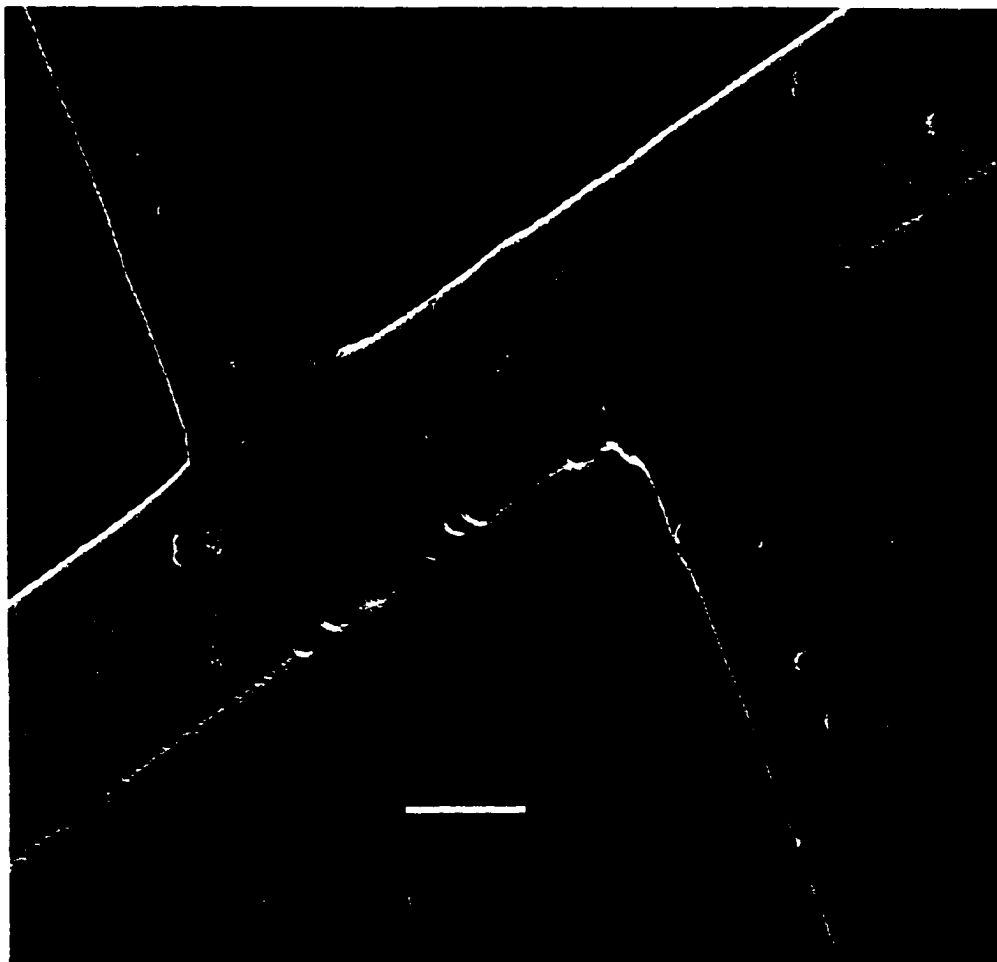


**Figure 4.6:** Scanning electron micrograph showing the “double T junction” of Figure 4.5 at a higher magnification.

Figure 4.5 shows a network of microchannels machined on GC substrate via base etching at 3 V for 15 min. The mask used here is specifically designed to fabricate microfluidic systems on glass chips [23]. The wider channels in Figure 4.5 are ~ 160  $\mu\text{m}$  wide while the more narrow ones range between ~ 25  $\mu\text{m}$  and ~ 35  $\mu\text{m}$ . The depth of the entire network of microchannels is ~ 7  $\mu\text{m}$ . Figure 4.6 is a magnification of Figure 4.5 at the “double T” junction. Harrison and coworkers have demonstrated that individual cells can be manipulated and reacted with various reagents using electroosmotic pumping on a micromachined glass chip [23]. Typical cross-sectional dimensions of the narrower channels fabricated on glass chips range from 10-50  $\mu\text{m}$  [23-26]. The dimensions of the microchannels machined on GC substrates shown in Figure 4.5 fall within this range. Thus, initial results reported here demonstrate the ability of the base etching procedure in fabricating microstructures on GC substrates.

### **Conclusion**

Results obtained in this Chapter indicate that the etched depth following ECP in basic media is dependent on anodization time and potential. Thus, the etched depth is controllable over the timescale and potential investigated. SEM results show that the sidewalls of the depressions etch inwards. Initial efforts demonstrate the potential of the etching procedure to micromachine structures on GC.

**References**

1. N. L. Pocard, D. C. Alsmeyer, R. L. McCreery, T. X. Neenan, and M. R. Callstrom, *J. Mater. Chem.* **2**:771 (1992).
2. K. Kinoshita, , John Wiley & Sons Inc., New York, 1988, p. 226 .
3. W. E. van der Linden and J. W. Dieker, *Anal. Chim. Acta* **119**:1 (1980).
4. R. L. McCreery, ,in *Electroanalytical Chemistry* Vol. 17 (A. J. Bard, ed.), Marcel Dekker, New York, 1991, p. 221.
5. S. Yamada and H. Sato, *Nature* **193**:261 (1962).
6. G. M. Jenkins and K. Kawamura, *Nature* **231**:175 (1971).
7. D. W. McKec, *Annu. Rev. Mater. Sci.* **3**:195 (1973).
8. R. C. Engstrom, *Anal. Chem.* **54**:2310 (1982).
9. R. Kosteki, X. Song, and K. Kinoshita, *Electrochem. Solid-State Lett.* **2**(9):465 (1999).
10. G. Sreenivas, S. S. Ang, I. Fritsch, W. D. Brown, G. A. Gerhardt, and D. J. Woodward, *Anal. Chem.* **68**:1858 (1996).
11. K. Morita and Y. Shimizu, *Anal. Chem.* **61**:159 (1989).
12. S. Ranganathan, R. L. McCreery, S. M. Majji, and M. Madou, *J. Electrochem. Soc.* **147**(1):277 (2000).
13. G. T. A. Kovac, K. Petersen, and M. Albin, *Anal. Chem.*:407 A (1996).
14. O. J. A. Schueller, S. T. Brittain, C. Marzolin, and G. M. Whitesides, *Anal. Chem.* **9**:1399 (1997).
15. F. Kong, J. Kim, X. Song, M. Inaba, K. Kinoshita, and F. McLarnon, *Solid-State Lett.* **1**:39 (1998).

16. J. Kim, X. Song, K. Kinoshita, M. Madou, and R. White, *J. Electrochem. Soc.* 145:2314 (1998).
17. W. H. Smyrl, R. T. Atanasoski, L. Atanasoska, L. Hartshorn, M. Lien, K. Nygren, and E. A. Fletcher, *J. Electroanal. Chem.* 264:301 (1989).
18. C. Kozlowski and P. Sherwood, *J. Chem. Soc. Faraday Trans. 1* 81:2745 (1985).
19. A. J. Arvia, *Surf. Sci.* 181:78 (1987).
20. A. A. Gewirth and A. J. Bard, *J. Phys. Chem.* 92:5563 (1988).
21. K. Itaya, K. Higaki, and S. Sugawara, *Chem. Lett.*:421 (1988).
22. K. E. Peterson, in *Proc. IEEE*, Vol. 70, 1982, p. 420.
23. P. C. H. Li and D. J. Harrison, *Anal. Chem.* 69:1564 (1997).
24. C. S. Effenhauser, A. Manz, and H. M. Widmer, *Anal. Chem.* 65:2637 (1993).
25. D. J. Harrison, A. Manz, Z. Fan, H. Ludi, and H. M. Widmer, *Anal. Chem.* 64:1926 (1992).
26. D. J. Harrison, K. Fluri, K. Seiler, Z. Fan, C. S. Effenhauser, H. Ludi, and H. M. Widmer, *Science* 261:895 (1993).

## CHAPTER V

### **Real time Mapping of the Electrochemical Oxidation of Glassy Carbon Electrodes with Friction Force Microscopy.**

#### **Introduction**

In Chapter II, the first application of phase contrast tapping mode scanning force microscopy (TM-SFM) for the compositional mapping of electrochemically pretreated (ECPed) glassy carbon (GC) electrodes was demonstrated. The work presented in this Chapter is aimed at applying scanning force microscopy (SFM) to track the initial oxidation mechanism of the ECP processess. In general, TM SFM is slow and imaging *in situ* is complicated by cantilever damping by liquid. Due to these experimental limitations, contact mode SFM is utilized to monitor, in real time, the compositional changes induced on GC surface by ECP. Specifically, friction (or lateral) force microscopy SFM is used to study the electrochemically modified surfaces.

The lack of a detailed understanding of the activation mechanism of the pretreatment methods greatly limits the ability of electrochemists to gain control of the reactivity at electrode surfaces. In this Chapter, the ability of *in situ* friction force SFM to track oxidation nucleation of ECP processes is exploited. Several research groups have demonstrated that lateral or friction force SFM (contact mode) is sensitive to surface chemistry and can be used to map differences in surface composition [1-3]. The amount of torsional

bending or twisting of the cantilever is a measure of the amount of friction between a SFM tip and surface. The friction ( $f$ ) between a SFM tip and sample contact can be described by Kendall's equation [4] as follows:

$$f = \mu F_N + 3\pi R\gamma^*\mu + \mu(6\pi R\gamma^*F_N + 9\pi^2 R^2 \gamma^{*2})^{1/2} \quad (5.1)$$

where  $\mu$  represents microscopic coefficient of friction,  $F_N$  is the normal force,  $R$  is the radius of the tip and  $\gamma^*$  is the interfacial free energy of the tip-sample contact. Interfacial free energy ( $\gamma^*$ ) depends on the surface-solvent (SL), tip-solvent (TL) and tip-surface (TS) free energies and is expressed as  $\dot{\gamma} = \gamma_{SL} + \gamma_{TL} - \gamma_{TS}$ . Equation 5.1 shows that the measured friction in lateral force SFM depends on normal force ( $F_N$ ), surface chemistry ( $\dot{\gamma}$ ) and tip-sample contact area (derived from  $R^2$ ). Images in friction force SFM are usually collected at constant imaging force. As a result,  $F_N$  and radius of the tip are kept constant in equation 5.1. Thus, a frictional image can be considered as a map of surface composition. Results obtained in this Chapter show frictional contrast between oxidized and non-oxidized regions on patterned GC electrodes. Importantly, frictional force SFM is able to map out initial nucleation sites for the electrochemical oxidation processes.

## Experimental

**Reagents.** The following reagents were used as received: acetone (Caledon), isopropanol (ACP Chemicals) and activated carbon (Caledon). Buffer solutions were prepared with reagent grade 5.0 mM  $\text{KHC}_8\text{H}_4\text{O}_4$  and 2.2 mM HCl (pH 3), 5.0 mM  $\text{KH}_2\text{PO}_4$  and 2.9 mM NaOH (pH 7), and 2.5 mM  $\text{NaHCO}_3$  and 1.1 mM NaOH (pH 10). All reagents were used as received. Aqueous solutions were prepared using distilled /deionized ( $18\text{M}\Omega/\text{cm}$ ) water (Barnstead, Dubuque, IA). All solutions used for electrolysis were purged with nitrogen gas for 10 min prior to use.

### **Electrode Preparation and Electrochemical Pretreatment (ECP).**

GC-20 electrodes (Tokai GC-20 Electrosynthesis Corp., NY) were prepared as described in Chapter II. Polished GC electrodes were patterned by using standard photoresist-based microfabrication techniques as explained previously in Chapter II. ECP was achieved by poisoning a polished GC electrode at +1.80 V vs Ag/AgCl (reference electrode) for a selected period of time in 1 M  $\text{H}_2\text{SO}_4$ . A three electrode cell was used with Pt wire as a counter electrode. The cell was connected to a model 175 (Princeton Applied Research, NJ) potentiostat. ECPed patterned GC electrodes were sonicated in acetone for 10 min to remove the photoresist mask.

**SFM Conditions.** *In situ* SFM experiments were carried out in the electrochemical fluid cell of a Nanoscope III MultiMode system (Digital Instruments, Santa Barbara, CA). Contact mode topographic and lateral force

images were collected simultaneously. Following ECP, the fluid cell was flushed with buffer solution (pH 3, 7 or 10) several times then allowed to equilibrate for at least 30 min before capturing images. Silicon nitride cantilevers (Digital Instruments) with nominal spring constants of 0.06 N/m were used. All the images shown here were collected at normal forces < 10 nN. The scan rate was between 5 and 10 Hz.

## **Results and Discussion**

As noted earlier in Chapter I, ECP of GC in acidic media at high positive potentials produces a surface film that has properties similar to graphite oxide [5, 6]. The mechanism responsible for the activation effects is believed to involve the generation of surface oxides [6-8]. In this Chapter, efforts are focused on tracking the nucleation and growth of the oxidation process. Towards this end, the frictional contrast between modified and unmodified regions on patterned GC electrodes is probed. First, SFM images collected in acidic and basic media for GC electrodes patterned with photo-resist and ECPed in acidic electrolyte are presented. This is followed by presentation of frictional mapping results for non-patterned GC electrodes ECPed in acidic media.

**SFM Imaging of Patterned GC Electrode ECPed in Acid.** The electrode preparation method developed in Chapter II (Figure 2.1) was used to produce patterned GC surfaces. Figure 5.1 contains 140 x 140  $\mu\text{m}^2$  topographic and lateral force images of a patterned, oxidized GC surface

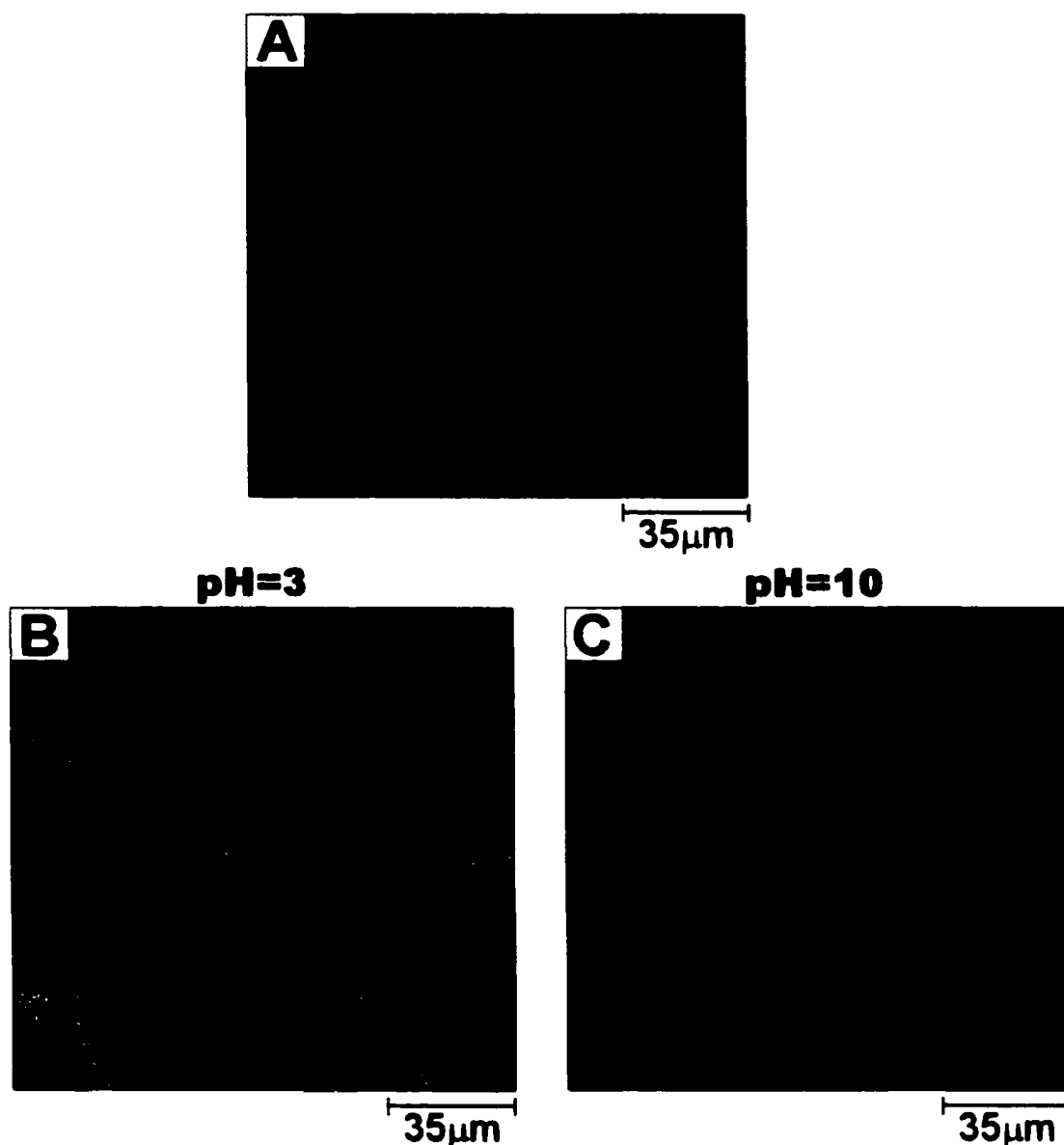


**Figure 5.1:** 140 x 140  $\mu\text{m}$  SFM images of GC surfaces oxidized at 1.8 V in 1 M  $\text{H}_2\text{SO}_4$  for 5 min through a photoresist pattern. (A) Topographic image of activated patterned GC surface collected in pH 3 buffer (z-scale 150 nm). Part B (z-scale 0.4 V) and C (z-scale 0.4 V) are the corresponding friction images collected in pH 3 and 10 buffer media respectively.

imaged in acidic and basic media. Figure 5.1A is the topographic image of a patterned GC electrode collected in pH 3 buffer after 5 min. oxidation in 1 M  $\text{H}_2\text{SO}_4$  at 1.8 V. The morphology of the modified region and that masked with photo-resist are indistinguishable. The main features in Figure 5.1-A are polishing scratches, which resemble those observed in Chapter II and reported in previous studies [5, 9-11]. Topographic images for a GC surface oxidized for 5 min. do not show any evidence for a distinct EGO layer, similar to results obtained in Chapter II using TM SFM. Since no evidence of the graphite oxide like layer was noted at lowered imaging forces with TM SFM, it is unlikely that the tip in contact-mode SFM is plowing through the oxide layer. Possibly longer anodization time is required for the EGO film to be observable with SFM. However, the color of the GC surface was observed to change from black to greenish upon ECP in acid, which is consistent with presence of a nearly transparent graphite oxide layer [6, 12].

Significant differentiation between oxidized and non-oxidized GC surface is observed in the friction force images of parts B and C of Figure 5.1. Figure 5.1-B was collected simultaneously with the topographic image in Figure 5.1-A in pH 3 buffer. The honeycomb regions were exposed for electrochemical modification while the grids were masked from ECP. In Figure 5.1-B the regions that were exposed to the ECP procedure exhibit a lower frictional signal than the unmodified polished GC.

Part C of Figure 5.1 is a friction force image obtained on the same area as Figure 5.1-B but under pH 10 buffer. In this case, an inversion in frictional

contrast is observed relative to Figure 5.1-B (pH 3 buffer). The modified regions now exhibit a higher frictional signal. The observed inversion of contrast with pH is reversible indicating that the EGO film is not dissolving in pH 10 buffer. Varying the pH of the imaging buffer did not induce any observable changes in the topographic images.

It is known that ECP of GC in acidic solution at high positive potentials (e.g. 1.8 V vs SCE) results in the formation of a surface film that exhibits properties similar to graphite oxide [5, 6, 13]. XPS [14] and FTIR [15] studies of the resultant graphitic oxide film formed in acidic conditions have revealed the presence of surface oxide functionalities such as phenolic and carboxylate groups. In addition previous studies have shown that carbon electrodes are responsive to changes in solution pH by exhibiting shifts in voltammetric features that arise from surface oxides [16, 17]. Thus, the pH of the buffer solution under which the modified GC surface is obtained determines the degree of ionization of the surface-confined acid groups. At high pH (e.g. pH 10), surface carboxylates should be deprotonated and at low pH (e.g. pH 3) the carboxylate groups are protonated.

The dependency of frictional contrast on pH in Figure 5.1 argues that the friction at the SFM tip-sample junction depends on ECP induced changes in surface chemistry. XPS analysis of polished GC ECPed in acid has revealed increase in O/C ratio [12, 18], and elemental analysis indicates that about 25% of EGO film is oxygen [6]. *In situ* FTIR spectroscopic study reported increase in surface oxides for polished GC ECPed in acidic media at

1.85 V. Results from this work suggest formation and/or transformation of phenolic-like groups into surface oxide species such as quinone, acid anhydride, and carboxylic groups following activation in acidic electrolytes [15].

XPS studies have also revealed that part of the oxygen on the modified GC surface is in the form of carboxylate groups [19]. Oxide catalysis at polished GC ECPed in acid has been reported for  $\text{Fe}^{+3/+2}(\text{aq})$ ,  $\text{Eu}^{+3/+2}(\text{aq})$ , and  $\text{V}^{+3/+2}(\text{aq})$  aquated redox systems. The inhibition of oxide catalysis on acid activated GC by silanization indicates the presence and involvement of  $-\text{OH}$ ,  $-\text{COOH}$  or similar hydroxyl-containing functional groups in the inner-sphere route [20]. The spatial distribution of carboxylates on ECPed carbon fiber electrode surfaces has been visualized by derivatizing the surface carboxylates with a fluorescence tag [21, 22]. In addition, significant increase in background currents measured on the acid modified surfaces is consistent with the presence of carbon-oxygen functionalities on the anodized GC surface [9, 18, 23, 24]. Thus, dependency of frictional signal on pH as evident in part B and C of Figure 5.1 is consistent with presence of surface oxides.

All frictional SFM images reported in this Chapter were collected at a constant load. Thus, observed frictional contrast is generated by differences in surface chemistry, which governs interfacial work of adhesion ( $W_{\text{st}}$ ) and /or mechanical properties, which influence contact area (equation 5.1). The dependency of frictional contrast on pH likely suggests that the observed contrast is governed by surface chemistry.

The  $\text{Si}_3\text{N}_4$  probe tip has a surface isoelectric point of  $\sim 6$  [25] and surface-confined carboxylic acid groups display a range of pKa values of 5.5 to  $> 8$  [26, 27]. At low pH (e.g. pH 3), the carboxylic acid groups are protonated while the tip is neutral. Adhesion measurements at pH 3 indicate a weaker tip-ECPed GC interaction ( $\sim 0.10$  nN) relative to the tip-polished GC ( $\sim 0.24$  nN). Since electrostatic interactions are likely inoperative at this low pH, results obtained here suggest a higher  $W_{\text{ts}}$  in the tip-polished GC junction. The layer of polishing debris is reported to contain carbon microparticles and is thus likely to be somewhat hydrophobic while the oxidized region is very hydrophilic. A higher solvent ( $\text{H}_2\text{O}$ ) reorganization energy at the more hydrophobic polished region may be responsible for the frictional contrast observed at pH 3.

The patterned GC surfaces ECPed in acid undergo an inversion of frictional contrast when imaged at high pH. This suggests the involvement of proton exchange. At pH 10, the  $\text{Si}_3\text{N}_4$  tip will be significantly de-protonated as well as the oxidized region. Adhesion measurements suggest a stronger tip-ECPed GC interaction ( $\sim 1.3$  nN) relative to the tip-polished GC ( $\sim 0.20$  nN). The adhesion values at polished GC are similar at both pH indicating that the contrast reversal is due to changing tip-sample interaction at the oxidized region. At pH 10,  $W_{\text{ts}}$  is higher at the oxidized region. Although a number of surface parameters may be operative, strong interactions such as dipole-dipole or ion-dipole bonding between the tip and surface may contribute at higher pH. Although the specifics of the observed frictional contrast are not

completely understood, the main focus of the work reported in this Chapter was to exploit the dependency of frictional contrast on pH in tracking oxidation nucleation of the ECP process. The results obtained from these efforts are presented below.

***In situ* SFM Imaging of Unpatterned GC Electrodes.** Results from Figure 5.1 demonstrates the ability of frictional force SFM to compositionally map oxidized GC surfaces. Importantly, the use of patterned GC electrodes allowed the calibration of the observed frictional contrast between oxidized and non-oxidized regions on the GC electrode. Oxidized regions exhibit a darker contrast than the background polished GC when imaged in pH 3 buffer. The contrast inverts when imaging in pH 10 buffer. Because regions of the GC electrode that are oxidized can be distinguished from the polished background, frictional force microscopy was applied to track the nucleation and growth of the ECP process. Towards this goal, the effect of ECP on polished GC electrodes was probed at very low anodization time scales (i.e.  $<1$  s). *In situ* SFM experiments were performed in the electrochemical fluid cell with the polished GC substrate being the working electrode (Figure 5.2). After ECP in acid, the imaging buffer was introduced into the fluid cell and upon thorough rinsing allowed to equilibrate for at least 30 min before collecting images.

Figure 5.3 shows SFM images of polished GC and acid-oxidized polished GC ECPed in 1M H<sub>2</sub>SO<sub>4</sub> for 0.5 s without pattern. All images in Figure 5.3 were collected at the same location on the GC electrode. Note the

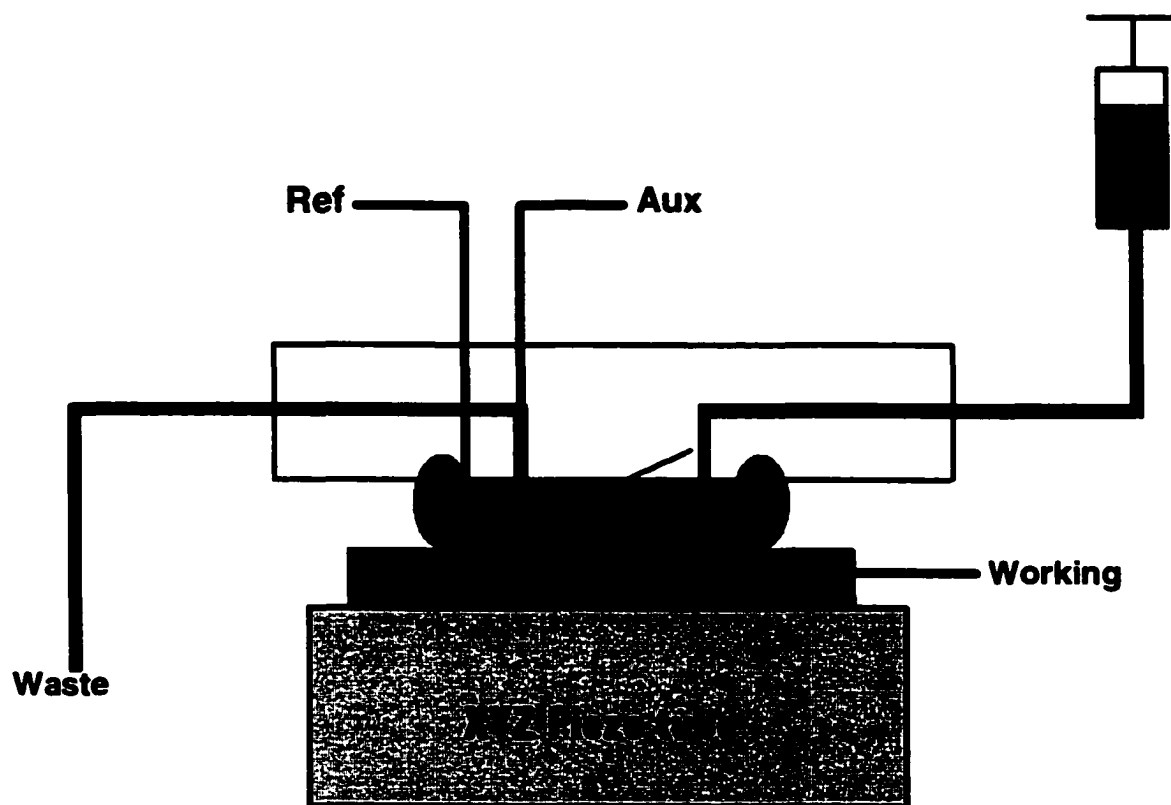


**Figure 5.2:** Schematic representation of a SFM electrolytic cell used for the *in situ* studies.

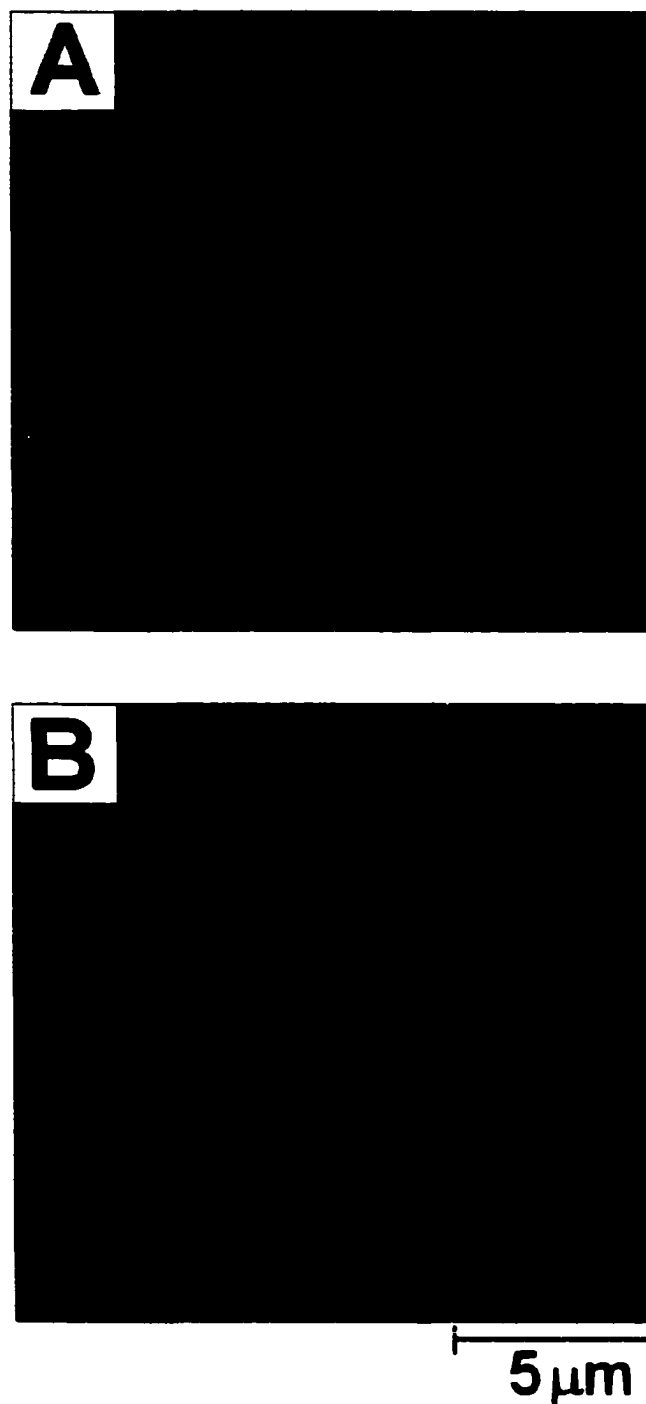


**Figure 5.3:** 15 x 15  $\mu\text{m}$  SFM images of GC surfaces collected *in situ*. (A) Topographic (z-scale 40 nm) and (B) Friction (z-scale 0.3 V) images of polished GC surface were collected simultaneously in pH 3 buffer. Part C and D (z-scale 0.3 V) are friction images collected at the same spot as Part A and B but after 0.5 s oxidation in acid in pH 3 and 10 buffer solutions respectively.

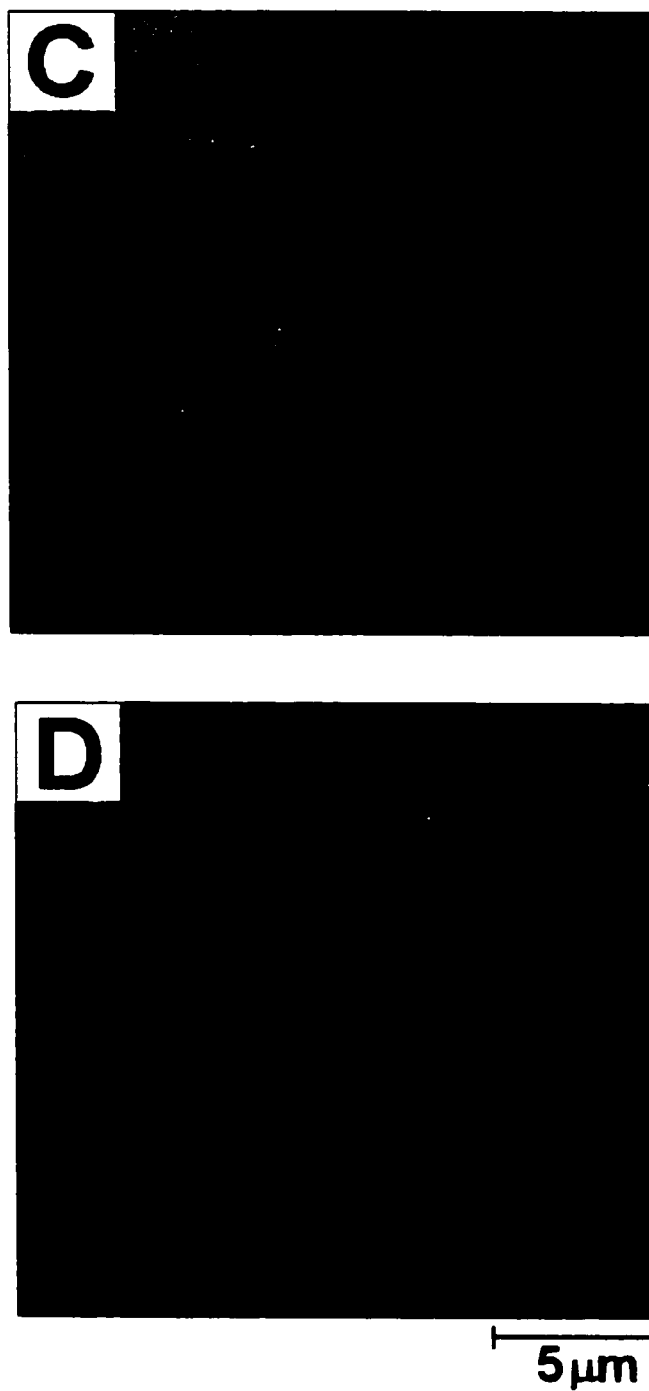


**Figure 5.3:** (continued)

“X” formed from polishing scratches near the center of each image. Parts A and B of figure 5.3 are the topographic and lateral force images, respectively of polished GC electrodes collected in pH 3 buffer. The topographic image (Figure 5.3-A) shows characteristic polishing scratches. The lateral force image of the polished GC (Figure 5.3-B) exhibits little contrast and displays a uniform friction signal. As noted earlier in this thesis, the surface of the unmodified polished GC electrode is covered with a thin layer of polishing debris. The polishing layer is stable at imaging forces of 1-10 nN and at scan rates from 5 to 10 Hz employed in this study. The constant frictional signal across the surface of the unmodified polished GC electrode is consistent with a uniform surface composition of the carbon microparticle layer.

After images for the polished GC electrode were collected, the cell was rinsed and filled with 1 M H<sub>2</sub>SO<sub>4</sub>. The GC electrode was then poised at a potential of 1.8 V for 0.5 s. The topographic image following this procedure (not shown) was similar to Figure 5.3-A, with no notable change in morphology. Part C of Figure 5.3 details the frictional image collected for the modified GC electrode in pH 3 buffer. This image was collected at the same spot as Figure 5.3-B. At this short oxidation time scale, alterations in the surface are evident. A lower frictional signal is observed along the polishing scratches while areas lacking these defects give a higher frictional signal. Based on earlier results obtained from calibrating the frictional contrast (Figure 5.1), a darker frictional contrast corresponding to oxidized regions in

pH 3 buffer. The regions exhibiting a higher frictional signal are not significantly altered at this low anodization time scale.

To further confirm this observation, a pH 10 buffer solution was introduced into the fluid cell and after a 30 min equilibration time, Figure 5.3-D was collected on the same spot as Figure 5.3-C. An inversion in frictional contrast is evident. The regions that showed lower frictional signal in acidic media now exhibit higher frictional signal at high pH consistent with results obtained in Figure 5.1-C. Importantly, the observed frictional contrast suggests that activation occurs initially at defects, namely the scratch sites. The polishing layer likely directs the nucleation of the oxidation process that results in the formation of carboxylate groups and other surface oxides.

As stated earlier, the microparticle layer is constituted of polishing debris and has been reported to have a thickness of ~20 nm [5]. During the polishing process there is uneven distribution of pressure on the GC surface. Surface alterations leading to the formation of polishing scratches result from high pressures induced by alumina particles on the GC surface. Thus, significantly reduction of the polishing layer thickness is expected at the high pressure points, namely the scratch sites. The variability in the polishing layer thickness results in a heterogeneous surface with the scratch sites being more readily exposed for activation. More studies aimed at exploring in greater detail the nucleation and growth mechanism of the EGO film were performed.

The evolution of the ECP process was further probed by sequentially expanding the period of time the electrode was held at 1.8 V versus Ag/AgCl. Figure 5.4 contains friction images collected in the same location in pH 3 buffer following several ECP steps. Thus, oxidized regions will exhibit a darker contrast. Part A of Figure 5.4 is the original polished surface. No significant change in friction signal is noted below an anodization time of 0.5 s. Figure 5.4-B depicts the friction image after 0.5 s oxidation in acid. The image shows a GC surface during the early stages of oxidation. This image is clearly distinct from the friction image of the unmodified polished GC (Figure 5.4-A). In this image, the scratch free regions appear relatively unmodified, exhibiting mainly a higher frictional signal. The observation of low friction contrast mainly at defects again suggests that oxidation leading to EGO film nucleates at these scratch sites.

Part C of figure 5.4 is the lateral force image of the electrode surface following 1.5 s activation. There is an increase in frictional contrast between the modified regions and the unmodified ones. In this image, more evidence is provided that nucleation of the EGO film nucleates at the scratch sites for polished GC electrodes. Further growth of the oxide film on the scratch-free sites is evident in images D and E of Figure 5.4 following 6.5 s and 16.5 s anodization times respectively.

During the collection of Figure 5.3 the SFM probe tip was withdrawn from the surface during ECP and thus, the tip is not expected to perturb the oxide film formation. Following 16.5 s oxidation time, a continuously oxidized

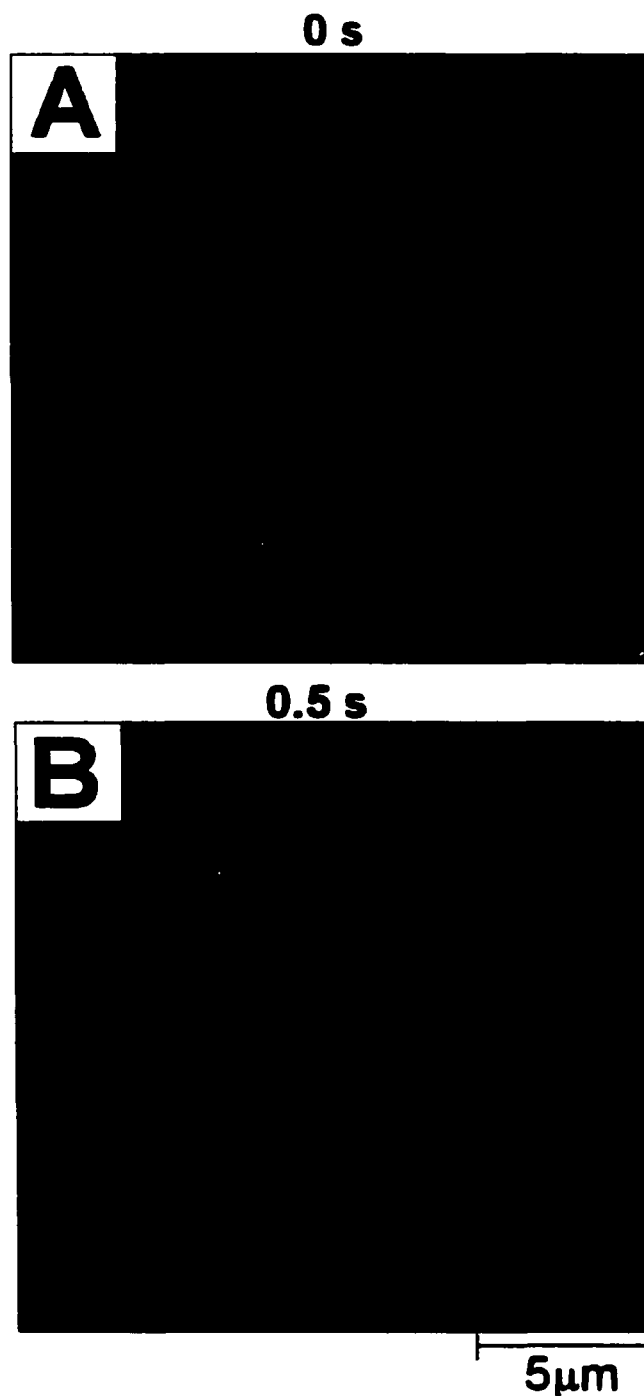


**Figure 5.4:** 15 x 15  $\mu\text{m}$  *in situ* SFM friction images collected in pH 3 buffer showing the nucleation and growth of the oxidation process. (A) Open circuit (B) After 0.5 s ECP in acid at 1.8 V versus Ag/AgCl. Parts C, D, and E are following 1.5, 6.5, and 16.5 s anodization time scales respectively. Z-scale is 0.3 V for all images.

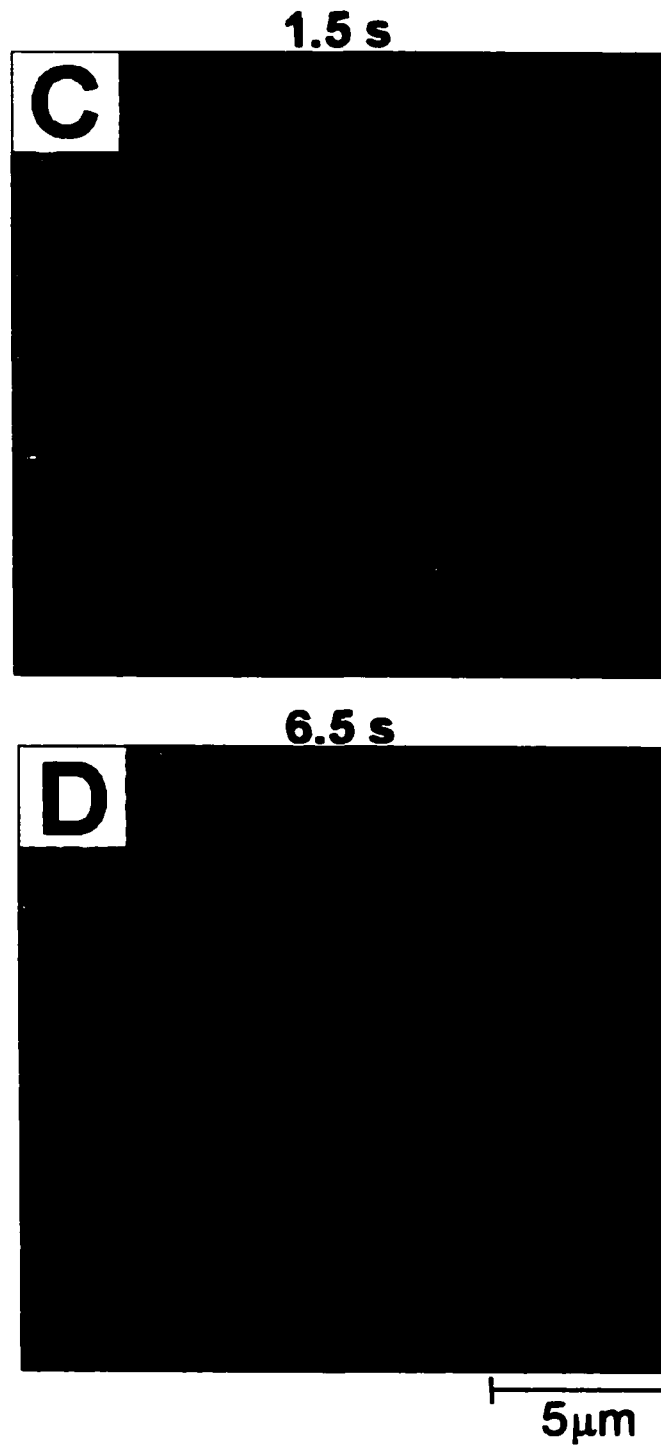


**Figure 5.4:** (continued)

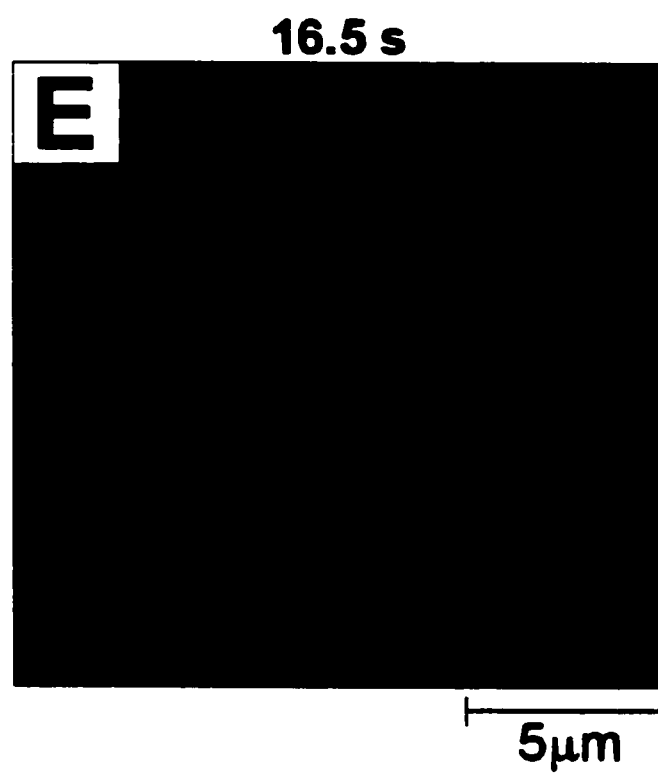


**Figure 5.3:** (continued)

surface results, as shown by the uniform friction in Figure 5.4-E. At longer anodization time (>16.5 s) there is no significant variation in friction signal across the GC surface. Thus, the friction images in figures 5.3 and 5.4 reveal that the ECP process initiates in polishing induced scratches and then continues to grow across the GC surface.

**Effect of the Polishing Layer on ECP Oxidation Nucleation Mechanism.** The surface of a GC electrode polished under aerobic conditions generally contains oxygen functionalities. XPS studies have reported increase in O/C ratio from 0.12 to 0.17 upon polishing in alumina/water mixture [28]. In addition, depth profile of the resulting polished surface revealed that the polishing procedure introduced oxygen to a depth of about 20-30 nm with majority of the oxygen existing in phenolic or hydroquinone form. Other studies have also reported the presence of carbon-oxygen functionalities on polished GC surface [18, 29-31]. Exposed surface oxides that are further oxidizable would likely act as nucleating sites for the ECP processes since they are easier to oxidize than the GC lattice.

XPS studies on carbon fibers ECPed in base have shown that alcohol/ketone groups already present at the edge sites of untreated carbon fibers undergo oxidation more readily than the graphite lattice [14]. Results obtained from Figure 5.3 and 5.4 suggest that oxidation proceeds most rapidly along the polishing scratches and at somewhat slower rate into the rest of the GC surface. This observation is attributed to a higher density of exposed oxidizable surface oxides present at defects. The ubiquitous

polishing layer is believed to be thinner in the scratches thereby allowing exposure of these surface oxides (Figure 5.5). These surface oxide functionalities act as nucleation chemical sites during the ECP processes.

To test this hypothesis, further studies were carried out with the aim of establishing if the polishing layer directs oxidation nucleation following ECP. Results obtained in Chapter III showed that ECP of polished GC in 0.1 M NaOH at 1.8 V for 10 s effectively removes the layer of polishing debris existing at the GC surface. This procedure was used to remove the polishing layer before ECP in 1 M H<sub>2</sub>SO<sub>4</sub>. Friction mapping studies similar to that in Figure 5.4 were then performed. Parts A and B of Figure 5.6 are 20 x 20 μm topographic and lateral force SFM images of unpatterned polished GC electrode ECPed in 0.1 M NaOH for 10 s at 1.8 V and collected in pH 3 buffer. Well defined and “focused” features such as polishing scratches are evident on the base etched surface (Figure 5.6-A), similar to images collected in Chapter II with TM SFM.

Part C of Figure 5.6 is a lateral force image obtained on the same area as Figure 5.6-B but after 2 s ECP in 1 M H<sub>2</sub>SO<sub>4</sub> at 1.8 V. This image was collected in pH 3 buffer. There is no significant differentiation between the starting surface (Figure 5.6-B) and the acid modified surface (Figure 5.6-C). Other lateral force images collected at both lower oxidation time scales (*e.g.* 0.1 s) as well as at longer oxidation time scales (*e.g.* >30 s) showed no significant frictional contrast. This suggests a different oxidation nucleation mechanism for GC surface free of the polishing layer. Prior removal of the

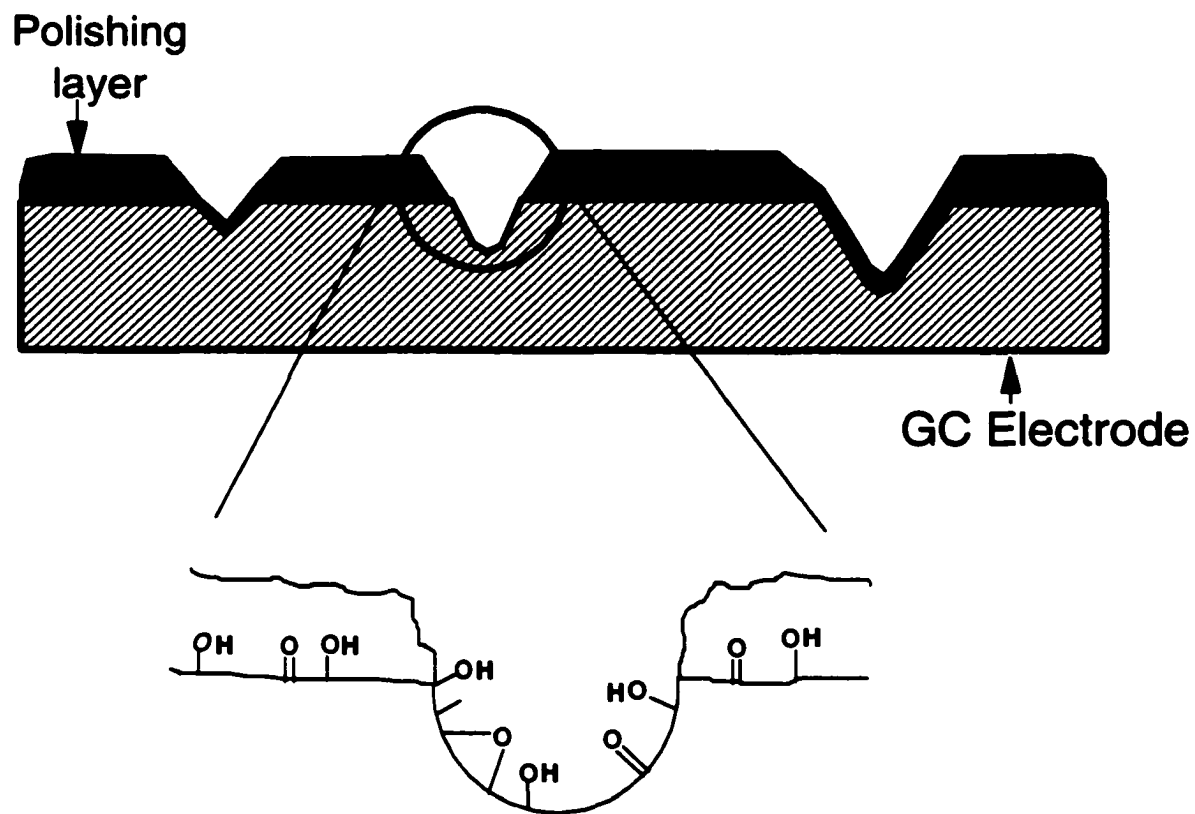


**Figure 5.5:** Schematic representation of a polished GC surface covered with a layer of polishing contaminants. Insert illustrates a magnification at a scratch site showing reduced polishing layer thickness which results in more exposed surface oxides.

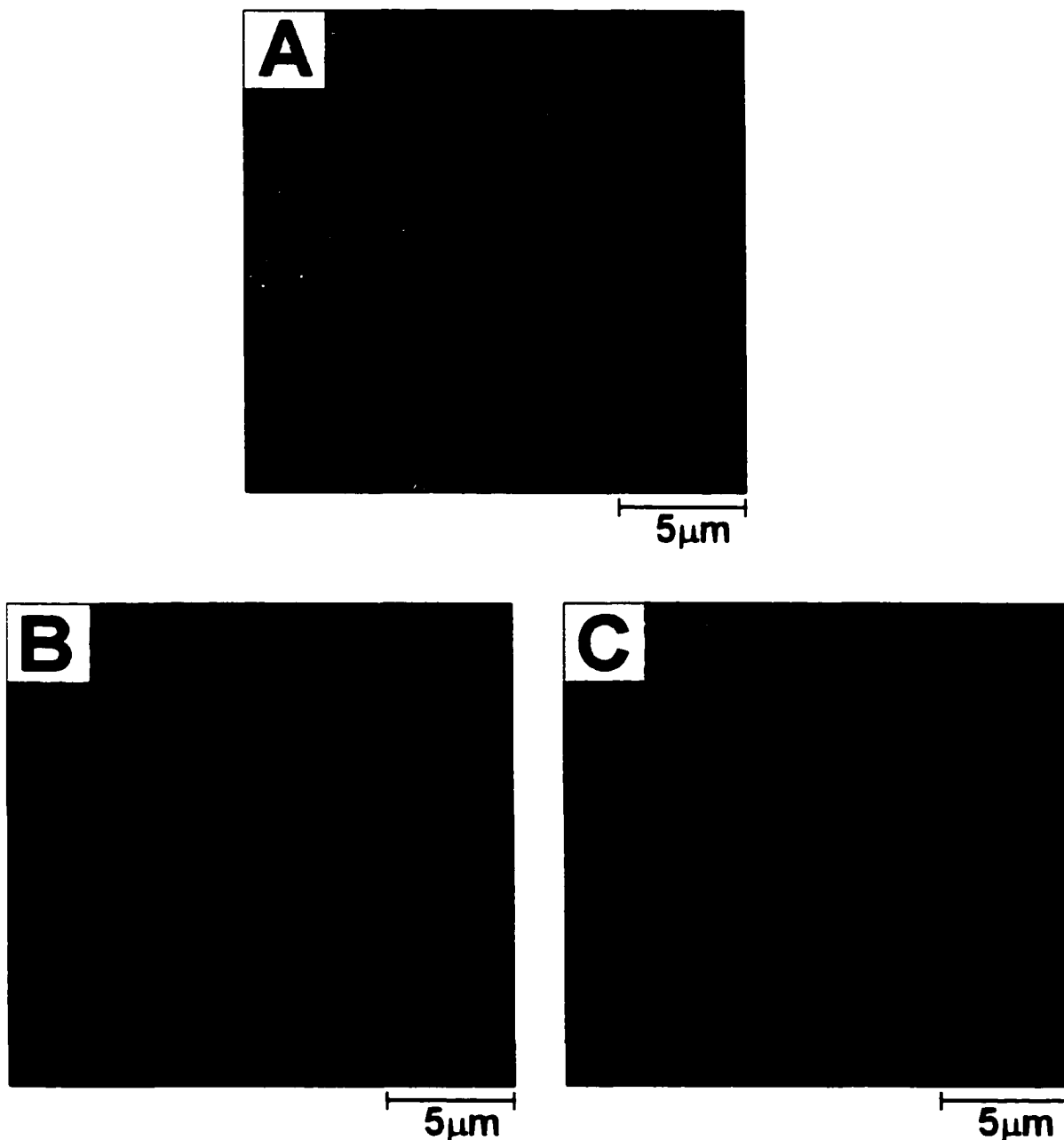


**Figure 5.6:** 20 x 20  $\mu\text{m}$  SFM images of GC surfaces collected *in situ*. (A) Topographic (z-scale 40 nm) and (B) Friction (z-scale 0.3 V) images of polished GC collected simultaneously in pH 3 buffer after 10 s ECP in 0.1 M NaOH. Part C (z-scale 0.3 V) is a friction image collected in pH 3 buffer at the same spot as Part B but after 2 s oxidation in  $\text{H}_2\text{SO}_4$ .

polishing layer by ECP in base for short time scales (~ 10 s) results in more nucleation sites being exposed for oxidation. A high density of the exposed nucleation sites would give rise to a more homogeneous GC surface. As a result, the oxidation process nucleates more uniformly across the GC surface in absence of the polishing layer.

### **Conclusion**

Results obtained in this Chapter show that transformations of GC surface induced by electrochemical modification can be tracked with friction force SFM. The use of patterned electrodes facilitated calibration of the observed frictional contrast between polished and acid oxidized GC surfaces in both acidic and basic media. Polished regions exhibit a higher frictional contrast than acid oxidized regions when imaging is done in acidic media. There is an inversion of frictional contrast when images are collected in basic media. The dependency of frictional contrast on pH probably suggests that the observed contrast is governed by differences in surface chemistry. Importantly, the dependency of frictional contrast on pH was extended to track oxidation nucleation mechanism of ECP process. *In situ* friction force SFM studies show that the electrochemical oxidation process nucleate at the defects, namely polishing scratches. Results obtained in this Chapter also show that nucleation of the electrochemical oxidation process is likely directed by the polishing layer.

**References**

1. C. D. Frisbie, L. F. Rozsnyai, A. Noy, M. S. Wrighton, and C. M. Lieber, *Science* 265:2071 (1994).
2. J.-B. D. Green, M. T. McDermott, and L. M. Siperko, *J. Phys. Chem.* 99:10960 (1995).
3. R. M. Overney, E. Meyer, J. Frommer, D. Brodbeck, R. Lüthi, L. Howard, H.-J. Güntherodt, M. Fujihira, H. Takano, and Y. Gotoh, *Nature* 359:133 (1992).
4. K. Kendall, *Nature* 319:203 (1986).
5. B. Kazee, D. E. Weisshaar, and T. Kuwana, *Anal. Chem.* 57:2736 (1985).
6. L. J. Kepley and A. J. Bard, *Anal. chem.* 1988:1459 (1988).
7. J. F. Evans and T. Kuwana, *Anal. Chem.* 49:1632 (1977).
8. R. M. Wightman, M. R. Deakin, P. M. Kovach, W. G. Kuhr, and K. J. Sturts, *J. Electrochem. Soc.* 131:1578 (1984).
9. G. K. Kiema and M. T. McDermott, *Anal. Chem.* 71:4306 (1999).
10. W. H. Smyrl, R. T. Atanasoski, L. Atanasoska, L. Hartshorn, M. Lien, K. Nygren, and E. A. Fletcher, *J. Electroanal. Chem.* 264:301 (1989).
11. M. T. McDermott, C. A. McDermott, and R. L. McCreery, *Anal. Chem.* 65:937 (1993).
12. G. E. Cabaniss, A. A. Diamantis, W. R. Murphy, R. W. Linton, and T. J. Meyer, *J. Am. Chem. Soc.* 107:1845 (1985).

13. D. M. Anjo, M. Kahr, M. M. Khodabakhsh, S. Nowinski, and M. Wanger, *Anal. Chem.* 61:2603 (1989).
14. C. Kozlowski and P. Sherwood, *J. Chem. Soc. Faraday Trans. 1* 81:2745 (1985).
15. Y. Yang and Z. G. Lin, *J. Appl. Electrochem.* 25:259 (1995).
16. K. T. Kawagoe, P. A. Garris, and R. M. Wightman, *J. Electroanal. Chem.* 359:193 (1993).
17. S. R. Jones, G. E. Mickelson, L. B. Collins, K. T. Kawagoe, and R. M. Wightman, *J. Neurosci. Methods* 52:1 (1994).
18. R. A. Engstrom and V. A. Strasser, *Anal. Chem.* 56:136 (1984).
19. K. M. Sundberg, *J. Electrochem. Soc.* 136:434 (1989).
20. C. A. McDermott, K. R. Kneten, and M. R. L., *J. Electrochem. Soc.* 140:2593 (1993).
21. P. Pantano and W. G. Kuhr, *Anal. Chem.* 68:1413 (1991).
22. P. Pantano and W. G. Kuhr, *Anal. Chem.* 65:2452 (1993).
23. T. Nagaoka and T. Yashino, *Anal. Chem.* 58:1037 (1986).
24. M. Poon and P. McCreey, *Anal. Chem.* 58:2745 (1986).
25. X. Y. Lin, F. Creuzet, and H. Arribart, *J. Phys. Chem.* 97:7272 (1993).
26. A. Noy, D. V. Vezenov, and C. M. Lieber, *Annu. Rev. Mater. Sci.* 27:381 (1997).
27. E. W. van der Vegte and G. Hadziioannou, *J. Phys. Chem. B* 101:9563 (1997).

28. G. N. Kamau, W. S. Willis, and J. F. Rusling, *Anal. Chem.* 57:545 (1985).
29. D. T. Fagan, I. Hu, and T. Kuwana, *Anal. Chem.* 57:2759 (1985).
30. R. DeClements, G. M. Swain, T. Dallas, M. W. Holz, R. D. Herrick II, and J. L. Stickney, *Langmuir* 12:6578 (1996).
31. P. Chen and R. L. McCreery, *Anal. Chem.* 68:3958 (1996).

## **Chapter VI**

### **Conclusions and Future work**

#### **Overall Conclusions**

This research was focused on probing in detail the effect of electrochemical pretreatment (ECP) on the morphology and surface architecture of glassy carbon (GC) electrodes at micrometer length scales using scanning force microscopy (SFM). The results presented in the proceeding Chapters have demonstrated that SFM is a powerful technique for probing topographic and compositional changes induced on GC electrodes following ECP.

The first application of phase contrast tapping mode scanning force microscopy (TM SFM) in the compositional mapping of relatively rough ECPed GC electrodes was demonstrated. Development of an electrode preparation method based on standard microfabrication techniques allowed direct comparison of modified and unmodified regions of polished GC in the same SFM image (Chapter II). Furthermore, the use of patterned GC electrodes provided direct evidence that ECP of polished GC electrodes in basic media etched away the carbon surface. All topographic SFM images obtained for GC electrodes ECPed in acidic media did not show any topographical changes.

Phase contrast TM SFM provided compositional information that correlated to topographic changes as well as electrochemical reactivity.

Although the surface composition of GC electrodes following ECP in acidic electrolytes varies significantly from that due to ECP in base [1, 2] the direction of the phase contrast and the overall trend of phase contrast measurements ( $\Delta\phi$ ) with oxidation time is found to be similar for both media. TM SFM images show that GC surfaces oxidized in acidic or basic media induce a lower phase lag in the oscillating cantilever than polished GC. Polished regions exhibit a darker contrast implying that more cantilever energy is dissipated at these areas. The results are surprising since the oxidized GC surface was expected to interact more strongly with the tip and induce a greater phase lag. Adhesion hysteresis measurements between the tip and the GC surfaces studied were made as well as nanoindentation measurements to determine surface parameters that govern the observed phase contrast. Results from these studies indicate that the observed phase contrast is derived from differences in mechanical properties between the modified and unmodified GC regions [3].

A simple and rapid electrochemical procedure was developed to remove contaminants resulting from polishing or other sources from electrode surfaces (Chapter III). It was discovered that 10 s ECP in 0.1 M NaOH at 1.8 V effectively removes contaminants present on polished GC surface. TM SFM and x-ray photoelectron spectroscopy (XPS) surface characterization techniques were utilized to track the removal of the contaminants. Electrochemical measurements obtained on the electrochemically cleaned

GC surfaces show a highly reproducible surface with reactivity comparable to polished GC.

Microstructures fabricated on GC substrates following ECP in basic media at high anodization potentials were shown in Chapter IV. Scanning electron microscopy (SEM) was used to image the fabricated microstructures. The etched depth was found to be controllable over the anodization time scales (up to ~15 min.) and potential (1.8 V to 3 V versus Ag/AgCl reference electrode) investigated. SEM micrographs show that the sidewalls of the depressions etched inwards.

Lateral or friction force SFM was employed in Chapter V to track the initial oxidation mechanism of the ECP process. Regions oxidized in acid exhibited a lower frictional signal relative to the unmodified regions for images collected in pH 3 buffer. An inversion in frictional contrast was observed when imaging was done in basic media. Dependency of frictional contrast on pH likely suggests that differences in surface chemistry dominated frictional contrast for the images consisting of oxidized and non-oxidized regions. Work presented in Chapter V also demonstrated for the first time the ability of *in situ* frictional force SFM to track oxidation nucleation mechanism of ECP process occurring on polished GC surfaces. Results from these studies show that electrochemical oxidation nucleate at the defects. The polishing layer was found to direct the oxidation nucleation mechanism.

## **Suggestions for Future Work**

TM SFM results obtained in this research suggest that interactions between the SFM tip and the polishing layer dominate the phase contrast observed in images consisting of both modified and unmodified GC. More research is needed to determine the viscoelastic properties of the different GC surfaces studied. The viscoelastic measurements may be performed with an AC nanoindenter. This may ascertain if differences in viscoelasticity contribute to the direction of the observed phase contrast.

Further work is also required to verify the surface parameters that govern the direction of frictional contrast observed in friction force SFM images presented in Chapter V. This may involve use of chemically modified SFM tips. Use of modified tips with tailored chemistry would verify if differences in surface chemistry dominate the observed contrast. Understanding the contrast mechanism in phase and friction SFM images would motivate wider application of SFM among electrochemists and other SFM users in characterizing electrode interfaces modified via various schemes.

More work is also needed to fully exploit the potential of base etching procedure in fabricating microstructures on GC substrates. This procedure may be extended to fabricate more complex carbon microstructures with potential applications in mechanical electromechanical systems (MEMS) such as interdigitated microcapacitors, microbatteries and microresonators. Base

etching may also be used to develop carbon arrays for selective modification and sensing.

It would be interesting to use SFM to probe the density of different surface oxide groups present on ECPed GC surfaces. This may be achieved by using selective substances that react with specific surface oxide groups. For example, studies have shown that dinitrophenylhydrazine and dinitrobenzoyl chloride selectively reacts with surface bound carbonyl [4] and hydroxyl [5] groups respectively. Derivatization of the various oxide groups present at the GC surfaces with SFM detectable molecules or beads would allow determination and distribution of surface oxides prior to and after ECP. Such information may allow better understanding of the oxidative nucleation mechanism and also facilitate better understanding of the role of specific surface sites in electron transfer kinetic. Results from the proposed studies may also likely permit control of reactivity at the electrode surface.

Various ECP procedures have been employed to activate carbon electrodes. Another common ECP procedure involves anodic treatment followed by partial reduction of the GC surface [6]. I propose studies similar to those reported in Chapter II on anodized GC electrodes. Together with tracking compositional changes on the partially reduced GC surfaces, it is possible that the results obtained may also provide more insight on the friction contrast mechanism observed in Chapter V.

**References**

1. A. L. Bielby, T. A. Sasaki, and H. M. Stern, *Anal. Chem.* 67:976 (1988).
2. C. Kozlowski and P. Sherwood, *J. Chem. Soc. Faraday Trans. 1* 81:2745 (1985).
3. G. K. Kiema and M. T. McDermott, *Anal. Chem.* 71:4306 (1999).
4. M. A. Fryling, J. Zhao, and M. R. L., *Anal. Chem.* 67:967 (1995).
5. P. Chen, M. A. Fryling, and R. L. McCreery, *Anal. Chem.* 67:3115 (1995).
6. R. L. McCreery, , in *Electroanalytical Chemistry* Vol. 17 (A. J. Bard, ed.), Marcel Dekker, New York, 1991, p. 221.